Evaluation of the purity and dispersion of single walled carbon nanotubes as potential pharmaceutical excipients

A Thesis Submitted to the College of Graduate Studies and Research
in Partial Fulfillment of the Requirements for the
Degree of Master of Science
in the College of Pharmacy and Nutrition, University of Saskatchewan
Saskatoon, Saskatchewan, Canada

By

Mukasa Tenyogtaa Bagonluri

PERMISSION TO USE

In presenting this thesis in partial fulfillment of the requirements for a Postgraduate degree from the University of Saskatchewan, I agree that the Libraries of this University may make it freely available for inspection. I further agree that permission for copying of this thesis in any manner, in whole or in part, for scholarly purposes may be granted by my supervisor who supervised my thesis work or, in their absence, by the Dean of the College of Pharmacy and Nutrition. It is also understood that any copying or publication or use of this thesis or parts thereof for financial gain shall not be allowed without my written permission. It is also understood that due recognition shall be given to me and to the University of Saskatchewan in any scholarly use which may be made of any material in my thesis. Requests for permission to copy or to make other use of material in this thesis in whole or part should be addressed to:

Dean of the College of Pharmacy & Nutrition

University of Saskatchewan

Saskatoon, Saskatchewan, S7N 5C9

CANADA

ABSTRACT

Single walled carbon nanotubes (SWNTs) are considered potential biomedical materials because of their flexible structure, hollow interior for fluidic transport, propensity for functionalization of the exterior walls, and biocompatibility. Research into exploiting these properties has focused on SWNTs as building blocks for novel drug-delivery systems, dosage forms, and biomedical substrates. However, the use of the internal nanochannels as conduits for trans-membrane drug delivery has not been explored. This research was initially designed to explore the latter.

It is postulated that due to their mechanical strength and the presence of an internal conduit, SWNTs can be used for nanofluidic transport. Using a magnetic field, the magnetically responsive SWNT are driven into intact stratum corneum, creating nanochannels, for trans-membrane drug delivery. Initial studies showed however that a bottleneck is the aggregation of SWNTs on the surface of stratum corneum. To achieve trans-membrane nanofluidic delivery, the SWNTs have to be well dispersed in an appropriate pharmaceutical medium, and the SWNT have to be of high purity. Similarly, the presence of impurities in SWNTs, and the dispersion state of these materials in pharmaceutical solvents may give an insight into the discrepancies in toxicity that is reported.

The purity of five commercially available SWNTs (AP-SWNT and P2-SWNT, from Carbon Solutions Inc, HMS-SWNT from Helix Materials, and NA-SWNT from Nanostructured and Amorphous Materials Inc. and CT-SWNT from ChepTubes Inc.) were analyzed by raman and electron dispersive x-ray spectroscopy (EDS) spectroscopy. Secondly, the dispersion states of SWNTs in various pharmaceutical solvents were evaluated by ultraviolet (UV) spectroscopy, scanning electron microscopy (SEM), dynamic light

scattering (DLS), zeta potential, and Raman spectroscopy to identify potential agents for exfoliation of SWNTs in selected pharmaceutical solution.

SWNTs were dispersed in various solvents (water, propylene glycol [PG], dimethylsulfoxide [DMSO], and ethanol) as well as in 0.1% w/v aqueous solutions of anionic, cationic and neutral surfactants at a SWNT concentration of 0.1 mg/mL. SWNT suspensions described as dispersed yielded an evenly coloured suspension with no visible precipitate. The most stable dispersions were obtained with the gemini surfactants, which were confirmed by SEM observation of exfoliated SWNTs. Zeta (ξ) potential measurements of the fully dispersed SWNTs showed typical values of greater than +30 mV, while non-dispersed samples were less than +20 mV. SEM images of the dispersed solution showed the presence of exfoliated SWNTs compared to the aggregated SWNT clusters observed in non-dispersed systems. Raman spectra of dispersed SWNTs showed G-band peak shifts (to higher wavelengths), confirming the presence of exfoliated SWNTs.

Even though the purity of SWNT did not correlate with amount of SWNT in dispersion, exfoliation of bundled SWNTs was accompanied by an increase in UV absorbance of the dispersion, with maximum exfoliation determined by a relatively stable UV absorbance.

As pharmaceutical excipients, we have demonstrated that gemini surfactants are suitable dispersing agents for SWNTs, and shown that the dispersion of SWNT for gemini surfactants (12-3-12) is achieved below the critical micelle concentration. The dispersion of SWNT bundles into individual strands is the first crucial step towards their use in biological systems as drug carriers.

ACKNOWLEDGEMENTS

I wish to extend my appreciation to my wife; Lisa, daughter; Moni, and sons; Landon and Liryck. I dearly appreciate the various sacrifices that were very instrumental in the completion of this thesis. To them, I dedicate this thesis.

TO

*I dedicate this work to my beloved wife (**Lisa**) and beautiful children (**Moni**,*

Landon** and **Liryck**) and to the memory of my father **Jacob Minnia Bagonluri

TABLE OF CONTENTS

LIST OF TABLES

LIST OF FIGURES

LIST OF ABBREVIATIONS

12-3-12	1,3-propanediyl-bis(dimethyldodecylammonium) dibromide
12-7-12	1,7-heptanediyl-bis(dimethyldodecylammonium) dibromide
12-7N-12	1,9-bis(dodecyl)-1,1,5,9,9-pentamethyl-5-aza-1,9-nonanediammonium dibromide
12-7NH-12	1,9-bis(dodecyl)-1,1,9,9-tetramethyl-5-imino-1,9-nonanediammonium dibromide
16-3-16	1,3-propanediyl-bis(dimethylhexadecylammonium) dibromide
18-3-18	1,3-propanediyl-bis(dimethyl-octadecylammonium) dibromide
AFM	Atomic force microscopy
AP-SWNT	As produced SWNTs from Carbon Solutions Inc.
BEI	Backscattered electron imaging
BNCT	Boron neutron capture therapy
cm^{-1}	Per centimeter. Unit of measure of Raman shift
CMC	Critical micelle concentration
CTAB	Cetyltrimethylammonium bromide
CTRL	Count rate too low.
CNT	carbon nanotubes
CNT-AmB	carbon nanotube- amphotericin B moiety
cp	carbonaceous purity of SWNTs
CT-SWNT	CheapTubes Single walled carbon nanotubes
C_{60}	fullerene,s composed of 60 carbons
CVD	Chemical vapour deposition
D-band	Disorder induced band of CNTs
DC	Direct current
DEA	*N,N*-diethylacetamide
D_H	Hydrodynamic diameter
DLVO	Derjaguin, Landau, Verwey and Overbeek
DLS	Dynamic laser light scattering
DMA	*N,N*-dimethylpropanamide
DMF	*N*-methyl-2-pyrrolidone

DMP	*N,N*-dimethylpropanamide
DMSO	Dimethylsulfoxide
DNA	Deoxyribonucleic acid
DTAB	Dodecyltrimethylammonium bromide
EAD	Electric arc-discharge
EDS	Electron backscattered electron imaging
ELISA	Enzyme-linked immunosorbent assay
ELS	Electrophoretic light scattering
EPO	Erythropoietin
eV	Electron volt, a unit of energy
FA	Folic acid
f-CNT	Functionalized carbon nanotubes
FE-SEM	Field Emission Scanning Electron Microscope
FMDV	Foot-and-mouth-disease virus
FWHM	Full width at half maximum
G	Unit of measurement of a magnetic field or the magnetic flux density
g	A measure of the centrifugal force
G-band	Raman peaks due to tangential vibration mode of CNTs
GFP	Green fluorescence protein
HLB	Hydrophile-lipophile balance
HMS-SWNT	Single walled carbon nanotubes from Helix Materials (90 % purity)
Hz	Hertz
I_D	Intensity of the D band in a Raman spectrum
IEP	Isoelectric point
IGP	Polyoxyethylene (100) nonylphenyl ether
I_G	Intensity of the G band in a Raman spectrum
IR	Infrared
iRNA	RNA interference
LA	Laser ablation
mg/mL	milligrams of solute dispersed/dissolved in a millilitre of solvent

mL	millilitre
mM	millimolar concentration
μL	microlitre
μm	micrometre
mTERT	mouse Telomerase Reverse Transcriptase
mV	millivolts
MW	molecular weight
MWNT	multi-walled carbon nanotubes
N/A	not applicable
NA-SWNT	SWNTs from Nanostructured and Amorphous Materials Inc.
nm	nanometer
NMP	*N,N*-dimethylformamide
NMR	Nuclear magnetic resonance spectroscopy
NNLS	Non-Negative Least-Squares
P2-SWNT	Low functionality SWNTs from Carbon Solutions Inc.
P3-SWNT	Acid purified SWNTs from carbon solutions Inc.
PEG	Polyethylene glycol
PLip	Phospholipid
PL	Phospholuminescence
RBM	Radial breathing mode of carbon nanotubes
RNA	Ribonucleic acid
RF	Radio frequency
SC	stratum corneum
SDS	sodium dodecyl sulfate
SDBS	sodium dodecylbenzene sulfate
SEM	Scanning electron microscope/microscopy
siRNA	Small interfering RNA
SLS	Static laser light scattering
S/N	Signal to noise ratio
SWNT	Single-walled carbon nanotubes
TGA	Thermogravimetric analysis

TEM	Transmission electron microscope/microscopy
USP	United States Pharmacopeia
UV	Ultraviolet
UV-Vis	Ultraviolet-visible
WDX	wavelength-dispersive x-ray spectroscopy
$^w/_v$	Weight of solute in a solvent to the volume of solvent.

1.0   CARBON NANOTUBES AS PHARMACEUTICAL AND BIOMEDICAL MATERIALS

1.1   CNTs in delivery of therapeutic agents

The applications of CNTs as drug excipients are of interest, given their capacity to interact with macromolecules such as proteins and DNA [1]. The salient characteristics of an efficient drug delivery system include its ability to perform controlled and targeted drug delivery, which CNTs have been shown to exhibit [2]. Three methods of interaction between CNTs and pharmaceutically active components are possible in drug delivery. The first method of interaction is as a porous absorbent for the entrapment of active components within a CNT mesh or CNT bundle (Figure1.1, *A*). The second is through functional attachment of the compound to the exterior walls of the CNTs (Figure 1.1, *B*). The third approach involves the use of CNT channels as nanocatheters (Figure 1.1, *C*).

Venkatesan et al. [3] used CNTs as a porous nanoparticulate absorbent in the controlled delivery of erythropoietin (EPO) in mice. The solubility of SWNTs was obtained by dispersing them in various surfactant solutions. An 11.5% increase in bioavailability of EPO in serum was demonstrated when EPO formulations contained CNTs, compared with formulations without CNTs. A more specific application of CNTs requires control at the nano-level, by attaching a drug to individual CNTs for drug delivery, rather than exploiting a bulk property of CNTs. The exohedral and potential endohedral attachment of pharmaceutically functional molecules is of interest. With exohedral binding, drug moieties are attached to the exterior of CNTs for subsequent delivery into cells. CNTs have a distinct outer surface that makes them amenable to functionalization. The diverse functional groups introduced onto the surface act as "linkers" to therapeutic moieties, for subsequent delivery into cells (Figure 1.1, *B*).

A   B   C
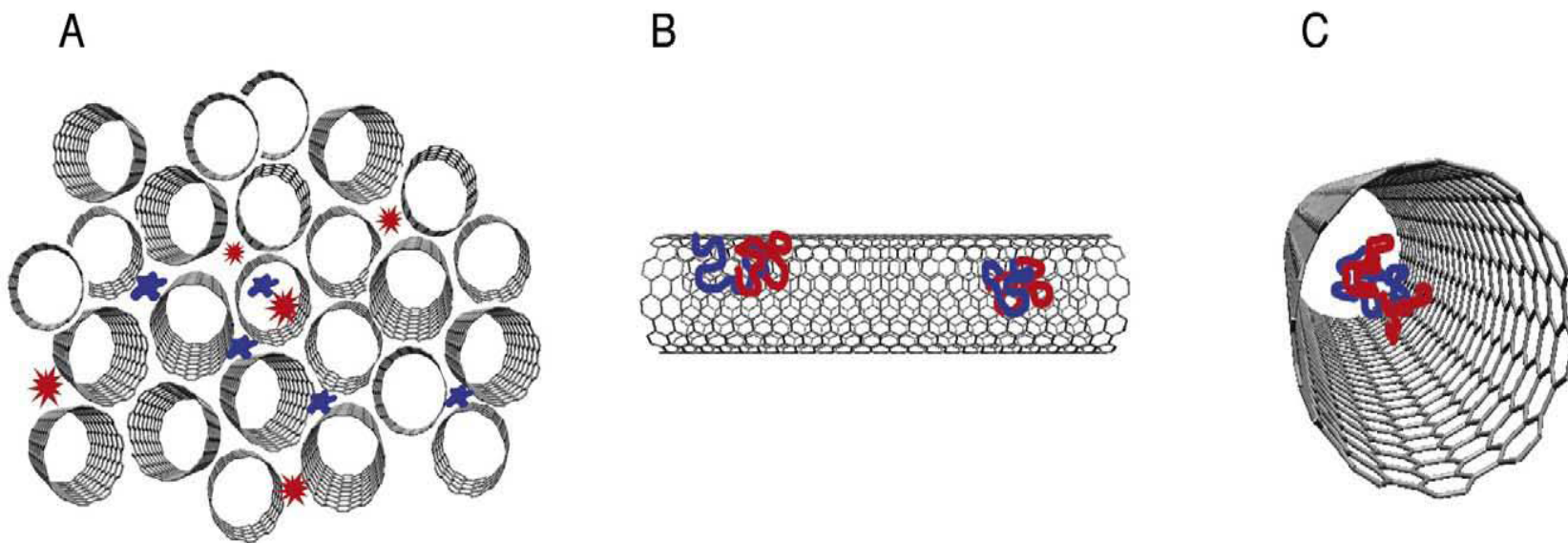
Figure 1.1   Schematic representation of (**A**) a bundle of CNTs as a porous matrix encapsulating drug molecules between the grooves of individual CNTs, (**B**) moieties attached to the exterior of a CNT either by covalent bonding to the CNT wall or by hydrophobic interaction of moieties with the CNT walls, and (**C**) the encapsulation of moieties within the internal nanochannel of a CNT.

With endohedral delivery, nanoparticles (particles with at least one dimension <100 nm) are encapsulated and transported through the inner cavities of CNTs (Figure 1.1, *C*). This raises the prospect of controlled nanofluidic delivery of therapeutic agents.

The application of CNTs as carriers is increased by their propensity to penetrate cells. Cationic functionalized CNTs (f-CNTs) can be bound to active molecules via stable covalent bonds or supramolecular assemblies based on electrostatic attractions. Two possibilities exist: (1) the more energetically feasible attachment onto the exterior either by covalent or non-covalent interactions, and (2) the encapsulation of these molecular assemblies within CNTs. Predominantly, reports on the use of CNTs in drug delivery have focused on the use of CNTs as carriers for large biomolecules. Tables 1.1 and 1.2 summarize the use of CNT-biomolecular conjugates in therapeutic delivery.

1.1.2 Functionalization of carbon nanotubes for pharmaceutical applications

Several approaches have been developed to functionalize CNTs (f-CNTs). They include the functionalization of defective CNT sidewalls, covalent functionalization of intact CNTs (Table 1.1), and noncovalent functionalization or adsorption onto CNT sidewalls (Table 1.2). Covalent functionalization of CNTs using the versatile 1,3-dipolar cycloaddition mechanism is the most widely used approach to covalently attach molecular moieties to CNTs (Table 1.1, structures *I-VII*) for the delivery of therapeutic molecules. The resulting amine-terminated reactive CNT-intermediates are the reactive centers for subsequent attachment of functional moieties. This has become the general synthetic strategy, allowing for the easy preparation of a common intermediate with a reactive group, for subsequent functionalization to the desired compound. By this scheme, the attachment of an ammonium-terminated triethylene glycol chain

(reactive intermediate) to CNT sidewalls allows for the synthesis of several CNT-functionalized compounds (Table 1.1, structures *I-VI*).

F-CNTs used as vectors for *in-vitro* delivery of therapeutic levels of amphotericin B (AmB) [4] are obtained from the 1,3-dipolar cycloaddition reaction (Table 1.1, *II*). Even though AmB is a very potent and effective antibiotic for the treatment of chronic fungal infections, its use is limited because of its potential toxicity to mammalian cells. This toxicity is attributed, in part, to the formation of aggregates because of low solubility. To avoid these concerns, AmB can be conjugated to CNTs, which increases its solubility and results in decreased aggregation. The decrease in toxicity and increased antifungal activity of the CNT-AmB conjugate was demonstrated in Jurkat cells, and modulation of antibiotic activity against three types of fungi: *Candida parapsilosis, C. albicans,* and *Cryptococcus neoformans* [4].

Chen et al. [5] obtained amine-terminated CNT conjugates via the derivatization of carboxylated CNTs with thionyl chloride ($SOCl_2$), and subsequent reaction with octadecylamine, yielding a versatile intermediate. Besides 1,3-dipolar cycloaddition, Yinghuai et al. [6] employed nitrene cycloaddition to covalently bind carborane cages to CNTs [6] (Table 1.1, structure *VII*), resulting in improved aqueous solubility of these boron containing chemotherapy moieties; a prospect for improved targeted delivery into cancerous tumours.

Functionalization with polyethylene glycol (PEG) moieties (also termed PEGylation) has been widely used to improve the solubility of the CNT-conjugate in aqueous solutions, as well as the biocompatibility of the moieties [7-10]. Kam et al. [9] reported the hydrophobic interaction between CNT sidewalls and the hydrocarbon chain of the phospholipid (PLip) component of a (PLip)-polyethylene glycol (PEG) moiety, to obtain noncovalent functionalization of CNTs. The PEG chains were functionalized with terminal amine (PLip-PEG-NH_2) and maleimide (PL-PEG-

maleimide) groups, resulting in positive interaction with a polar aqueous solvent. The amine and maleimide terminal groups provide another functionalization site for biomolecules. The heterobifunctional cross-linker sulfosuccinimidyl 6-(3'-[2-pyridyldithio]-propionamido)hexanoate (sulfo-LC-SPDP) was conjugated with the phospholipid, forming a thiol bond. Upon reacting with the thiol functional groups from biomolecules, a disulfide bond is formed (Table 1.2, *III*).

1.1.3   Delivery of therapeutic proteins, peptides, and genes by CNTs

F-CNT-DNA and f-CNT-protein conjugates are adept at crossing the cell membrane and subsequently lodging in the nucleus [11, 12]. This makes them a potential vector for transporting proteins [9, 11, 13-19] and genes [12, 20-23] into the nucleus, where the payload is released. Proteins are known to adsorb spontaneously onto the sidewalls of carboxylic f-CNTs, creating protein-CNT conjugates [17]. However, the binding of proteins onto the sidewalls of CNTs is highly selective. In an experiment to determine the complement activation of CNTs in blood, Salvador-Morales et al. [13] determined that of the 35 proteins in the human complement system (a group of 35 defense cell-surface proteins that recognize and clear invading moieties), fibrinogen and apolipoproteins were the proteins that bound onto CNTs in significant amounts [13]. Protein delivery, however, has been mediated by both anionic and cationic f-CNTs. In a study of the uptake of CNT-protein conjugates, Kam et al. [17] investigated the transfection of HL60 and Jurkat cell lines with acid-purified CNT-streptavidin conjugates. A higher expression of the protein was observed for the CNT-streptavidin conjugate transfection, compared with the streptavidin-only transfection. To establish that proteins bind non-specifically to acid-purified CNTs and that the mechanism of CNT-protein uptake by cells occurs by
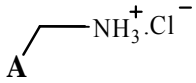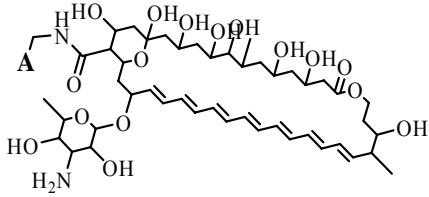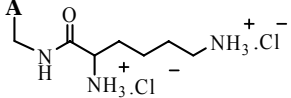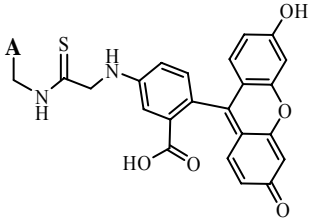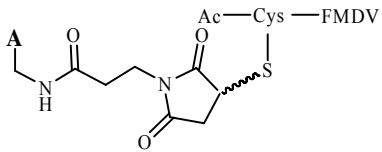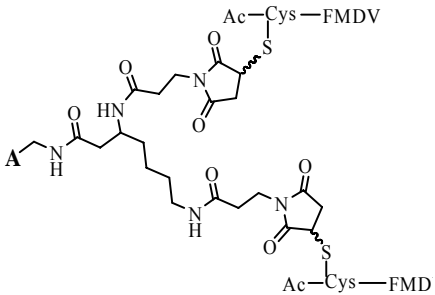
endocytosis, Kam et al. [16] investigated the uptake of several other proteins (Protein A, bovine serum albumin, and cytochrome c) into adherent and non-adherent cell lines (HeLa, NIH-3T3 fibroblast, HL60, and Jurkats cells).

Gene silencing, the introduction of short interfering RNA (siRNA), is a quickly emerging approach to genetic intervention. Using the complex ($-CONH_2-(CH_2)-NH_3^+Cl^-$), messenger telomerase reverse transcriptase (mTERT), siRNA was successfully attached to SWNTs without losing its conformation. The attached moiety was successfully delivered into the cell cytoplasm, resulting in the suppressed expression of the TERT gene [19]. Kam et al. [9] synthesized (Table 1.2, *III*) a "smart" siRNA delivery system, by coupling SWNTs to siRNA, through an enzymatically cleavable disulfide bond. The transfection of this moiety with HeLa cells showed significantly increased RNA interference (RNAi) activity. The process of CNT-mediated gene/protein delivery *in vitro* is illustrated in Figure 1.2, *A* (pathway 1).

Cationic f-CNTs have been used as carriers to deliver genes. Unlike the non-specific binding of proteins onto f-CNTs, the binding of DNA to these f-CNTs is by the electrostatic interactions between the phosphate backbone of DNA and the cationic functional groups.

Table 1.1   **Covalent binding of bioactive molecules to CNTs**

CNT properties		Bioactive molecule	Study aim/results	Dispersion solvent	Refs.
Type	Functional group or structure				
SWNT/ MWNT	A —NH$_3^+$.Cl$^-$ **I**. Ammonium-terminated triethyl glycol	i. pCMV-ß-gal plasmid	i. Effect of attached functional group on DNA compaction and subsequent transfection	i. Aqueous	i.[22]
		ii. Mouse splenocyte	ii. Immunology; *in-vivo* study of the antigenicity, and immune response of FMDV peptide-CNT conjugate in Balb/c mice	ii. Aqueous	ii.[14]
		iii. ODN CpGs	iii. Increased production of immunostimulatory CpG motifs in mouse splenocytes	iii. Aqueous	iii. [18]
		iv. G family of proteins	iv. CNT-bound peptides successfully transfected in human 3T6 and murine 3T3 fibroblasts	iv. Aqueous	iv. [11]
SWNT/ MWNT	A (Amphotericin B structure) **II.** Ammonium-terminated triethyl glycol	Amphotericin B	Transfection and increased antifungal activity demonstrated in Jurkat cells against three species of fungi: *Candida parapsilosis, C. albicans,* and *Cryptococcus neoformans*	Aqueous	[4]
SWN⌐	A (structure with O, N–H, NH$_3^+$.Cl$^-$, NH$_3^+$.Cl$^-$) **III**. Ammonium-terminated triethyl glycol	i. ß-gal plasmid	i. Transfection efficiency increased with increasing charge ratio (f-CNT:DNA)	i. Aqueous	i.[11]
		ii. pCMV-ß-gal plasmid	ii. Effect of attached functional group on DNA compaction and subsequent	ii. Aqueous	ii. [22]

		transfection			
SWN T	**IV**. Functional group attached to CNT	i. Streptavidin ii. ODN CpGs	i. Gene delivery and cytotoxicity study ii. Increased production of immunostimulatory CpG motifs in mouse splenocytes	i. Aqueous ii. Aqueous	i. [12] ii. [18]
SWN T	**V.** Triethylene glycol- coupled to a maleimido linker. Functional group attached to CNT.	i. G-family of proteins ii. Peptides derived from VP1 protein of FMDV	i. Protein delivery in human 3T6 and murine 3T3 fibroblasts ii. Immunology; *in-vivo* study of the antigenicity, and immune response of FMDV peptide-CNT conjugate in Balb/c mice	i. Aqueous ii. Aqueous	i. [11] ii.[14]
SWN T	**VI**. N-terminal and side chain N-deprotected lysine; functional group attached to CNT	Peptides derived from VP1 protein of FMDV	Immunology; *in-vivo* study of the antigenicity and immune response of FMDV peptide-CNT conjugate in Balb/c mice	Aqueous	[14]

∞
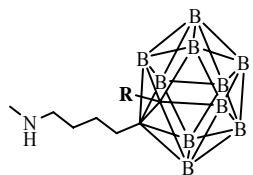
| SWNT | **VII**. Carborane bound to SWNT | None | Cell targeting by selective recognition of EMT6 cell with potential use in boron neutron capture therapy | Aqueous / DMSO | [6] |

Structure VII is directly bound to CNT sidewall, whereas structures I-VI are attached to a moiety defined below. R represents an alkyl chain of variable length.

The moiety represented by A in structures I-VI =
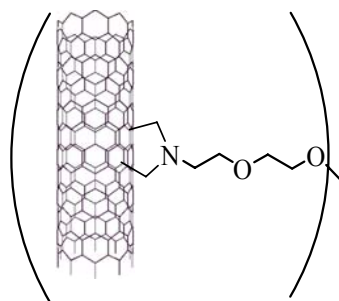
Table 1.2   Non-covalent binding of bioactive molecules to CNTs

CNT properties		Bioactive molecule	Study aim/results	Dispersion solvent	Ref.
Type	**Functional group**				
SWNT	None	Erythropoietin	Controlled release of EPO	Mixed in several component formulations	[3]
SWNT	**I**. PL-PEG and PL-PEG-FA molecules	Cys-DNA	Selective tumor marking and subsequent NIR irradiation in HeLa cells	PL-PEG surfactant	[24]
SWNT	**II**. None	Streptavidin protein A (SpA), bovine serum albumin, and cytochrome *c*	Non-specific binding of proteins onto CNT sidewalls, and increased transfection of conjugates	Aqueous	[16]
SWNT		siRNA	Gene silencing (siRNA) obtained by relative ease of cleavage of disulfide bond	PL-PEG surfactant	[9]
	III. PL-PEG-NH$_2$ and PL-PEG-maleimide				
Aligned CNT	None	pEGFP-cI plasmid	Increased transduction by magnetofection of Bal17 B-lymphoma and B cells *ex vivo*	Nanosperse AQ™ surfactant	[23]

A

- Attached moiety
- Functionalized carbon nanotube
- Chiral recognition
- Receptor

Pathway 1

Pathway 2

B

- Laser radiation
- Encapsulated hyperthermic device

C

- Carbon nanotube template
- Neuron
- Neural extension

D

- Cover slip
- Ni-embedded CNT with coupled plasmid
- Cell
- Magnet

11
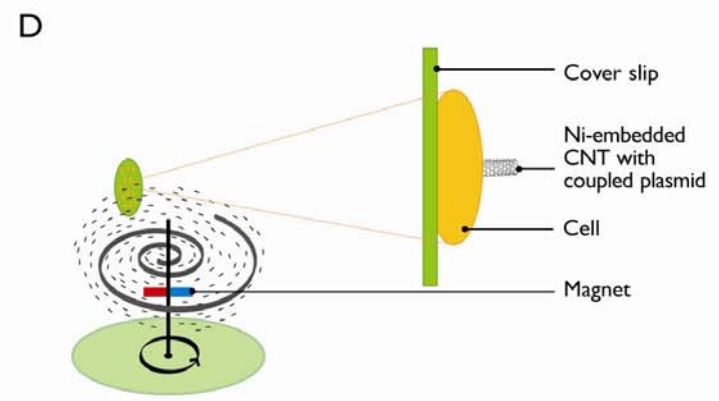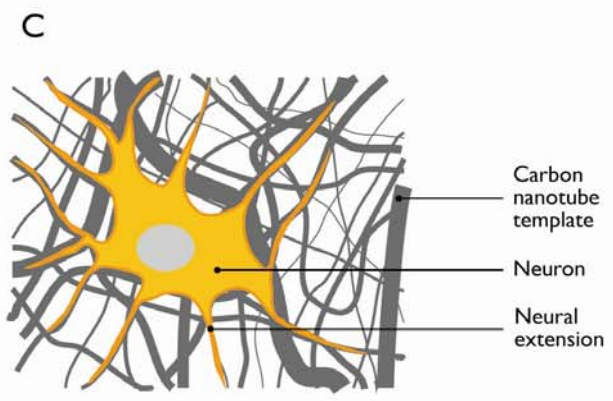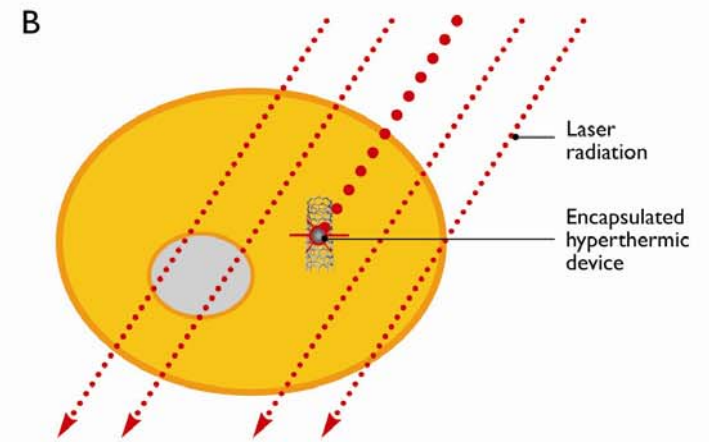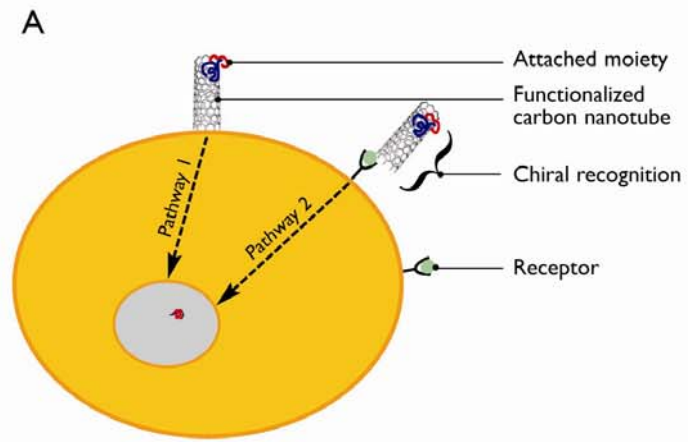
Figure 1.2   Conceptual diagrams of selected pharmaceutical and biomedical applications of CNTs. (A), The two approaches for in vitro delivery of pharmaceutically active moieties into cells via endocytosis. Pathway 1 exploits the propensity of cationic f-CNTs to penetrate cells and their ability to bind these moieties as carriers for delivery. Pathway 2 uses f-CNTs for cell targeting by incorporating moieties that bind selectively to epitopes or receptors on cells. (B), The concept of hyperthermic cell destruction, either by irradiating "endocytosed" CNTs directly or by triggering a hyperthermic device within the endocytosed CNTs. (The latter example is shown.) In either case, specific cell destruction is achieved without harming surrounding cells. (C), The use of CNTs/aligned CNTs as templates, as signal transfer substrates, and as nonbiodegradable substrates for the growth and support of neurons. CNT templates have been demonstrated to promote the growth and extension of neural extensions, as illustrated by the extensive neurite branching that follows the contour of the CNT bundle. CNTs can conduct electricity, so a neural signal can be detected and recorded by placing a probe on a conducting CNT matrix. (D), Spearing of immobilized cells with nickel-embedded ferromagnetic CNTs under the influence of a rotating magnetic field. CNTs spear cells cultured on a coverslip.

Pantarotto et al. [21] successfully transfected HeLa and CHO cell lines with a plasmid (β-galactosidase encoded gene, β-gal), using ammonium f-CNTs as a vector (Table 1, *II*). As with most cationic DNA delivery vectors, the level of marker gene expression (transfection efficiency) seems to be related to the f-CNT:DNA charge ratio. Significantly higher gene expression was reported for a f-CNT:DNA charge ratio of 6:1 than with a charge ratio of 2:1. The efficiency of the delivery vector in plasmid transfection was confirmed by a 10-fold increase in gene expression levels compared with that achieved with DNA alone. The association of the cationic f-CNTs with plasmid DNA is explained as an electrostatic interaction between the anionic phosphate backbone of DNA and the cationic centers on the surface of the f-CNTs. Similar to other cationic molecules, such as cationic lipids, f-CNTs condense plasmid DNA for gene delivery [25, 26].

Having established that f-CNTs increase transfection [21] , Singh et al. [22] evaluated the effect of CNT type and the attached functional group on transfection efficiency of pCMV-β-gal in A549 cells. Three different cationic f-CNTs were evaluated (Table 1, *I* and *II*, lysine f-CNTs) to determine the effect of different attached functional groups on gene expression. The findings indicated that even though both cationic f-CNTs condense DNA, the extent of condensation depended on charge (cation) density. These findings also suggested that the large surface area of f-CNTs resulted in more efficient pCMV-β-gal condensation. However, this did not result in higher gene expression of transfected A549 cells. What is yet to be established is the extent to which DNA condensation affects the release of the plasmid within the cell and subsequent gene expression.

So far, the approach to cellular uptake of CNT-plasmid conjugates has been to incubate cell cultures with the respective f-CNT-plasmid conjugates. Cai et al. [23] reported the use of

CNTs to spear nanochannels into Bal 17 B-lymphoma and B cells *ex vivo*. Vertically aligned nanotubes grown by PECVD with ferromagnetic nickel particles embedded at the tips were used as carriers for enhanced green fluorescent protein (EGFP) coding plasmids, and were driven into cells membranes under the influence of a magnetic force, as shown in Figure 2, *D*. This technique resulted in a high transduction efficiency and viability after transduction. The approach not only delivers the plasmids in a relatively short time, but, by varying the magnetic field, it can also be used to tune the efficiency of spearing. The potential of magnetofection delivery includes a drastic lowering of vector dose since close to 100% of cells were reported to express EGFP protein [23].

At present, several *in-vitro* trials point to the potential of CNT-DNA/protein conjugates as delivery vectors. Nonetheless, several fundamental issues remain to be addressed in the use of CNTs as potential biological transporters. One such issue is the entry mechanism that regulates the cellular internalization of CNTs and their cargos. Kam et al. [12, 16] propose that SWNTs traverse the cellular membrane via endocytosis, whereas Pantarotto et al. [21] suggest a nonendocytotic mechanism that involves insertion and diffusion of nanotubes through the lipid bilayer of the cell membrane. The plasmid/protein uptake findings of Pantarotto and colleagues reveal a novel combination of properties attributable to soluble CNTs and establish the potential of these structures as components of advanced delivery systems for a variety of therapeutics, even though the preliminary comparative gene expression data for lipid:DNA and f-CNT:DNA delivery systems showed that their f-CNTs were less effective for *in-vitro* transfection than were lipid:DNA systems [21].

1.1.4   Delivery of vaccines by CNTs

Efforts are ongoing to develop novel systems for the delivery of protective antigens. The basic idea of using CNTs in vaccine delivery entails linking an antigene to CNTs, without losing its conformation, thereby inducing an antibody response with the right specificity. However, it is equally important that the incorporated CNTs do not possess intrinsic immunogenicity and, hence, trigger an immune response. CNTs therefore act as templates, upon which chiral molecules are attached, which in turn act as centres for molecular recognition [13-15, 27, 28] (Figure 1.2, *A*, pathway 2).

Pantarotto et al. [15] reported the use of CNTs in eliciting an improved immune response. Peptides derived from VP1 protein of the foot-and-mouth-disease virus (FMDV) were coupled to SWNTs (Table 1, *V* and *VI*). Serum samples from inoculated (by injection with CNT conjugates) BALB/c mice were collected and analyzed by enzyme-linked immunosorbent assay (ELISA) for presence of anti-peptide antibodies. Peptide-CNT complexes were shown to elicit greater immune response against the peptides, with no detectable cross-reactivity to the CNTs, confirming the non-immunogenicity of the carrier. It was also observed that the CNT-protein complex enhanced the immune response when attached to an antigen, which strengthens the possibility of incorporating CNTs in vaccines.

Bianco et al. [18] demonstrated that the presence of cationic f-CNTs (Table 1.1, *IV*) in the delivery of synthetic oligodeoxynucleotides containing CpG motifs (ODN-CpGs) improve the immunostimulatory properties of ODN-CpGs *in vitro*. Synthetic oligonucleotides containing CpGs are reported to confer nonspecific protection against cellular pathogens and enhance antigen-specific immune responses. These properties have made them target candidates for incorporation in vaccines. To evaluate the immunostimulatory properties of CNTs, various ratios

of CNT-ODN CpG complexes were incubated with splenocytes. The efficiency of the process was measured by the amount of IL-6, a proinflammatory cytokine whose production is stimulated by ODN-CpG secretion in the supernatant of the culture. The results showed higher levels of IL-6 when f-CNTs were complexed to ODN-CpGs than when only ODN-CpGs were incubated with splenocytes. From the forgoing, f-CNTs could potentially be used as non-replicating vectors for proteins, peptide antigens, and CpGs.

1.1.5   CNTs for delivery and targeting of biophysical treatments

Several uses of CNT moieties have been reported for targeted delivery and subsequent treatment. These range from the use of f-CNTs in cell targeting and biologically triggered drug release control [9, 24, 28, 29], in hyperthermia (i.e., destruction of cancerous cells by local heating) [24], and as carriers of biomolecules for gene therapy and gene silencing [6, 19, 30]. Because of the strong optical absorbance of CNTs and their propensity for endocytosis, they have become candidates for a method to hyperthermically destroy cancerous cells.

Functionalizing CNTs with recognizable epitopes results in endocytosis of f-CNTs by cancerous cells only. Subsequently, IR laser radiation is used to locally heat the endocytosed f-CNTs, resulting in thermal destruction of cancer cells without harming surrounding healthy cells (Figure 1.1, *B*) [24]. This selective killing of cancerous cells that contain CNTs is attributed to the strong optical absorbance of SWNTs in this spectral window. Using this approach of selectively targeting tumor cells, Kam et al. [24] functionalized SWNTs with a phospholipid-polyethylene glycol moiety (PL-PEG) and with folic acid (FA) collectively described as PL-PEG-FA (Table 1.2, *I*). Transfection of the SWNT-(PL-PEG-FA) with HeLa cells expressing the folate epitope results in transfection, together with uptake of SWNTs. Hyperthermic treatment of

a mixture of healthy and folate-expressing tumor cells resulted in the death of only folate-expressing cells. McDevitt et al. [28] developed a tumor targeting CNT construct by attaching the monoclonal antibodies Rituximab and Lintuzumab to the f-CNT (Table 1.1, *I*). To establish specific binding, these constructs were shown to specifically bind to Daudi (CD20+) and HL60 (CD33+) cells, with no binding observed for HL60(CD20-) and Daudi (CD33-) and tumor cells to the exclusion of healthy cells. Using the high aspect ratio of the SWNT, several other moieties, such as fluorescent probes (GFP and Luciferace proteins), and radiometal-ion chelates [^{111}In] were simultaneously bound to the f-CNT together with the antibodies for improved detection.

Yinghuai et al. [6] reported the potential of substituted carborane (a polyhedral cluster of carbon and boron atoms) f-CNTs as a new delivery system for an efficient boron neutron capture therapy (BNCT). BNCT is an experimental radiotherapeutic treatment of cancerous tumors that uses a neutron beam to interact with boron injected into the blood stream. The injected boron collects in tumor cells, which are later irradiated and killed by a neutron beam. Cell-specific uptake of the CNT-carborane complex was observed (Table 1.1, *VII*). Orally administered carborane f-CNTs in *in-vivo* experiments showed a concentration of carborane in tumor cells, to the exclusion of healthy cells, blood and other organs. Using what appears to be a rather simplistic approach, Zhang et al. [29], successfully achieved the dual goal of selective uptake of CNT moieties via folic acid (for cell targeting) and controlled release of the payload (doxorubicin, anticancer drug), by using an intermediate of carboxylated CNTs linked to selected polysaccharide molecules as intermediates.

In view of these results, f-CNTs represent a new, emerging class of nano-delivery system for targeting cancerous cells. It will be necessary, however, to further evaluate the metabolism, biodistribution, and clearance of the CNT conjugates.

1.1.6 CNTs as matrices for compounds that stimulate neuronal growth

CNTs are also potential biocompatible materials that can serve a dual capacity: as a supportive matrix [31-37] and as a conduit for delivering electrical signals [31, 38-40] on which neurons can grow into a specific neural bundle or network, resulting in the formation of neuron-CNT hybrids (Figure 1.2, *C*).

These capabilities allow CNTs to form scaffolds to guide neurite growth [23, 31-35, 38, 41-43]. The growth of neurites during neuron development and regeneration is controlled by a highly motile structural specialization at the tip of the neurite called the growth cone. F-CNTs aid neurite growth by providing a platform for the growth cone to grasp onto rather than growth relying on physisorption alone [33].

The growth of neurons on CNTs suggests that they are biocompatible. Additionally, it has been demonstrated that selective chemical modifications of the tips/walls of CNTs enhance and control neurite outgrowth and branching. Hu et al. [34] observed that the number of neurite growth cones, length of neurite outgrowths, and the degree of branching on positively charged polyethyleneimine f-CNT templates was significantly higher than on neutral or negatively charged CNT substrates. Similarly, enhanced neurite growth and branching was observed when CNTs were coated with a bioactive neuron growth enhancer (4-hydroxynonenal) [32]. Upon establishing that positively charged f-CNTs can potentially support and enhance neurite growth, Lovat et al. [31] and Zhang et al. [35] both suggested the use of positively charged and aligned

CNTs as a template, patterned guide to grow an elaborate, and controlled neuronal network. This concept of a patterned CNT array allows the control of a three-dimensional neuronal network, a prerequisite for signal transmission and, ultimately, regeneration [31, 34, 35].

Several research groups have explored the possibility of using conducting CNTs for transmitting and receiving electrical signals to and from neurons. Wang et al. [39] developed a prototype neural interface based on a CNT microelectrode that is capable of transmitting current pulses to hippocampal neurons preloaded with Fluo-4 AM ester, which responded by increased fluorescence because of influx and binding of Ca^{2+} to the dye. Lovat et al. [31] also demonstrated an increase in spontaneous postsynaptic currents in hippocampal neurons grown on a CNT substrate even when the neurons were randomly spaced apart on the substrate, suggesting that electric coupling had occurred between neurons and the CNTs. Similarly, Liopo et al. [38] demonstrated the direct stimulation of NG108 neuroblastoma and rat dorsal root ganglion cells grown on a SWNT-polyethylene terephtalate film, by an electrode that was attached to the film at a remote site. Gabay et al. [40] have shown that electrical signals can be transmitted in the opposite direction as well. The CNT-multielectrode array, made up of 60-80 μm diameter CNT islands, not only transmitted electrical signals from rat cortical cells grown on its surface, but also transmitted signals that could be recorded with high sensitivity.

The multiple functions of CNTs, such as being a biocompatible substrate, and electrical signal conductor and carrier of neural growth-promoting substances on their surfaces or within their cavities, may be important in neural tissue regeneration and/or stimulation, leading to their use as implantable prosthetic templates for the growth and support of neurites. As CNTs are not biodegradable, these scaffolds can be useful as implants in cases where long-term extracellular molecular triggers for neurite outgrowth are required. They could therefore be employed as an

extracellular scaffold to guide directed neurite outgrowth, the potential use of which is desirable after spinal cord or brain injury [34].

1.1.7   Encapsulation of molecules in CNTs

The unique enclosed nanochannels within CNTs make them potential nanofluidic delivery devices for pharmaceuticals, as well as protective structures for environmentally susceptible pharmaceuticals. Because of the size of CNTs and their propensity for cell entry/uptake, targeted delivery of CNT-ferried pharmaceuticals at the cellular level could be enhanced, and the discomfort associated with current intrusive techniques minimized. The first possible use of CNTs to protect therapeutic moieties is as structures to encapsulate the moiety within the CNTs. Shaitan et al. [44] modeled a non-immunogenic CNT nano-container, which encapsulated a bioactive peptide (pentadecapeptide and cholesterol) and an explosive agent. Once transplanted within a cell, an external trigger sets off the explosive agent, releasing the encapsulated peptide into the cytoplasm of the cell. Leonhardt et al. [45] proposed incorporating a ferromagnetic material, together with a therapeutic agent and a temperature sensor, into CNTs. This would allow for the manipulation of CNTs, using an external magnetic field and trigger, to destroy cancerous cells via hyperthermia.

The second possible use of CNTs is as structures for nanofluidic delivery of therapeutics. Table 1.3 summarizes studies of the type of pharmaceutically active molecule encapsulated, the diameter and type of CNT, and the conditions of encapsulation. One simple approach to fill nanotubes is to use capillarity forces [46-51].

Table 1.3   Encapsulation of molecules in CNTs

CNT	Diameter of CNT	Molecule/size of encapsulated entities	Conditions of encapsulation	Ref.
MWNT	10-20 nm	DNA	400K and 3 bar	[51]
SWNT	1-2 nm	DNA	"Plasma ion irradiation" of DNA electrolyte by applying direct current and radio frequency	[52]
SWNT	1.5 nm	RNA	Electrophoretic transport through cavity enhanced by changes in RNA conformations	[53]
MWNT	500 nm	Fluorescent-labeled beads/50 nm	Capillary inbibition of beads	[46]

However, to use the inner channels of CNTs for nanofluidic delivery, it is essential to understand capillary behavior at the nanoscale. First, the nanochannels must be sufficiently wet, i.e., have the ability for a liquid to spread along the walls of the nanotube. It is a direct reflection of the competitive cohesive forces within the liquid and the strength of interaction between the liquid and the CNT material [47, 48]. Second, surface tension of the filling fluid should be low enough to achieve wetting. For graphitic materials like CNTs, wetting is possible only if the surface tension at the fluid-CNT interface is less than a threshold value of 200 mN/m [47]. Beside the liquid wetting properties, certain structural properties of CNTs also influence capillarity. Molecular dynamics simulations and initial experimental results [47] both suggested that CNTs are hydrophobic. However, recent experimental results indicate that hydrothermal and CVD-synthesized CNTs are indeed hydrophilic, suggesting an increasing ease in wetting and hence capillarity. The efficiency of capillary imbibition was also established to be diameter dependent [54].

Cui et al. [51] reported the encapsulation of Pt-labeled DNA molecules in MWNTs (10-20 nm internal diameter) as depicted in Figure 1.3, *C*. However, encapsulation was achieved under rather extreme conditions (400K and 3 bar), which might not be suitable for most pharmaceutical compounds (Table 1.3). Hence, a better approach to encapsulation, rather than improved capillary action, would be more suitable in this application. Kaneko et al. [52] reported the encapsulation of DNA by "plasma ion irradiation," by applying direct current (DC) to an electrolytic solution of DNA in water. SWNTs were immobilized on the anode (aluminum support) and an applied DC drove the negatively charged DNA towards the anode. Encapsulation of DNA increased when a radio frequency field (RF) was simultaneously applied with the DC. The application of the RF changes the native random-coil structure of the DNA, to a stretched

form, thereby reducing its diameter. By compromising the nano-dimensions (i.e., increasing the diameter), 50-nm fluorescent-labeled polystyrene beads in ethylene glycol/water were encapsulated in 500-nm diameter CNTs by capillary action (Table 3) [46]. Using CNTs of similar dimensions, Nadarajan et al. [55] encapsulated 10-100 nm nanoparticles in a viscous solution by optimized centrifugation. However, nanofluidic delivery was greatly enhanced when a particulate driving mechanism was introduced. By using electrophoresis as a driving force, a charged nanoparticle (ssRNA) laden solution was shown to flow through 1.5-nm CNT nanochannels [53].

Measurements of the hydrophobicity of vertically aligned carbon nanotubes (VANTs) indicate that they are even more hydrophobic that individual CNTs [56], having been described as "superhydrophobic". The implication of such a property is the increased difficulty in wetting VANTs. However, by electro-wetting their superhydrophobicity is significantly reduced, which allows for wetting and reduced surface tension at the water-CNT (solid/liquid) interface, improving capillary imbibition [57].

From the foregoing, it is envisioned that CVD- and hydrothermal-synthesized CNTs, with large enough diameters, should imbibe and subsequently maintain consistent nanofluidic delivery. Alternatively, the rather prohibitive superhydrophobicity exhibited by an array of CNTs can be overcome by electro-wetting and subsequent use of the numerous nanochannels for nanofluidic delivery. Fluid flow through CNTs has been demonstrated to be much faster (four to five orders of magnitude greater) than conventional estimates suggest [50].

A novel system could be designed to deliver charged therapeutic molecules using a nano-dispensing system by taking advantage of diameter-selective encapsulation, coupled with electrophoresis and electro-wetting.

1.1.8 Toxicity of CNTs

Despite the widely demonstrated potential of CNTs in drug delivery, research indicates these particles can potentially cause adverse effects because of their small size and extreme aspect ratio(length-to-diameter ratio) [58]. The microscopic size and weight of CNTs allows for their easy distribution in the environment and human body. The general approach has been to consider and treat CNTs as toxic, since nano-sized particles are markedly more toxic than larger-sized particles. However, controversy surrounds the interpretation ascribed to CNT toxicity data. What is apparent however, is that toxicity is related to properties of the CNT material, such as their structure (SWNT vs. MWNT), length and aspect ratio, surface area, degree of aggregation, extent of oxidation, surface topology, bound functional group(s), and method of manufacturing (which can leave catalyst residues and produce impurities). Toxicity of CNTs is also related to their concentration and the dose to which cells or organisms are exposed [59].

1.2 Parameters of quality; Purity and quality of dispersions

The prospects of carbon CNTs as excipients in drug delivery has gained currency, mainly because of the high aspect ratio, ease attaching bioactive functional moieties to the external sidewalls via functionalization [1, 18, 20, 60-63], propensity to penetrate into cells, and the presence of an inner cavity that can be exploited for controlled nano-fluidic delivery [59, 64].

To this end, CNTs have been demonstrated as functional biomedical particles in for the *in vivo* delivery of proteins[11-18, 30, 63], DNA[16, 20-22, 65, 66]. The attachment of functional groups onto these biocompatible materials have allowed for their use centers of chiral recognition for the attachment of functional chiral moieties, which are subsequently used for molecular targeting [9, 24, 28, 66-68].

Even with the ongoing research into new and improved CNT synthetic techniques; there has been little improvement in the control of CNT quality, controlled chirality and diameter. CNTs obtained from different synthetic methods have different physical properties. The quality, quantity, and type of nanotubes synthesized depend on the synthetic method used. For example, CNTs from an electric arc-discharge (EAD) source have a higher Young's modulus and fewer defects than those from a CVD source. Hence, the choice of synthetic method is guided by the intended use of the CNTs. Invariably; the inherent reaction conditions will also have an effect on the product.

A major bottleneck bedeviling the CNT community is the lack of a standard for CNT quality analyses [69]. The disparity between reported purity of CNT (presence of CNT in sample) materials and those obtained from independent analyses [69, 70], and those reported by the suppliers From commercial sources) has been a long standing problem. Typically, commercial CNT from vendors are accompanied by what is described as product information sheets, purported to contain the quality analysis of the accompanying material (Table A1, Appendix A). These typically consist of a Raman spectrum and an electron micrograph (either by SEM/TEM) with the accompanying elemental analysis. It is now common practice to advertise CNT as >95 % purity when in deed the sample contains >95 % carbon content and not nanotube content. Since it is well accepted that neither Raman spectroscopy, electron microscopy, nor elemental analysis can by themselves or in combination with the others state the purity of the CNT material, this raises fundamental questions; How are the stated purity levels quoted by the vendors obtained, can the quoted purity levels be re-produced, and what do the various terminology of percentage of CNT, percentage of carbon, weight purity, volume purity, carbon content etc. represent?

Typically, excipient standards for pharmaceutical use are defined in the form of a monographs in the United States Pharmacopeia (USP) [71]. For excipients, the USP contains three major components; positive identification of the excipient, presence of impurities, and specialized assays [72]. The positive identification of the excipients pertains to a collation of both physical (boiling and melting points, dissolution, particle size, specific gravity, and chemical (molecular weight, chemical identifier) as well as organoleptic description (odour, colour etc). The monographs also include the identity of impurities (often residual starter materials in the synthesis). The tests also establish such parameters as the stability and dispersibility in routinely used pharmaceutical solvents. Often, a reference standard, with defined purity and impurity content, determined by standardized experimental procedures are established for purposes of calibration. Subsequent excipient samples/batches are evaluated against this standard.

However, with new pharmaceutical excipients such as CNTs, no such standards have been established yet. Despite the extensively reported use of CNTs in drug delivery research, and biomedical applications, the purity (quality) analysis has often been incomplete. It is therefore not surprising that contradictory reports have been published regarding the toxicity of pristine CNTs [73-77]. Lam et al. [74] ,Shvedova et al. [78] and Muller et al. [77] reported that CNTs possessed inherent toxicity whereas Warheit [76] et al. and Pulskamp et al [79] found otherwise. Pulskamp et al .[79], reported that oxidative stress due to the presence of remnant catalytic iron particles in the pristine SWNTs was responsible for the observed toxicity rather than an inherent property of the CNTs. Interestingly however, there appears to be a consensus that functionalization of CNTs with cationic moieties does improve their toxicity profile [80, 81].

Gao et al. [80] reported that toxicity of cationic f-CNTs is a function of CNT surface cation density. These observations indicate that soluble f-CNTs are biocompatible and exhibit a significantly improved toxicity profile than do pristine CNTs. The dichotomy in toxicity of pristine CNTs versus functionalized CNTs can be attributed to the size distribution of particles in the formulation. Pristine CNTs have a tendency to aggregate in aqueous solutions as a result of their hydrophobicity, resulting in increased cytotoxicity, whereas functionalization generally increases the solubility and hence dispersion of CNTs in solution, resulting in a reduced toxicity [81].

To the best of our knowledge, no CNT supplier has indicated a set of qualities that would make their nanotubes suitable for use as pharmaceutical excipients. For pharmaceutical applications, a set of parameters reflecting the purity, physical (diameter, length, chirality), chemical (surface defects, functional groups) properties and dispersion characteristics of CNTs, will have considerable impact on the biological fate of carbon nanotubes. A standard set of parameters and consistent protocols must be developed to evaluate these properties. Although various techniques have been used to characterize CNTs, there appears to be issues with reproducibility of the reported purity values. It is not surprising that the reported quality (percentage purity) of commercially available CNTs is contentious. The material safety data sheets that accompany CNT samples usually indicate the purity of CNTs (presumably obtained from qualitative electron microscopy techniques) and the diameter of material (estimated from Raman spectroscopy).

It would be ideal that CNT raw material for pharmaceutical applications have comparatively low carbonaceous impurities, and a more homogenous size and length distribution. Applying these criteria, CVD-synthesized CNTs would be the preferred choice of

synthetic method. However, removing the metallic catalyst residue is still required. CNT samples may contain a significant amount of other carbonaceous materials (graphite, amorphous carbon etc), as well as residual catalytic particles left over from the synthesis, and embedded within the CNT. To explore the use of CNTs in the pharmaceutical industry, high purity material is essential for pharmaceutical excipients.

1.2.1 Structure and Properties of Carbon nanotubes

Carbon nanotubes belong to the fullerene family of carbon allotropes. They are cylindrical molecules consisting of a hexagonal arrangement of sp^2-hybridized carbon atoms (C-C distance of ~1.4 Å). They are described as hollow cylinders formed by rolling single or multiple layers of graphene sheets into seamless cylinders [82]. These cylindrical structures have two forms: single-walled carbon nanotubes (SWNTs) and multi-walled carbon nanotubes (MWNTs). SWNTs are comprised of a single cylindrical graphene layer capped at both ends in a hemispherical arrangement of carbon networks (Figure 1.3). The closure of the cylinder results from the inclusion of pentagonal and heptagonal C-C structures during the growth process. MWNTs comprise several to tens of concentric cylinders of graphitic shells, each one forming a SWNT. MWNTs generally have a larger outer diameter (2.5-100 nm) than SWNTs (0.6-2.4 nm) and consist of a varying number of concentric SWNT layers, with an interlayer separation of ~0.34 nm. SWNTs have a better defined diameter, while MWNTs are more likely to have structural defects, resulting in a less stable nanostructure [83].

A

B

C

D

SWNT

Armchair (10, 10)

Zig-zag (10, 0)

Chiral (10,5)
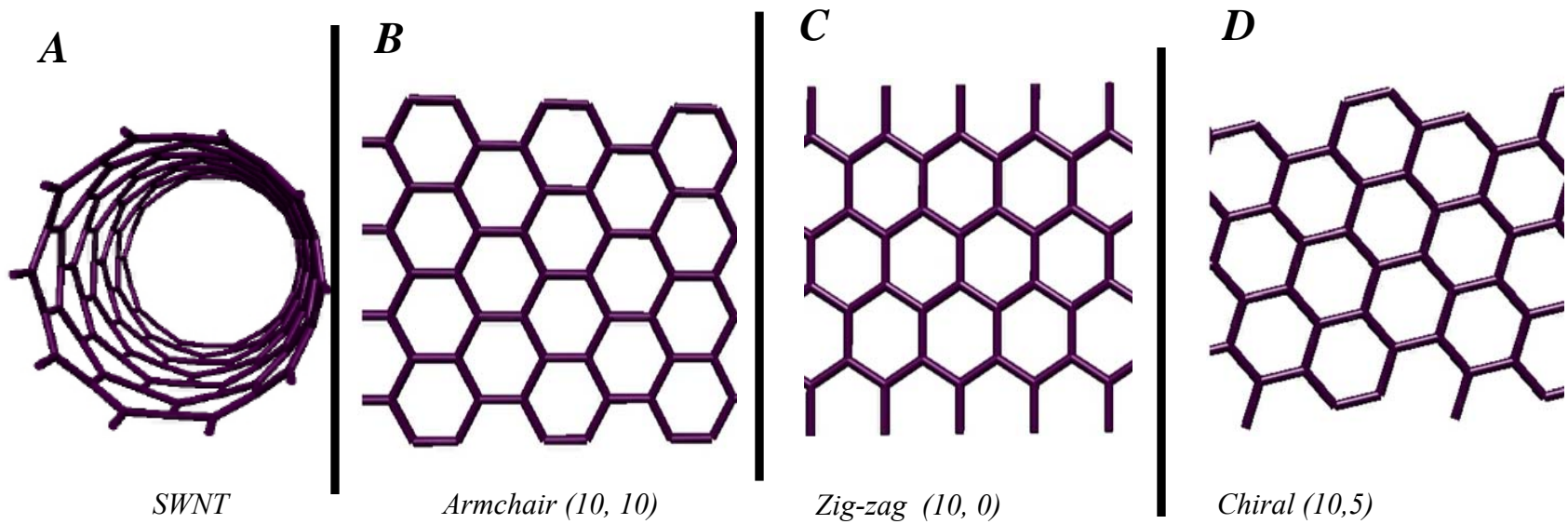
Figure 1.3 Computer-generated images of carbon nanostructures using Nanotube Modeler© 2005 from JCrystalSoft, showing the structures of (A) cylindrical shape of a single-walled carbon nanotube (SWNT) that can be obtained from the various orientation (conformations) of the graphene hexagons of (B) an armchair with chiral , (C) zig-zag, and (D) a chiral/helical.

CNTs combine high stiffness with resilience and the ability to buckle and collapse reversibly. The high C-C bond stiffness of the hexagonal network produces an axial Young's modulus (measure of the stiffness) of approximately 1 TPa and a tensile strength of 150 GPa [84], making CNTs one of the stiffest materials known, yet with the capacity to deform (buckle) elastically under compression [85].

SWNTs exist in a variety of structures, corresponding to the many ways a sheet of graphite can be rolled into a seamless tube (Figure 1.3 *B-D*)). This arrangement can make SWNTs behave as a well-defined metallic, semiconducting, or semi-metallic structure, depending on chirality and diameter.

The chirality of a SWNT is obtained from its chiral vector C which considers the arrangement of the graphite hexagons with respect to the SWNT axis and is completely defined by specifying a pair of two integer numbers *(n,m)* identifying the two components of C with respect to the lattice parameters of the graphene sheet. Examples of chiral vectors for the various configurations are defined along the illustrations in Figure 1.3. The armchair configuration has chiral vectors (*n,n*), are characterized by the perpendicular shape of the chair to the tube axis as in Figure 1.3 B, whiles the zigzag conformation is characterized by vectors (*n,0*), and have a V shape perpendicular to the tube axis as in Figure 1.3 C. The remaining SWNT (i.e. neither armchair nor zigzag), are described as chiral or helical, as depicted in Figure 1.3 D.

1.2.1.1 *Methods of production and expected quality issues*

Since the discovery of CNTs [86], research into new and improved CNT synthetic techniques has been toward improved yield, better CNT quality, and controlled chirality and diameter. The major synthetic approaches include electric arc-discharge (EAD), catalytic chemical vapor deposition (CVD), and laser ablation (LA) [87].

CNTs obtained from different synthetic methods have different physical properties. The quality, quantity, and type of nanotubes synthesized depend on the synthetic method used. For example, CNTs from an EAD source have a higher Young's modulus and fewer defects than those from a CVD source. Hence, the choice of synthetic method is guided by the intended use of the CNTs. Invariably, the inherent reaction conditions will also have an effect on the product. In the EAD set-up, a plasmon is generated across carbon electrodes, resulting in the deposition of CNTs on a substrate. In its original configuration, the anode was constructed from pure graphite, resulting in MWNTs as the main product. However, the incorporation of nanometer-sized metal catalysts in the anode material yielded SWNTs. The limitations of EAD are its inability to produce either SWNTs or MWNTs to the exclusion of the other, control over CNT diameter, the rather tangled/bundled nature of the products, and the presence of metal impurities. This necessitates difficult and time-intensive purification stages by chemical and thermal treatment [87, 88].

LA uses a laser beam to vaporize a graphite target mixed with a transition metal catalyst [89]. As with EAD, LA can yield both SWNTs and MWNTs. The introduction of a secondary laser improves the quality of CNTs by optimizing the vaporization of the target and minimizing the amount of carbon deposited as soot by the breakdown particles ablated by the primary laser [90]. The limitations of this technique are the narrow diameters of SWNTs produced, and the presence of tangled ropes and bundles along with graphitic particles, metals, and carbonaceous impurities.

Unlike LA and EAD, the feedstock in CVD synthesis is a vaporized hydrocarbon, typically mixed with an inert gas [91]. The feedstock is fed into a furnace where it decomposes, depositing CNTs onto a substrate. The substrate is prepared by embedding nanometer-sized

catalyst particles (e.g., nickel or cobalt) onto its surface [92, 93]. Various adaptations, such as plasma enhanced-CVD (PECVD) [94], thermal CVD (TCVD) [93], laser-assisted CVD (LACVD) [95], and high-pressure CVD (HiPco), have been made to the initial method [91]. CVD is currently the only method that allows for the direct synthesis and deposition of CNTs on patterned substrates and control of nanotube diameter [96].

Of the three synthetic approaches, CVD allows for more control over the morphology and structure of the produced nanotube, resulting in well-separated individual CNTs, either supported on flat substrates or suspended across trenches [97]. The length and diameter of CNT are controlled by the synthetic conditions. Whereas the length of both SWNT and MWNT (typically tens of microns) are controlled by the length of the synthetic time (the longer the time the longer the length), the diameter of SWNTs is controlled by the size of the catalyst, and typically 0.7-3.0 nm wide. For larger sized catalyst particles, SWNT fail to grow, and instead the larger diameter MWNTs are formed [98].

It is imperative that CNT purity for pharmaceutical applications have comparatively low carbonaceous impurities, and a more homogenous size and length distribution. Applying these criteria, CVD-synthesized CNTs would be the obvious choice of synthetic method. However, removing the metallic catalyst residue is still required.

1.2.2 Dispersion of CNTs in biocompatible media

The dispersion of carbon nanotubes (CNTs) in aqueous solvents is a pre-requisite for biocompatibility; hence the use of CNT composites in therapeutic delivery should meet this basic prerequisite. Similarly, it is important that such CNT dispersions be uniform and stable to obtain accurate concentration data. In this regard, the solubilization of pristine CNTs in aqueous

solvents remains an obstacle to the realization of their application potential, due to the rather hydrophobic nature of the graphene sidewalls, coupled with the strong π-π interactions between the individual tubes, causing the assembly to aggregate as bundles.

The current carbon nanotube synthetic approaches yield CNTs, together with carbonaceous and metallic impurities, as tangled and aggregated clusters. These clusters are not discernible to the eye and are observable only via high magnification. This tangled and aggregated morphology is attributed to the rather strong π-π interactions between the individual tubes causing them to aggregate, and their high aspect ratio (ratio of length to diameter of individual CNTs) resulting in an entangled mass.

The most widely used approach to obtain individual and smaller bundle sizes of these materials has often been achieved by exploiting the solution chemistry to overcome the strong attractive forces (either by chemical of physical functionalization of the sidewalls). For biomedical and pharmaceutical purposes, the use of common excipients and solvents routinely used in pharmaceutical formulations is of interest. In the same vein, it is equally important that the resultant dispersions in pharmaceutical solvents and/or dispersions are characterized in terms of stability and size of CNT in dispersion. The size/aggregation state of the dispersions has a direct consequence on the toxicological profile of these nanomaterials [99-101].

Kim et al. [102] classified CNT dispersions into two categories; macro-dispersions consisting of "dissolved" CNT bundles in solution, and nanodispersions consisting of "dissolved", exfoliated/individual CNTs in solution. Several publications estimate the amount of individual CNTs in a dispersions by the statistical comparison of the fraction of CNTs with diameters within the defined range of CNT diameters as a function of the CNT concentration [103-106].

To obtain CNT dispersions, four basic approaches have been used; covalent functionalization of CNT sidewalls, surfactant assisted dispersion, solvent dispersion and biomolecular dispersion [59].

1.2.3 Dispersion of CNTs via covalent functionalization

The covalent functionalization of CNTs results in the attachment of a desired functional group onto the sidewalls and/or tips of CNTs, often resulting in a break in the π–electron network. The most common approaches to functionalization involves strong acid treatment (resulting in carboxylic/ hydroxyl functional moieties) [107], fluorination [108] and amine [22] treatment. Chemical functionalization of these kind result in the introduction of hydrophilic sites on the hitherto hydrophobic CNT surface.

Chemical functionalization is perhaps the most efficient form of obtaining well dispersed CNT in aqueous solution due to the presence of polar functional groups on the CNT surfaces [16]. However, functionalization of CNTs is invariably accompanied by shortening of the CNT lengths and damage to the sidewalls [109].

Dispersion is achieved through the attenuation of the van der Waals forces between individual/bundles of CNT due to the introduction of functional groups on the surfaces. The most common functionalization approach is via carboxylation. In addition to improving the purity of CNT, carboxylation increases CNT dispersion by reducing the van der Waals forces between individual tubes, and bundles. However, the oxidation by acids introduces defects on the CNT walls (i.e. by disrupting the seamless graphene network), shortens the length of tubes, and invariably changes the intrinsic chemistry of the CNT.

1.2.4 Dispersion of CNTs via non-covalent methods

However, for the incorporation of CNT in pharmaceutical formulations, it is not only essential that these materials be exfoliated into individual CNT entities; the relative concentration of the exfoliated individual entities should be known. Table 1.4 below is a summary of the quantitative values reported for pristine CNT (i.e. this does not include pretreated acid purified/functionalized CNTs) dispersed in various solvents [104, 110, 111], surfactants [106, 112-122], and polymers [118, 122, 123]. The most common and frequently used dispersants for CNTs are surfactants. Of these, the anionic surfactants sodium dodecyl sulfate (SDS) [112-118, 122] and sodium dodecylbenzene sulfate (SDBS) [106, 113, 114, 117, 118, 122] are the most frequently used. Table 1.4 contains a summary of the quantitative dispersions of CNT in relevant pharmaceutical solvents/excipients.

Islam et al [124] were the first group to investigate the effect of surfactant type and concentration on the yield of exfoliated SWNTs. Dispersions were deemed suitable when no visible aggregates were observed. Of the surfactants investigated, only SDBS, SDS and Triton X-100 (polyethylene glycol p-(1,1,3,3-tetramethylbutyl)-phenyl ether)) showed dispersion of SWNTs at concentrations above 0.1 mg/mL. Using the height of particles in an AFM micrograph, the population of exfoliated SWNTs for SDBS, SDS and Triton X-100 were 74, 16 and 36 % respectively. The superior dispersing ability of SDBS and Triton X-100 to SDS is attributed to the presence of an aromatic moiety in its structure resulting in increased interaction with the graphitic SWNT surface. Similarly, SDBS disperses SWNT better that Triton X-100 due the presence of a longer alkyl chain (12 compared to 8), and a smaller headgroup. Shin et al. [112] investigated the effect of the chemical structure of surfactants (neutral, anionic and cationic) and concentration on the dispersion of SWNTs. They established optimum surfactant

concentrations for 0.04 mg/mL concentration of SWNT. The optimized surfactant concentration was established by qualitatively examining TEM micrographs, coupled with the presence of characteristic Van Hove transitions in the optical absorbance spectra due to the metallic and semiconducting SWNTs. The optimized surfactant concentrations of all surfactants were slightly greater than their respective critical micelle concentration (CMC) values, suggesting SWNT stabilization through the formation of hemimicelles structures, covering the surface of the SWNTs [118, 125]. The stability of dispersions is attributed to the strength of interaction of the surfactant with the graphitic surface of the SWNT, the length of alkyl chain in the surfactant, the head group size, and charge. Thus, the presence of an aromatic ring as in IGP (polyoxyethylene (100) nonylphenyl ether) results in the structure of the surfactant produces a superior dispersion, compared with an alkyl chain (SDS and CTAB). Similarly, the CTAB has a lower optimized concentration than SDS due to the presence of a longer alkyl chain. Sun et al. [113] studied the optimized surfactant concentration required to disperse 10 mg/mL SWNT (Table 1.4), by measuring the fraction of CNT remaining after centrifugation for a wide concentration range for each of the selected surfactants. Contrary to the previous findings [112], the optimized surfactant concentration in all cases was found to be close to 10 mg/mL. It is therefore not yet certain if the optimized concentration of surfactant for CNT dispersion is a function of concentration, surfactant type, or even CNT type.

Yoon et al. [115] developed a multi-step SWNT dispersion method which involves several centrifugation and steps (at different speeds). The extent of SWNT exfoliation was monitored by the intensity of a specific radial breathing mode (RBM) peak; while quantification of exfoliated SWNTs was by fluorescence spectroscopy.

Yurekli et al. [116] investigated the mechanism of SDS absorption onto SWNT surfaces using small angle neutron scattering (SANS). Their investigation suggested a structureless interaction since the SANS data neither pointed to the cylindrical micelle structure proposed , not the wormlike model proposed [112, 124].

Coleman's research group [106, 110, 111] have investigated the population/fraction of exfoliated SWNTs as determined by analyzing several frames of AFM images of SWNT dispersions. The major finding of this group is that ultracentrifugation is not required to obtain exfoliated SWNTs, and secondly, at the optimized sonication condition, the percentage of exfoliated SWNTs is a function of concentration.

Table 1.4   CNT dispersion, solubilization, debundling and stabilization by selected agents

CNT type	Dispersing Agent(s)	Solubility	Comment	Reference
SWNT (HiPCO)	SDS IGP*1 CTAB*2	0.0.87mM CO-990 in 0.12 mg/mL SWNT, 1.51 mM CTAB in 0.08 mg/mL SWNT, and 9.00 mM SDS in 0.16 mg/mL SWNT	Optimization of surfactant concentration and mass percent conversion of SWNT	[112]
SWNT (HiPCO)	SDBS, SDS, LDS*3, TTAB*4 SC*5	Optimized dispersions were obtained close to 10 mg/mL for all surfactants (1 mg/mL SWNT)	Statistical analysis of AFM micrographs to determine the aggregation state of each dispersion	[113]
SWNT (HiPCO)	SDBS, NaOBS, sodium benzoate SDS, sodium butylbenzene sulfonate, Triton X-100, DTAB*6; dextrin, PS-PEO	Maximum dispersion for SWNT; SDBS (20 mg/mL), SDS (0.5 mg/mL), Triton X-100 (0.8 mg/mL), All others less than 0.1 mg/mL	Determination of suitable surfactant: SWNT concentration ratios. Stability established by visual monitoring.	[124]
SWNT (HiPCO)	SDS	Maximum concentration of 26 mg/L ($\equiv$ 0.026 mg/mL) SWNT in 1 w/v % SDS.	Qualitative and quantitative exfoliation monitored by 267 cm^{-1} RBM peak intensity. and statistical analysis of AFM micrographs respectively.	[115]
SWNT (HiPCO)	SDS (in D_2O) at 0.1, 0.25 and 0.5 w/v %	7 mg/L (=0.7mg/100mL) 9 mg/L, 12 mg/L	Qualitative study of SDS-SWNT binding.	[116]
Purified SWNTs (HiPCO)	SDBS (5 mg/mL)	10 % mass dispersion at 0.06 mg/mL nominal dispersion	Max. partial conc. of individuals of ~0.006 mg/mL at a total concentration of ~0.07 mg/mL	[106]
SWNT	Encapsulation in poly(styrene)-block-polyacrylic acid copolymer	0.5g/L (0.05 g/100 mL= wt%) For polymer concentrations of 1- 10^{-4} mg/mL	Established by UV spec., using the $\varepsilon_{500} = 2.86 \times 10^{-14}$ g/cm^2	[123]
SWNT	N-methyl-2-pyrrolidone	0.02 mg/mL (=2mg or 0.002g/100 mL) i.e. below this conc. No	Fraction of dispersed SWNT obtained from the ratio of	[104]

		aggregates observed. At 0.004 mg/mL 70 % of all dispersed particles are individual nanotubes)	absorbance (650 nm) before and after centrifugation.	
SWNT (HiPCO)	The max. ratio (of 0.1 mg/mL SWNT :Surfactant) SDBS (1:10), SDS (1:10) SC[*5] (1:100), CTAT (1:1), CTAB[*2] (1:5)	Weight of SWNT (mg) in supernatant; SDBS (0.065), SDS (0.045), SC (0.025), CTAB (0.04), CTAT (0.04)	Quantification by UV, TGA. The subtraction method accounts for the non-dispersed impurity component of the SWNT	[117]
SWNT	γ-butyrolactone	0.004 mg/mL	Fraction of dispersed SWNT obtained from the ratio of absorbance (660 nm) before and after centrifugation	[110]
SWNT (HiPCO)	Anionic surfactants: SDS, SDSA, SDBS, Sarkosyl, TREM, PSS-70. Non ionic surfactants: Pluronic® surfactants (P103, P104, P105, F108, F98, F68, F127, F87, F77, F85), Brij 78 and 700, Tween 85, Triton X-405, and PVP-1300 Cationic surfactants: CTAB[*2], DTAB[*6]	Mass percent conversions of SDS (3.3 %), SDBS (3.9 %), SDSA (6.0 %), Sarkosyl (2.8 %) TREM (4.0 %), PSS-70 (4.7 %), P 103 (1.9 %), P 104 (3.0 %), P 105 (4.8 %), F 108 (8.7 %), F 98 (9.4 %) , F 68 (5.8 %), F 127 (7.1%) , F 87 (8.8 %) , F 77 (2.5 %), F 85 (0 %), Brij 78 (4.3 %), Brij 700 (6.4 %), Tween 85 (3.9 %), Triton X-405 (5.0 %), PVP-1300 (4.1 %) CTAB (5.1 %) DTAB (5.6 %)	0.3 mg/mL SWNTs in 200 mL of aqueous surfactant or polymer (2 wt %).	[118]
SWNT (HiPCO)	Triton X-100 in D_2O	Optimized dispersion at 0.1 mg SWNT in 0.5-1.0 % w/v (dispersed in D_2O)	SANS study of optimized surfactant concentration for dispersion.	[119]
MWNT (Shenzhen Nanotech Port Co. Ltd., China)	DTAB*[6] Hexyl-α,β,-bis(dodecyldimethylammonium bromide) ($C_{12}C_6C_{12}Br_2$)	Maximum dispersion for 2 mg/mL MWNT obtained at 2 and 30 mM for $C_{12}C_6C_{12}Br_2$ and DTAB respectively.	surfactant structure on the stability of carbon nanotubes in aqueous solution	[126]
MWNT	Pluronic F127 [*7]	180 µg/mL MWNT in 0.1 % Pluronic	Pretreatment by stirring at 70	[121]

(Nanothinx, Greece)		F127 from an [MWNT] of 0.5 mg/mL i.e. 36 % dispersion.	^{o}C before sonication. Concentration determined by UV spectroscopy	
SWNT (HiPCO)	hvimBr[*8], SDBS, SDS, CTAB	The optimized surfactant:SWNT ratio, and the respective dispersion are: SDS; (10:1) at 45%, SDBS (13:1) at 79 %, CTAB; (5:1) at 40 %, and hvimBr; (13:1) at 99 %.	Investigate the use of long chain ionic liquid for dispersion	[122]

[*1]- Polyoxyethylene (100) nonylphenyl ether

[*2] -Cetyltrimethylammonium bromide

[*3]- Lithium dodecyl sulfate

[*4] - Tetradecyl trimethyl ammonium bromide

[*5] - Sodium Cholate

[*6] - Dodecyltrimethylammonium bromide

[*7] - Polyoxyethylene-polyoxypropylene block copolymer

[*8] - 1-hexadecyl-3-vinylimidazolium bromide

1.2.4.1   Dispersion of CNTs via solvents

The most common approach to CNT processing requires its dispersion in a liquid medium [111]. However, due to the unique physicochemical properties of "as produced" CNTs such as high aspect ratio, bundled nature, and strong van der Waal's forces between individual tubes, the choice of a solvent, capable of debundling (breaking up aggregate tubes into individual tubes) the tubes has been under investigation. The most promising group of solvents for CNT dispersion are the amide containing solvents [111, 127-129].

Several authors attribute the ease of dispersion to the basicity (availability of a free electron pair) of the solvent, a low hydrogen bond donation parameter and a high solvatochromic parameter [127, 130], it has become evident that solvents such as dimethylsulfoxide (DMSO), which meet both of these parameters, have a rather low dispersion efficiency [129]. It is nonetheless agreed that even though these two parameters are a pre-requisite to the dispersion, they are by no means the sole contributors to dispersion.

In their investigation on the effect of electron pair donicity (β) of organic solvents in the production of stable nanodispersions of CNTs, Ausman et al.[127] concluded the presence of Lewis basicity (i.e. ability to donate a free electron pair) was the single most influential parameter in the production of a stable CNT dispersion. Consequently, the reported order of dispersion efficiency as determined by the optical density of the resultant dispersions was *N,N*-dimethylformamide (DMF)> *N*-methyl-2-pyrrolidone (NMP)> hexamethylphosphoramide> cyclopentanone > tetramethylene sulfoxide>caprolactone (oxypanone). The presence of a lone pair of electrons on the nitrogen of the amides (i.e. increasing the basicity) appears to aid the dispersion, while the less available lone pair of electrons on the oxygen atom of the ketones reduces their dispersion efficiency.

Landi et al. [129] studied the effect of amide solvent structure on their dispersion efficiency for five alkyl amide solvents; NMP, *N,N*-dimethylpropanamide (DMA), *N,N*-dimethylpropanamide (DMP), *N,N*-diethylacetamide (DEA) and DMF. The dispersions were prepared from 0.1 mg/mL stock solutions prepared by sonication at 38.5-40.5 kHz for 30 min at 40 °C, from which desired concentrations were obtained by serial dilution. Prior to determining the optical absorbance, each sample was centrifuged at 5000 rpm for 10 min prior to measurements. It was concluded that the dispersion was improved by increased CNT purity, optimized solvent geometry due to increased π-stacking (i.e. increased π-orbital overlap between amides and CNT sidewalls).

It was reported that the order of increasing dispersion efficiency DMA>DMP>DEA> DMF>NMP was attributed not just to the presence of a lone electron pairs, but an optimized geometry (bond lengths and bond angles) [129]. The maximum dispersion limit for these amide solvents as determined, using Beer's plots based on the presence of sediments after centrifugation, were DMF (1.56 μg/mL), DMA (6.25 μg/mL), DEA (3.13 μg/mL), DMP (3.13 μg/mL).

1.2.4.2   Surfactant dispersion of CNTs

Surfactants in general can be useful for dispersing CNTs, although the chemical structure of the surfactant is important. Moore et al. [131] and Ham et al. [130] have independently shown that the dispersibility by nonionic surfactants is a function of the hydrophobic alkyl chain length of the surfactant. Ham et al. [130] determined that if adequate dispersibility is to be achieved, an alkyl chain length greater than C10 was required, and that dispersibility increased with increasing alkyl chain length [130]. Moore et al. [131] determined that within a series of nonionic Pluronic® surfactants (P103, P104, P105, F108, F98, F68, F127, F87, F77, F85),

solubility (i.e. measured by UV spectroscopy of individually dispersed CNTs) generally increased with increasing molecular mass. The highest efficiency of solubilization was achieved with Pluronic® F108 (MW: 14,600) and F98 (MW: 13,000), where solubilities of 8.7 and 9.4 mg/L, respectively, were measured. These solubility levels were higher than those achieved by the other surfactants examined (Brij 78 and 700, Tween 85, Triton X-405, and PVP-1300). The higher molecular weight surfactants and polymers increased the solubility of CNTs through steric stabilization by adsorbed surfactant/polymer onto the walls of the CNTs, thereby impeding aggregation [132]. For ionic surfactant dispersion, Vaisman et al. [133] determined that the controlling factor for dispersion appears to be the charge of the head group, rather than the hydrophobic alkyl chain length.

The current limitations of surfactant-based solubilization are the relatively low levels of solubility and that the surfactant often remains as an impurity in downstream processes [133]. Nevertheless, this approach could be potentially useful in pharmaceutical applications, where surfactants are routinely incorporated in formulations for improved delivery.

1.2.5   Analytical techniques for characterizing CNT parameters of quality and dispersions

For pharmaceutical applications, a consistent protocol must be developed to evaluate the purity, dispersion, and physical and functional properties of CNTs. These properties include nanotube size and type, surface defects, electronic characteristics, mechanical strength, and thermal conductivity. Although various techniques have been used to characterize CNTs, there is no industry standard to evaluate the quality of produced CNTs. It is not surprising that the reported quality (percentage purity) of commercially available CNTs is contentious. The material safety data sheets that accompany CNT samples usually indicate the purity of CNTs (presumably

43

obtained from qualitative electron microscopy techniques) and the diameter of material (estimated from Raman spectroscopy).

Several techniques have been used to characterize the structure and morphology of CNTs, to determine the purity of CNT materials, and to establish the presence or absence of exogenously bound moieties onto the walls of CNTs. The most extensively used techniques are thermogravimetric analysis (TGA) [69, 134], scanning electron microscopy (SEM) [69, 135], transmission electron microscopy (TEM) [15, 46, 136], atomic force microscopy (AFM), Raman spectroscopy [69, 107, 137-139], infrared (IR) spectroscopy [69, 140], and nuclear magnetic resonance (NMR) [15, 141-143]. Whereas TEM, SEM, and AFM have been used predominantly to qualitatively establish the general morphology of CNTs, IR spectroscopy, Raman spectroscopy, and NMR have been used to confirm the presence of functional groups on CNTs. Each technique has advantages and disadvantages for purity evaluation and each is complementary to the others.

1.2.5.1   *Purity by electron microscopy and energy dispersive X-ray spectroscopy*

Transmission and scanning electron microscopy, are used in the preliminary evaluation of CNT morphology [69, 85]. It can be used as a qualitative confirmation for the presence of CNT, and carbonaceous material in the "as-produced" CNTs. These techniques are also used to evaluate the quality of CNT dispersions (extent of exfoliation into individual/small bundle sizes) [85]. The limitation of the EM imaging as a representative of the dispersion state is that the dried sample on a substrate is not representative of the dispersed state.

This technique is limited, however, by its inability to differentiate catalyst and carbonaceous impurities from CNTs [69]. However, coupled to an energy dispersive X-ray

spectroscopy (EDX/EDS), it is principally a qualitative tool for the elemental analysis of a sample. Another variation of this technique that could be employed for CNT analysis is the wavelength-dispersive x-ray analysis (WDX). This is often used in conjunction with SEM [144] and TEM for the morphological mapping of CNT surfaces (i.e. by SEM/TEM), and qualitative confirmation of the identity and location of residual catalysts in a CNT sample [144-154]. These techniques utilize the characteristic x-rays generated when a sample is bombarded with electrons, to identify the constituents of a sample. The peaks in the resultant spectrum are specific to certain x-ray lines, allowing for the identification of the constituent elements in a sample.

EDX/WDA will be used to identify the residual catalysts materials in each CNT sample. This is important as the presence of residual ferromagnetic particles in CNT samples, could significantly affect their magnetic susceptibility.

1.2.5.2   *Purity of CNTs by thermogravimetric analysis*

As produced CNT samples are often accompanied by significant amounts of other carbon allotropes (graphite, soot, spherical fullerenes), and residual catalytic impurities. TGA relies on the differences in oxidative temperature of the various allotropes of carbon, and the catalytic impurities, to establish a definitive quantitative amount of either CNT type [69].

However, significant variations in TGA traces, from samples of the same batch suggest a wide variation and difficulty in obtaining reproducibility. Even though this has been attributed to CNT heterogeneity, a relatively high number of repeats (>3), each requiring a significant amount of CNT material (~20-100 mg) will be required to establish a representative purity values.

1.2.5.3   Purity and dispersion quality by Raman spectroscopy

Raman spectroscopy has been used to evaluate the synthesis and purification processes of SWNTs. Carbonaceous impurities (graphite, spherical fullerenes, amorphous carbon, etc.) present a major obstacle in interpreting Raman spectra of SWNTs, as these impurities have characteristic Raman features (D- and G-bands) identical to that of SWNTs. A typical Raman spectrum of SWNTs has three intense bands. The low-energy vibrational band (100–400 cm^{-1}) results from the radial movement of carbon atoms, resulting in the expansion and contraction of SWNT diameter [137, 138], hence the name radial breathing mode (RBM). For SWNT samples from an identical source, the frequency of the RBM peak is inversely proportional to tube diameter. Typically, the RBM and electron microscopy data are complementary in determining tube diameter. As only the Raman spectra of SWNTs show the RBM peak, the presence of such can be used to distinguish SWNT samples from all other carbonaceous materials.

The mid-energy vibrational band (D-band, ~1300-1400 cm^{-1}) is a disorder-induced band, characteristic to all graphitic material. In SWNT samples, it is indicative of both the presence of defective sites on the SWNT (including functional attachments) and carbonaceous impurities. Similarly, the presence of functional groups on the walls of the SWNT is inferred from the D-band [137]. The third band (G-band, ~1500-1600 cm^{-1}) is a tangential vibrational mode, characteristic to all graphitic material. The ratio of intensities of the D-band (I_D) to G-band (I_G) is often used as an estimate of carbonaceous-impurity content and defect-site density [139]. Raman

spectroscopy is the most widely used tool in characterizing SWNT quality, even though it is unable to detect metallic impurities in a sample. It is often used as a complementary technique to electron microscopy.

A shift in peak position is generally observed for both the RBM and the G-band when CNTs disperse. The binding of the dispersing agent to the CNT results in an increase in the elastic constant of the harmonic oscillator of the coated CNT, thus increasing the energy required for vibration to occur, and thus an upward shift in the frequency of the band. One distinguishing difference between a covalently attachment, and a non-covalently attachment, is in the intensity ratio of the D band (I_D) and the G band (I_G). Generally, a shift in peak is indicative of an interactive force between the dispersing agent, and the SWNT. However, shifts in peaks are also accompanied by a simultaneous decrease in D band intensity (I_D) and an increase in G band intensity (I_G). Covalent modifications to the sidewalls are characterized by a significant change in the D band and I_G/I_D ratio compared to the values obtained from pristine SWNT from the same batch [109, 155, 156].

1.2.5.4   *Dispersion quality by light microscopy*

This is the first technique in qualitatively evaluating dispersion quality. It enables the qualitative determination of the degree of macro-dispersion under an optical microscope. The presence of visible precipitates will be an indicator of non-dispersion. This will be used to evaluate the efficiency of the centrifugation method. However, the presence and or extent of smaller sizes aggregates in the nano-range (<200 nm) can not be established by this technique.

1.2.5.5   *Dispersion quality by particle size and zeta potential*

The length distribution of nanotubes in solution has been measured within hydrodynamic approximations by using dynamic and static laser light scattering (DLS/SLS) [109, 157-160].

DLS provides information for length distribution, whereas electrophoretic light scattering (ELS) generates the zeta potential, which provides information for the stability of ionic surfactant aided dispersions [85, 109, 159, 161].

Zeta potential measurements of nano-dispersions are based on the well known Derjaguin-Landau-Verwey-Overbeek (DLVO) theory. The DLVO theory states that the stability of a colloidal system is determined by the sum of these van der Waals attractive and electrical double layer repulsive forces that exist between particles as they approach each other due to the Brownian motion. It is postulated that the adsorption of ionic surfactants onto CNTs imparts a net charge on the surfactant-CNT composite. Consequently, a more diffuse layer of surfactant counter ions engulfs the composite, resulting in an electrical double layer, thus leading to colloidal stabilization via electrostatic repulsion.

In a CNT-surfactant composite, the mechanism of stabilization will be by steric repulsion (surfactant absorbed onto the surface of the CNT and preventing the individual CNTs coming into close contact). The use of DLS for the estimation of size for non-spherical particles is not necessarily valid due to the hydrodynamic approximations introduced. However, in combination with zeta potential measurements, the nano-/micro-dispersion sizes (measure over time), will explain stability i.e. as particles aggregate, the mass of the aggregates increase, resulting in slower movement and hence smaller zeta potential, whereas the presence of sufficient charge, particles tend to repel each other, preventing aggregation, and hence larger zeta potential [159].

1.2.5.6 *Dispersion quality by ultraviolet (UV) and photoluminescence spectroscopy*

Dispersed CNTs are UV active because of their conjugated systems. Their concentration in solution, therefore, can be determined by Beer's law, where a higher absorbance is obtained for dispersed CNTs in a solution than for an equivalent non-dispersed solution. In larger clusters

(bundles) of CNTs, however, the apparent absorption coefficients tend to decrease because of the similarity in size of CNTs to the wavelength of light [162, 163]. This has been used to evaluate the dispersion efficiency of various dispersing agents and conditions [130, 162-164], CNT dispersion stability over time [130], and the effect of SWNT diameter on dispersion [165]. The UV absorbance of the dispersion increases as exfoliation of bundles into individual tubes progresses, reaching a constant maximum value as the exfoliation process attains an equilibrium [132].

The use of photoluminescence (PL) spectroscopy in determining the amount of exfoliation into individual CNT robes relies on the distinct difference in the amount of PL of single tubes (isolated tubes), and aggregated bundles [166-169]. Semiconducting SWNTs, which statistically constitute 66.7 % of any SWNT sample, are direct bandgap semiconductors and hence photoluminescence arising from the recombination of electron-hole pairs is expected [168, 170]. The presence a metallic SWNT (either as an individual tube or within bundle) quenches the electronic excitation from adjacent semiconducting SWNTs, significantly reducing photoluminescence [166, 171].

A limitation of PL lies in the ability of aggregates of the SWNT in solution to quench the PL. Ultracentrifugation of the dispersed SWNT solution has been reported to increase the PL yield [171]. Therefore PL may provide a unique quantitative method for the evaluation of the dispersion efficiency of SWNT in the selected pharmaceutical excipients.

1.2.6   **Research issues**

      The effective application of CNTs as pharmaceutical and biomedical functional materials hinges on the effective control of the purity and aggregate (particle size) control. The efficacy and toxicity profile of a pharmaceutical excipient is largely controlled by the purity of the materials, particularly for nanoparticles. Two major research questions will be addressed in this work; purity of SWNTs, and dispersion in pharmaceutical agents.

2.0   HYPOTHESIS AND OBJECTIVES

2.1   Aims and hypothesis

The use of CNTs as excipients in pharmaceutical delivery will require the development of a set of quality control criteria including purity analysis and dispersibility in aqueous solutions. The difficulty of the solubilization of pristine CNTs in aqueous solvents is a potential obstacle to realizing their application as excipients, due to the rather hydrophobic character of the graphene sidewalls, coupled with the strong π-π interactions between the individual tubes, causing CNTs to aggregate as bundles. It is particularly necessary to understand the properties of CNTs in aqueous media in the presence of pharmaceutical dispersing agents that may be used to prepare exfoliated monodispersed SWNTs. The aim of the project is two-fold; to characterize the purity of selected commercially available CNT ("as produced" materials) and, to characterize the dispersibility of selected SWNTs prepared using pharmaceutically relevant surfactants and solvents. These objectives will rely on the suitability of Raman and UV spectroscopy, dynamic light scattering and zeta potential as quantitative analytical methods to describe the dispersions and characterization of CNTs.

It is hypothesized that selected pharmaceutical surfactants and solvents will be suitable to produce dispersed SWNTs in aqueous media by sonication. However, dispersibility could be dependent on the original purity of the starting CNT raw material.

2.2   Specific Objectives

The specific objectives of the research will include

51

2.2.1 Purity evaluation of commercial SWNT and selection of SWNT for further studies

i.   Comparative purity analysis of six SWNT samples by Raman spectroscopy. A comparison of the RBM peaks will be used to evaluate the diameter distribution of SWNT samples, while the ratio of the G/D peak intensities, will be used to determine the purity (i.e. SWNT content) of SWNTs.

ii.   Evaluation of the dispersion efficiency of selected pharmaceutical solvents and surfactants for a chosen SWNT sample.

iii.   Determine the relation between purity and dispersion efficiency of commercial SWNT samples for a selected dispersion medium.

2.2.2 Physicochemical characterization of SWNT dispersions

The physicochemical characterization of SWNT dispersion will entail the development and optimization of a dispersion method and a quantitative analytical method; First, a method will be developed for the dispersion of one SWNT in a surfactant solution previously described in the literature (1% w/v SDS) by optimizing the conditions of sonication, centrifugation and surfactant concentration. Specifically,

i.   Determine the length of sonication required for maximum dispersion (no further change in UV absorbance) of a selected SWNT sample

ii.   Determine the optimum centrifugal force and centrifugation time required to separate impurities and aggregated nanotubes from dispersed nanotubes

iii.   Select pharmaceutical surfactants and solvents that have potential as dispersing agents based on their biocompatibility, ionization state, HLB and polarity of the solvents (see Table 3.1).

Table 2.1 Panel of potential pharmaceutically relevant solvents and surfactants for initial screening.

Solvent / Surfactant	Physicochemical properties		
	MW (gmol^{-1}) *[1]	HLB*[2]	CMC (mM)
Solvents			
Ethanol (100%)	46.07		
Propylene glycol	76.09		
Dimethylsulfoxide	78.13		
PEG 300	190 - 210		
Glycerol	92.0		
Anionic surfactants:			
SDS	288.4	40	8.1
Monocationic surfactants			
Benzalkonium Chloride	424.2		5.0
Bis-cationic surfactants			
12-2-12 gemini surfactant	614.7		0.89 ± 0.04 [172]
12-3-12 gemini surfactant	628.7		0.98 ± 0.04 [172]
12-7-12 gemini surfactant	684.8		0.85 ± 0.07 [173]
12-16-12 gemini surfactant	754.9		0.12 ± 0.01 [172]
16-3-16 gemini surfactant	740.8		0.026 ± 0.001 [174]
18-3-18 gemini surfactant	797.0		0.013 ± 0.001 [173]
Neutral surfactants			
Poloxamer 188	8,400	>20	8.33
Poloxamer 338	14,600	>20	
Poloxamer 407	12,600	>20	0.079
Tween 20	1227.5	16.7	0.050
Tween 60	1311.7	14.9	0.021
Tween 80	1310	15.0	0.010
Span 20	346.5	8.6	0.025
Span 40	402.6	6.7	0.010
Span 60	430.6	4.7	0.009
Triton X-100	625	13.5	0.241
Myrj 52	2043	16.9	N/A

▓   - No data available

NOTE: HLB values are only relevant for non-ionic surfactants, whiles CMC values are relevant for ionic surfactants only.

* MW – Molecular weight of solvent molecules and surfactants were take from Ref [175]

3.0   MATERIAL AND METHODS

3.1   Evaluation of CNT samples for magnetic susceptibility

Both SWNTs (AP-SWNT, P3-SWNT, CT1-SWNT) and MWNTs (MWNT-15, MWNT-40 and MWNT-50) were evaluated for their magnetic susceptibility. Subsequently, only the responsive CNT sample was used for magnetophoresis, using a magnetic field created by an electromagnet.

3.1.1   Materials and Methods I – Magnetic susceptibility

Six samples of CNTs were evaluated in the first batch of experiments; three being SWNT and three being multi-walled carbon nanotubes (MWNT). For the single-walled carbon nanotubes, AP-SWNT (Batch # 155) and P3-SWNT were purchased from Carbon Solutions Inc, whiles CT1-SWNT from CheapTubes Inc. P3-SWNT is described as carboxylated SWNTs, and hence soluble in deionized water. The MWNT samples of MWNT15 (external diameter <15 nm) MWNT40 (external diameter <40 nm) and MWNT50 (external diameter >50 nm) were all purchased from CheapTubes Inc (See Appendix A for quality details).

To evaluate the magnetic susceptibility of the CNT samples, a 0.1 mg/mL dispersion of the CNT was dispersed in deionized water (without sonication). The samples were then placed on a magnetic stirrer (Auto Mixer, Fisher Scientific), and allowed to settle prior to turning on the magnetic stirrer. When the magnetic stirrer was turned on, a rotating magnetic field was generated. The rotating magnetic field caused the responsive CNT samples to be agitated/moved, while no movement was observed for non-responsive CNT samples. Using this technique, AP-SWNT was the only sample observed to be responsive. This was subsequently used to evaluate

the efficiency of the spearing of intact *SC* by these CNTs, under the influence of a magnetic force.

3.1.2   Materials and Methods II – SWNT magnetophoresis of stratum corneum

Stratum corneum (*SC)* was harvested from excised human skin using the method described in Appendix C. *SC* was then sandwiched between two layers of parafilm, with a window cut into one side of the parafilm, exposing the *SC* (the exposed outer layer of the *SC*, usually exposed to the elements is oriented to be exposed in the window). A model non-porous lipophilic synthetic material, Silastic membrane (SM) was also used.

The sandwiched *SC*-parafilm is then fastened onto the top of a 20 mL glass vial (Kimble®), containing 0.1 mg/mL dispersion of SWNT in deionized water. With the *SC* securely held in place, the container is then introduced into the cavity between the two poles of an Electron Spin Resonance (ESR) Spectrometer (Bruker EMX EPR Spectrometer, equipped with Win-EPR software) for 5 minutes (Fig. 3.1). The effect of the generated magnetic field strengths on the efficiency of magnetophoresis was evaluated by exposing the membranes to two different magnetic field strengths ; 5000 and 9800 G, each with a sweep width of 100 G. After exposure to the magnetic field, the vial was removed, and the membranes (*SC* and parafilm) carefully removed and dried in a desiccator for SEM analysis. To better observe the nanosized channels created under the influence of the magnetic field, the above set-up was repeated using parafilm as the membrane, rather than *SC*.

The surface of the CNT treated *SC* and parafilm were examined for pores and location of CNT bundles by scanning electron microscopy (SEM) using a Leo FE-SEM at the WatLabs (University of Waterloo).
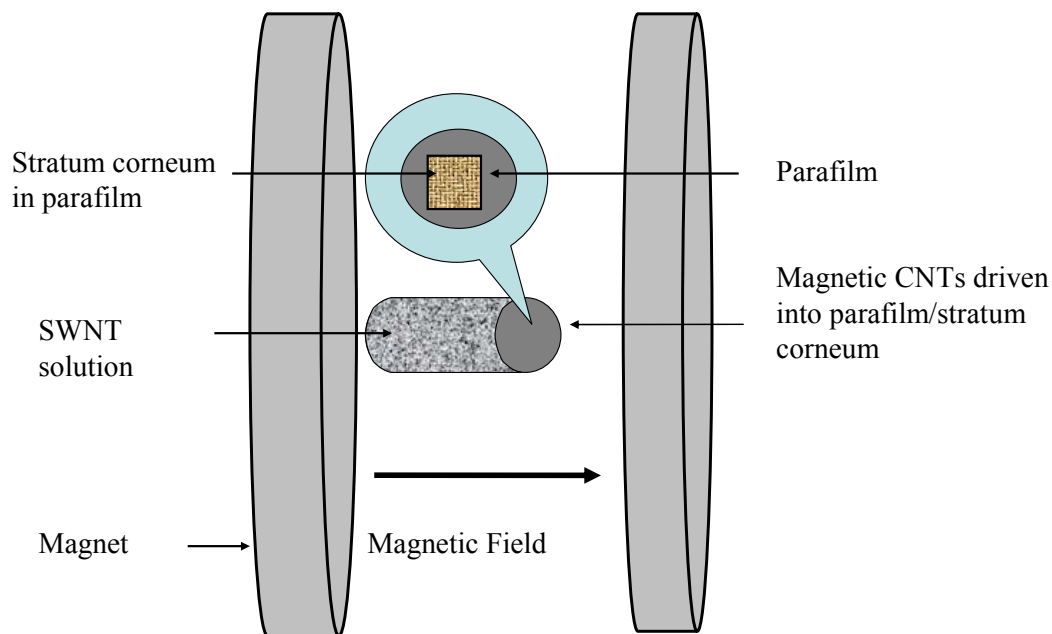
Figure 3.1   Schematic representation of magnetically responsive CNTs driven into stratum corneum (sandwiched between two layers of parafilm) under the influence of a varying magnetic field strength using the magnetic field generated between the poles of an Electron Spin Resonance Spectrometer (Bruker EMX EPR Spectrometer)

3.2 Materials and methods- Evaluation of SWNTs quality

Five of highest quality (as described by the suppliers) SWNT were purchased from commercial source, and analyzed by Raman and electron dispersive x-ray spectroscopy (EDS). These SWNT samples are; AP-SWNT and P2-SWNT, from Carbon Solutions Inc, HMS-SWNT from Helix Materials, and NA-SWNT from Nanostructured and Amorphous Materials Inc. (See Table 5.1 for purity details).

3.2.1 Raman spectroscopy –Purity of SWNT

The purity of as-received SWNTs samples were determined on a Renishaw system 2000 equipped with a 784 nm laser. A 10-40 mg portion of each SWNT sample was transferred into a clean aluminum sample pans (Perkin Elmer). Generally, the laser beam was focused on the sample with a 5 X objective of the Raman microscope. To obtain relatively high signal to noise ratio (*S/N*), 10 scan accumulations, with each scan collected for 10 seconds. The Raman spectral peaks were calibrated using a silicon peak position of 520 cm^{-1}.

3.2.2 Qualitative EDX Analysis of SWNT Samples

About 5mg of each SWNT sample was surface mounted to glass thin-section slides using conductive double sided carbon tape, followed by the application of carbon emulsion paint between the glass slide and sample holder to maintain electrical contact.

Analysis of the mounted samples were conducted on a JEOL 8600 Superprobe electron microprobe analyzer (EMPA) operating at an accelerator voltage of 15 kV and a focused beam at a current of 10 nanoamps. By scanning over the surface of the samples, impurities are identified in backscattered electron imaging configuration at a raster area of ~ 0.4 mm. This method of

imaging causes particles composed of elements heavier than carbon to appear brighter than the CNT on the monitor. Once identified, these particles were analyzed qualitatively using energy dispersive spectrometry (EDS) to determine their chemical composition.

3.3 Dispersion in selected pharmaceutical solvents - Materials and methods

P2-SWNT was used for the initial evaluation of dispersion of selected pharmaceutical solvents. All the surfactants were NF quality (See Table 5.5), purchased from Spectrum except for gemini surfactants which were synthesized in our research group [172, 173] . AP-SWNT was used without further purification.

P2-SWNT dispersion were prepared by adding a 0.10 % $^w/_v$ of ionic and non-ionic surfactants in de-ionized water (nominal resistivity greater than 18.0 MΩ cm) and in various pharmaceutically relevant solvents to the appropriate amount of P2-SWNT to obtain a SWNT concentration of 0.1 mg/mL. The dispersions were sonicated at low power (50 kHz) for 24 hours on a Branson 5210 waterbath sonicator (Branson Ultrasonics) at 25 ^{o}C. For the optimization of the excipient concentration for dispersing 0.1 mg/mL of SWNT, several concentrations of the excipient (the gemini surfactant 12-3-12) was used in the method development. After sonication, the dispersions were centrifuged on an Allegra™ 25R centrifuge (Beckman Coulter).

SWNT stability of the SWNT dispersions was evaluated by UV spectroscopy. Zeta (ζ) potential measurements, dynamic light scattering (DLS), Raman spectroscopy, optical microscopy, and scanning electron microscopy (SEM).

The extent of exfoliation into individual/smaller bundled tubes, and stability of the SWNT dispersions were monitored by UV spectroscopy, optical microscopy, and scanning electron microscopy (SEM), and Raman spectroscopy.

For dispersion in ionic surfactants, the stability (i.e. ability of SWNT to remain in dispersing medium without phase separating) of the dispersion was monitored by zeta (ζ) potential measurements, while the particle size distribution of all dispersions was obtained by dynamic light scattering (DLS). Raman spectroscopy, was again used to ascertain the exfoliation if dispersed samples.

3.3.1 Microscopy

Optical Microscopy - For optical imaging, 50 µL of the dispersion was carefully drawn using and dipped on a glass slide to settle. Images were taken at a 40X magnification on a Reichert (Microstar IV) microscope, fitted with an Olympus (Q Color 5 RTV) camera and software.

Scanning Electron Microscopy (SEM) micrographs were taken using a using a LEO 1530 FE-SEM (Zeiss). SEM samples were prepared by transferring 5 µL of dispersed SWNTs onto pre-heated (~150°C) silicon substrates.

3.3.2 Particle size and zeta potential

Carbon nanotube dispersion size and zeta potential measurements were carried out on a Malvern NanoZS instrument (Malvern Instruments, Worcestershire, UK) equipped with a 633 nm He-Ne laser. The system was calibrated for size measurements using Nanosphere[TM] (Duke Scientific Corporation) standards of mean diameter of 60 nm ± 2.5 nm, whiles ζ-potential transfer standard (Malvern, DTS1050); -50 ± 5 mV was used for used for ζ-potential calibrations.

Size and ζ-potential measurements were performed by transferring ~800 μL of dispersion into a clear disposable folded capillary cell (Malvern, DTS 1060) at 25 °C and at the natural pH of the dispersing medium. The zeta potential was obtained using by laser Doppler microelectrophoresis at a frequency of 1000 Hz, while particle size (electrophoretic diameter) was obtained using the Non-Negative Least Squares (NNLS) algorithm to distinguish between particle size populations. Zeta potential data was fitted using Smoluchowski approximation and reported as intensity distribution. Each data point was automatically repeated in quadruplets, with the average reported.

3.3.3   Raman spectroscopy – Evaluation of dispersion

The dispersion characterization by Raman spectroscopy was carried out on a Renishaw system 2000 equipped with a 784 nm laser. The dispersed sample (200 μL) was transferred into a clean aluminum sample pans (Perkin Elmer). All measurements were taken at room temperature, and for each sample the Raman data were collected at different light spots on the sample surface. Generally, the laser beam was focused on the sample with a 40 X objective of the Raman microscope. To obtain relatively high signal to noise ratio (S/N), 20 scan accumulations, with each scan collected for 10 seconds. The Raman spectral peaks were calibrated using a silicon peak position of 520 cm^{-1}.

3.3.4   Ultraviolet (UV) spectroscopy

UV absorption measurements were taken using an Agilent 8453 UV-VIS spectrophotometer at λ=500 nm. The UV absorbance spectrum at 500 nm is relatively unaffected

by CNTs conditions (such as charge transfer between CNTs and dispersing agents) and has been used to estimate NTs dissolved in solutions [109, 128, 176, 177] .

The wavelength was selected as dispersed CNT absorbance values followed the Beer-Lambert law, and more significantly, the absorbance values are unaffected by ambient conditions [109, 176-179]. One (1.0) mL of the SWNT dispersions was transferred into a quartz cuvette, with a path length of 1 cm. A blank sample of the dispersing agent (surfactant or solvent) was used as a reference for background correction.

To monitor the exfoliation of CNTs in various dispersion solutions, 1.0 mL of the dispersion was withdrawn at set time intervals and the UV absorbance measured as above. Similarly, to evaluate the process of centrifugation, 1 mL aliquots of the supernatant (after centrifugation) were measured similarly.

4.0　　RESULTS AND DISCUSSION

4.1　　Magnetic Carbon nanotubes in *Stratum Corneum*

An initial research objective was based on the immobilization of magnetically driven SWNT, as drug delivery nanoparticles, into *stratum corneum* (*SC*). Our preliminary investigation showed that the CNT aggregated as non-dispersed clusters on the surface of the *SC*, with no observable damage to the *SC*. Hence to achieve our initially set goal, it is paramount that CNTs are dispersed in an appropriate medium prior to magnetophoresis.

4.1.1　　Results and discussion – Magnetic susceptibility and magnetophoresis of SWNT on *Stratum Corneum*

The initial experimental design was to use the magnetic field generated by an electromagnetic (EPR machine) to drive CNTs into *SC*. By modulating the magnetic field, aggregates of the magnetically responsive SWNTs were observed to migrate in a set direction, with the target membrane (*SC* and parafilm) immobilized perpendicularly against the direction of CNT magnetophoretic movement.

AP-SWNT, P2-SWNT and P3-SWNT were magnetically susceptible owing to their observed movement when their dispersions were exposed to a magnetic field. The source of such magnetism susceptibility can be attributed to one of two sources. The first and most often cited source is from remnants of catalytic superparamagnetic particles often used in the synthesis of SWNTs [180-185]. These nested (at the tip of SWNTs) paramagnetic nanoparticles have in inherent magnetic susceptibility, resulting in a response to magnetophoretic force [180, 184, 186-189], dragging the SWNTs with them . The second source of magnetic susceptibility is suspected to arise from structural defects in carbon based nanoparticles in general [190], and the inherent

paramagnetism of carbon nanotubes [191, 192]. Exposing these paramagnetic materials to a strong magnetic field, such as that generated in the EPR magnet, can result in observed magnetic susceptibity. Following the treatment of SC and parafilm by magnetophoresis, the now "treated" *SC* pieces were retrieved and surface examined by SEM for the presence of SWNT aggregates, and any resulting nanochannels/pores that would have been created by magnetophoresis.

In the experimental design, two magnetic field strengths were selected (5000 G and 9,800 G), and the magnetophoretic migration of AP-SWNT and P3-SWNT (dispersed in deionized water) towards immobilized *SC* and parafilm. The maximum field strength generated by the EPR machine was 10,000 G. By modulating the field strength at either setting by 200 G, the magnetic field created generates a magnetophoretic force, resulting in the movement of aggregated/clusters of SWNT. In the aggregated CNT dispersion (i.e. CNT in deionized water), magnetophoresis [193, 194] was inferred from the movement of the aggregates in a set direction, stopped only by the membrane cap. These visible aggregates were observed to completely migrate onto the surface of the membranes in less than 5 minutes. Hence, the time of exposure to the magnetic field was set at 5 minutes.

The SEM micrographs performed with AP-SWNT dispersed in deionized water are shown in Figure 4.1. SEM images of the control *SC* (no SWNT treatment) treated *SC*, and treated silastic membrane. As expected, the control *SC* sample shows no visible pores (Fig. 4.1 A), confirming an intact piece of *SC*. An examination of the AP-SWNT (Figure 4.1 B) and P3-SWNT (Figure 4.1 *C* and *D*) treated *SC* samples showed no visible pores on the surface of the *SC*. However, as the SWNT were dispersed in deionized water, these persisted in the dispersions as aggregates, which aggregates were observed as clusters on the surface of the *SC*.

In portions of the P3-SWNT treated *SC*, smaller clusters of SWNT were observed on the *SC* (Figure 4.1 *D*), however, the non-rigid nature of SWNTs imply that these clusters tend to coil upon contact with the *SC*, rather than penetrate the membrane. A similar trend is observed when a silastic membrane (Figure 4.1 *E* and *F*) is used instead of *SC*. However, dark spots appear on the membrane which were absent from the control sample.

The investigation into the use CNT created nano-channels on *SC*, under the influence of a magnetic force under the current experimental set-up did not appear feasible for the following reasons. Firstly, to successfully create individual nano-channels on the stratum corneum via spearing of the individual CNTs, it is imperative to obtain a nano-dispersion (CNTs as individual strands, or smaller bundle sizes). Secondly, this could be due to one of several reasons; the magnetic properties of the CNT are too weak to be driven by a magnetic force of the order of 1 tesla (10,000 G), and/or the magnetic field strength of 1 tesla is too weak to cause any observable damage to the stratum corneum.

To address the issue of aggregated SWNT observed on the *SC*, it is necessary to disperse SWNT in an appropriate media prior to magnetophoresis across the *SC*. The successful and reproducible dispersion of SWNT in selected pharmaceutical solvents will address issues such as SWNT purity, an optimized SWNT and surfactant concentration, optimized dispersion conditions, and a characterization of the dispersion (stability and size distribution). To this end, the specific objectives of the research were subsequently modified to reflect this.

65
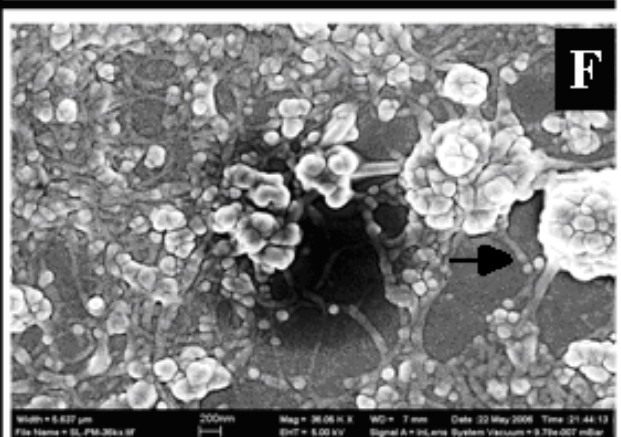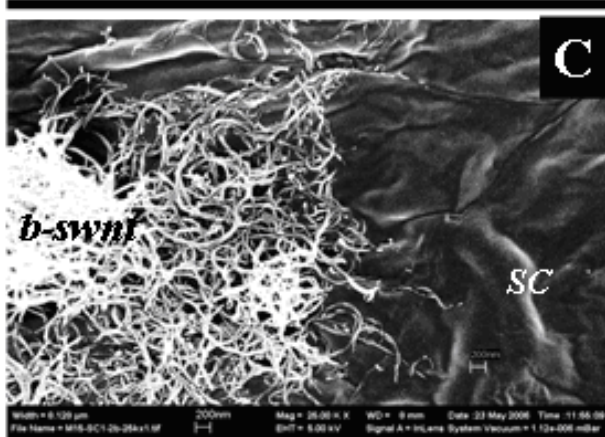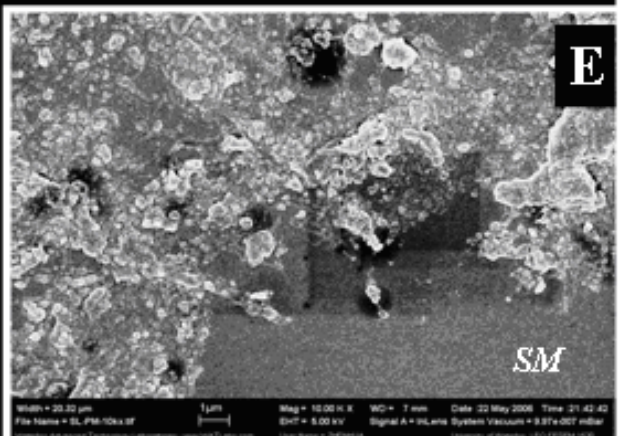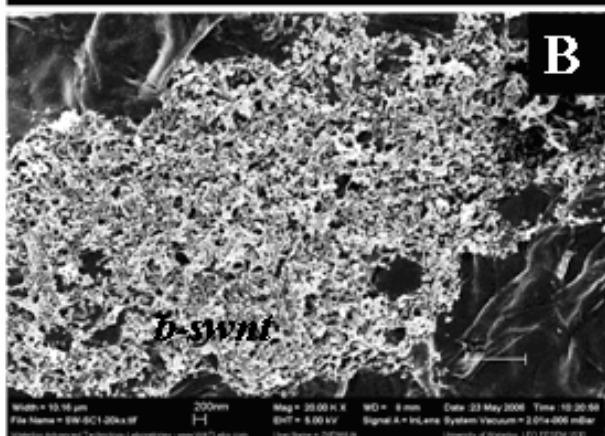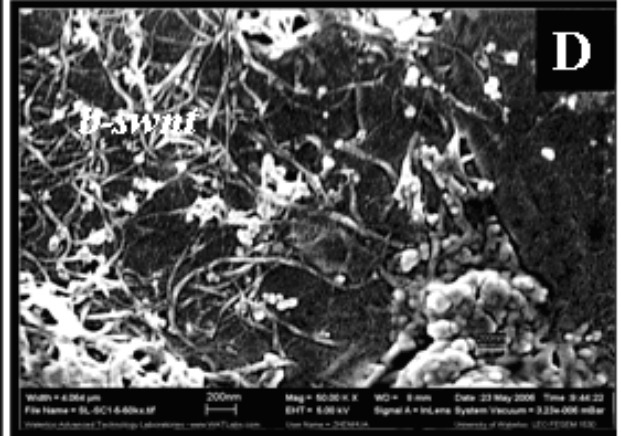
Figure 4.1   Magnetically susceptible AP-SWNT treatment of intact human stratum corneum and parafilm membranes, using the magnetic field created between the poles of a Bruker EMX Electron Spin Resonance Spectrometer; **A**-Control stratum corneum (SC) shows no visible signs of damage. Inserts **B, C** and **D** have been exposed to 0.1 mg/mL dispersions of SWNT magnetically driven AP-SWNT 9,800 G into SC shows no visible damage to the SC whiles aggregates of AP-SWNT are observed on the surface of the SC; **C**-No damage is observed in the magnetically susceptible acid purified P3-SWNT in SC; **D**-In places where P3-SWNT appear more exfoliated, P3-SWNT lies flat on the SC surface rather than penetrate the SC surface; **E-**On the hydrophobic silastic membrane, P3-SWNT appear to cause dark coloration at the surface of the membrane at 9,800 G; **F**- At a higher magnification, the dark spots appear to be indents on the parafilm.

4.1.2 Conclusion from SWNT-magnetophoretic study

Preliminary investigation into this resulted in two major observations: spearing of SC did not appear to be possible at magnetic field strengths of up to 1 tesla, and SWNTs appear as bundled aggregates, preventing/obscuring the spearing of stratum corneum by individual CNTs.

To overcome these challenges, it was necessary to identify the nature of metals present in the SWNT samples, as these could impart magnetic susceptibility to the bulk material. To generate the desired nanochannels, using magnetophoresis, it is necessary to disperse/exfoliate the SWNT bundles into individual strands prior to magnetophoresis. These findings have thus dictated the redefinition of the research objectives.

4.2 Evaluation of SWNTs and the establishment of minimum quality requirements

A major bottleneck in the utilization of carbon nanotubes in medicine is the lack of a standardized quality analysis [69]. For medical and pharmaceutical purposes, it is imperative that the quality of CNT (purity, impurity content and identity, diameter, length, and functionalization state) materials be well defined, with little ambiguity. However, a survey of CNT from various suppliers at best include a few of these descriptors (see table 4.1 below).The disparity between reported purity of CNT materials and those obtained from independent analysis [69, 70] are largely due to the heterogeneous nature of the CNT. Typically, CNT from commercial sources are accompanied by what is described as product information sheets, purported to contain the quality analysis of the accompanying material. Table 4.1 is a collation of the information accompanying CNTs. These list the synthetic method, size (diameter and length), purity, amorphous carbon content, metallic content, ash, specific surface area, density, melting point and aqueous solubility. The details of the accompanying product quality sheets are in Appendix A.

The reported purity values have different descriptors; carbonaceous purity (cp) is used for AP-SWNT, P2-SWNT and P3-SWNT), while weight percentage (wt %) is reported for Cheap Tubes Inc (CT-SWNT), no specific units listed for HMS-SWNT, while for NA-SWNT, percentage SWNT is used. There are no specified units used for the products of Helix Material Solutions and Nanostructured & Amorphous materials Inc.

By definition, carbonaceous purity will refer to all carbon allotropes within the sample, and hence gives little information on the CNT purity of the sample. It is particularly known that MWNT are by-products of SWNT synthesis using EAD. Similarly, the use of ambiguous terminology such percentage (or percentage SWNT) has several interpretations, e.g. percentage volume or weight. The most appropriate descriptor of purity will therefore be by weight. Carbon nanotube samples contain two categories of impurities; metallic catalytic impurities used for in the synthesis of CNTs, and carbonaceous impurities. These typically consist of a Raman spectrum and an electron micrograph (either by SEM/TEM) with the accompanying elemental analysis. It is now common practice to advertise CNT as >95% purity when indeed the sample contains >95% carbonaceous content and not nanotube content.

Solutions Inc. The internal diameters reported are either as an average as in AP-SWNT, P2-SWNT, P3-SWNT, HMS-SWNT and NA-SWNT, or a range as in CT1-SWNT and CT2-SWNT, suggesting a degree of heterogeneity of the particle size.

Table 4.1   **Summary of synthetic methods, properties, and purity of carbon nanotubes**

Description and Code	Synthetic Method	Internal/External Diameter (nm)	Purity*	Ash Content	Amorphous carbon	Length (μm)	SSA (m^2/g)
AP-SWNT	EAD	1.4 [#1]	40-60 cp	▓	▓	1-5	▓
P2-SWNT	EAD	1.4 [#1]	70-90 cp	▓	▓	0.5-1.5	▓
P3-SWNT	EAD	1.4 [#1]	80-90 cp	▓	▓	0.5-1.5	▓
CT-SWNT	CCVD	0.8-1.6/1-2	>90 wt %	<1.5 wt %	<3 wt %	5-30	407
HMS-SWNT/HP-SWNT	CVD	~1.3 [#2]	>90 %	<2 %	< 5 %	0.5-40	300-600
NA-SWNT/N&A-SWNT	CVD	NA/1.1	>90 % SWNT	▓	▓	5-30	400

[#1]   – The diameter of all SWNT samples from Carbon Solutions Inc is reported to have an average of 1.4 nm.

[#2]   – The diameter of all HMS-SWNT samples from Helix Material Solutions Inc. per the certificate of analysis is reported to have an average of ~1.3 nm.

*   – The reported purity values have different descriptors: Carbonaceous purity (cp) is used for products from Carbon Solutions Inc., while weight percentage (wt %) is reported for Cheap Tubes Inc. samples. There are no specified units used for the products of Helix Material Solutions and Nanostructured & Amorphous materials Inc.

N/A – Information not available from the MSDS and certificate of analysis.

▓   - No data available

It is imperative that CNT purity for pharmaceutical applications have comparatively low carbonaceous impurities, and a more homogenous size and length distribution. The ash content refers to the nonvolatile inorganic matter of CNT which remains after subjecting it to a high decomposition temperature. This contains oxidized metallic impurities. The amorphous carbon content identifies the amount of non-CNT carbonaceous impurity (e.g. graphite, fullerenes) content of each sample. This information is not available for samples purchased from Carbon

Since it is well accepted that neither Raman spectroscopy, electron microscopy, nor elemental analysis can, by themselves be used to establish the purity of the CNT materials, fundamental questions regarding the purity values often reported (often times listing only one of the aforementioned method) arise. How are the stated purity values obtained; are the quoted purity levels reproducible; what do the various terminologies of percentage CNT, percentage carbon, weight purity, volume purity, carbon content etc often used by vendors mean?

For pharmaceutical applications, the development of a set of parameters reflecting on the purity, physical (diameter, length, chirality) and chemical (surface defects, functional groups) properties and dispersion state of CNTs is necessary. It is imperative that CNT purity for pharmaceutical applications have comparatively low carbonaceous impurities, and a more homogenous size and length distribution. Several commercially available CNT samples were purchased for purity evaluation. Using the technique of Raman spectroscopy, a comparative purity evaluation is used to rank the SWNT samples.

4.2.1 Results and Discussion –SWNT Quality by Raman spectroscopy

A typical Raman spectrum of CNT has three intense bands; the radial breathing mode ("RBM" band), the D-band, and the G-band. The RBM mode arises from a low-energy vibration

(100 – 400 cm^{-1}) of CNT due to the movement of the carbon atoms radially, causing the nanotube diameter to expand and contract (radial movement) [138, 195] and partly from the tube–tube interactions [196] (Figure 4.2A).

The D band appears around 1350 cm^{-1} and is due to defects in the hexagonal C-C network in the nanotubes, and characteristic of all graphitic material. The G-band (1500-1600 cm^{-1}) is a tangential vibrational mode, arising from the motion of carbon atoms tangential to the surface of the nanotube. Two peaks, arising from the vibrations parallel to and perpendicular to the axis of the SWNT, are often observed in the tangential mode.

The intensity of the D-band, relative to the G-band, is therefore an indication of the amount of graphitic impurities in the sample, and often used as an accepted index for the estimation of CNT purity [197-199]. By using the ratios of the intensities (G to D bands), the issues of fluctuations in the Raman beam and counts are eliminated, as each sample acts as an internal standard to itself. Table 4.2 contains a summary of the intensity (counts) values of the D (I_D) and G (I_G) bands of SWNT samples analyzed. The purity of these SWNTs as reported by the vendors is also listed. These are reported as percentage weight purity values unless otherwise stated. Other terminology used to describe SWNT purity include carbonaceous purity (used for AP-SWNT), percentage CNT and percentage SWNT. Even though these terminologies might accurately describe the quality of the SWNT, their definitions could be arbitrary. Two criteria, both based on Raman measurements, will be used to rank the purity of six samples of SWNT obtained from various commercial sources. The purity of the materials were evaluated using two criteria; the ratio of the I_G /I_D, and full-width-at-half-maximum (*FWHM*)

The first criterion was a comparison of I_G /I_D ratios of the various SWNT samples. There is a direct correlation between the value of the intensity ratios and the purity of the SWNT

samples; the higher the ratio, the higher the CNT content/quality [200]. The D-band occurs in the range 1200-1400 cm^{-1} is characteristic of any graphitic material. This is a disorder induced band, and hence its intensity mimics the amount of graphitic impurities (non CNT material), as well as the defects in the sidewall i.e. defective sites on the continuous hexagonal carbon network, introduce some disorder-induced features into the spectra [195].

Table 4.2   Purity evaluation of SWNT by Raman spectroscopy

	Purity*	I_G	I_D	I_G/I_D	$FWHM_D$
P2	70-90 % ^{cp}	1419820	82209	17.27	41.25
AP	40-60 % ^{cm}	994864	150182	6.62	52.25
CT	90 % ^{wt}	490789	84339	5.82	55.04
NA	95 % ^{CNT}, 90 % ^{swnt}	152449	193469	0.78	57.41
HMS	>90 % ^{p}	561926	110286	0.592	44*

* reported purity of SWNT from commercial source
^{cp} carbonaceous purity. CT1*- SWNT sample purchased from CheapTubes in 2005, while CT2* were purchased (also from CheapTubes) in 2007.
NA describes the purity of the SWNT in terms of carbon nanotube content (^{CNT}) and single walled carbon nanotube content (^{swnt}).
$FWHM_D$ represents the full width at half maximum for the D-band

The G-band appears around 1500-1600 cm^{-1} and, similarly characteristic of all graphitic materials. Its origin is the tangential mode of vibration of carbon atoms relative to the surface of the nanotube. Two peaks, arising from the vibrations parallel to and perpendicular to the axis of the SWNT, are often observed in the tangential mode. This purity comparison can not be compared from the information contained in the accompanying material analysis report due the use of varying terminology to describe the purity of these materials (Table 5.2).

The Raman spectra were fitted using the Laurentian model of peak fitting. To obtain the various intensities of the bands, the area under the fitted curves were used. For the G-band, two prominent peaks were routinely fitted; hence the peak with the greater intensity (by area) was used in the analysis. Table 4.2 contains the intensity (counts at maximum peak height) of the D (I_D) and G (I_G) bands of six SWNT samples, and the calculated I_G/I_D ratio. The samples are arranged in decreasing order of I_G/I_D ratio (i.e. P2-SWNT > AP-SWNT > CT-SWNT > NA - SWNT > HMS-SWNT).

An alternative approach to estimating the purity of CNT samples was suggested by Dillon et al.[139]. By measuring the full-width-at-half-maximum (*FWHM*) of the D and G bands, a comparative qualitative estimate of the purity of CNTs is made. The origins of the disorder induced D-band and G-bands are a convolution of in-plane vibrations (D-band) of the various carbon allotropes (graphite, C_{60}, and other carbonaceous materials), and CNTs. However, the *FWHM* of the D-band of other carbon allotropes are much broader than that of CNT, and a direct indicator of the level of carbonaceous impurities.

This is measured at the full width of a spectral band at a height equal to half of the height at the band maximum. The *FWHM* is a better descriptor of spectral width when the spectra do not have sharp edges. The D-band of CNT, as described earlier, is a convolution of several vibrations from CNTs and other carbonaceous material in the sample.
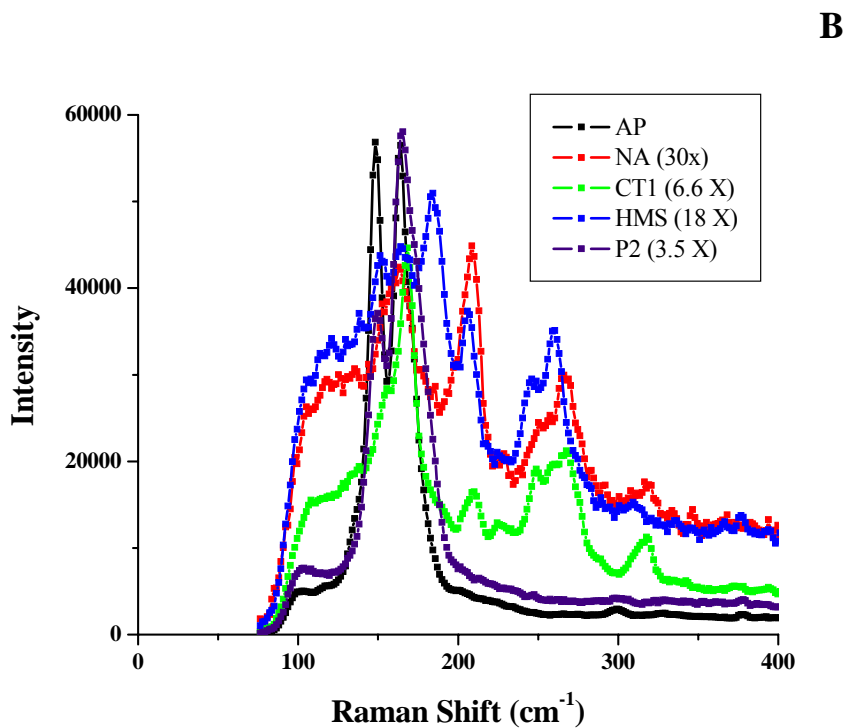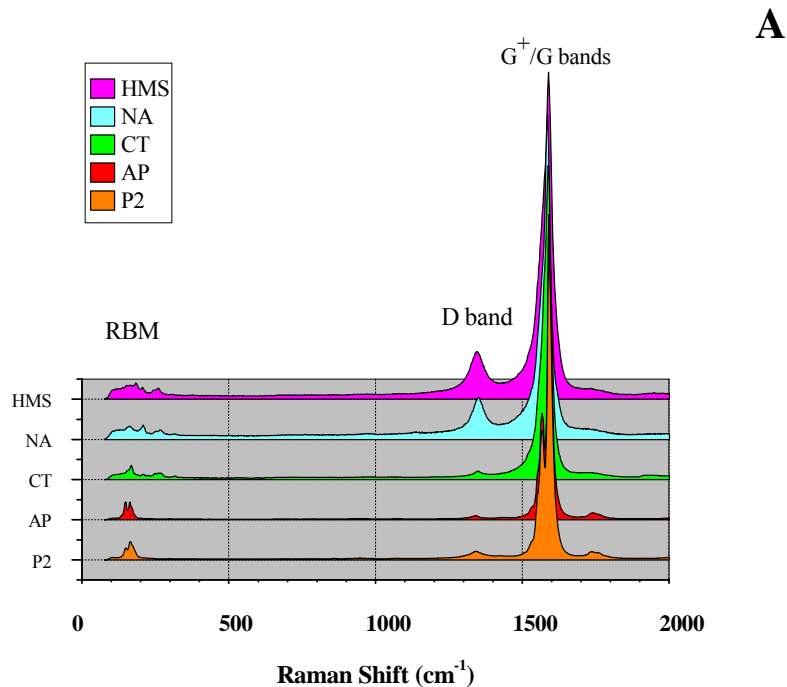
Figure 4.2 Stacked Raman spectra of SWNT from various commercial sources showing (**A**) the relative peak intensities of the RBM (100-400 cm^{-1}), D (1100-1400 cm^{-1}) and G (1500-1650 cm^{-1}) and (**B**) the intensity distribution of their relative peaks in the RBM region.

Since the RBM is a characteristic feature of only SWNT, the presence of RBM peaks in all six samples (Figure 4.2 B) confirms the existence of SWNT in each sample. Even though the use of one excitation wavelength (i.e. only specific chiralities are excited) can not be used to estimate the diameter distribution of these samples, the spread of the peaks in this region is an indicator of the diameter distribution (and hence homogeneity) of the individual SWNT. Whereas the two sharp and narrow peaks are observed for P2-SWNT (149, 164 cm^{-1}) and AP-SWNT (148, 164 cm^{-1}), several peaks are observed for HMS (152, 164, 182, 205, 260 cm^{-1}), NA (164, 208, 266, 316 cm^{-1}), and CT (166, 210, 266 and 316 cm^{-1}). This suggests a narrower diameter distribution for P2- and AP-SWNTs. However, since the RBM values are inversely proportional to the diameter, this narrower diameter distribution will be larger than the smallest diameters found in HMS-, CT- and NA-SWNT, since they have RBM active vibrations at > 165 cm^{-1}).

Figure 4.2A shows stacked Raman spectra of the six SWNT samples analyzed. The disorder induced D-bands (~1353 cm^{-1}) are indicated by arrows whiles the G-bands (1588 cm^{-1}) as shown in Figure 4.2A. The peak positions of both bands in all six samples are relatively fixed. The ranking of purity obtained by the *FWHM* method (i.e. P2-SWNT > AP-SWNT >CT-SWNT > NA-SWNT > HMS-SWNT), is significantly different from the intensity ratios.

However, this approach appears to be much less sensitive, with the values appearing are close in magnitude (47.0-56.6). It is essential to note however, that the purity evaluation as defined by Raman spectroscopy takes cognizance of the carbonaceous materials only. Even though a sample might have a significant amount of SWNT, the presence of defective sites on the tubes will increase the D-band with resulting in a reduced I_G/I_D ratio.

Using the two criteria (I_G/I_D, and *FWHM*) set for purity comparison, Raman spectral analyses indicated that P2-SWNT was the best quality of the six samples, while HMS-SWNT was the least pure. Based on the purpose of the comparative purity analysis, it has been established that P2-SWNT has the best carbonaceous purity, and will subsequently be used for dispersion evaluation.

O'Connell et al. [166] established that ultracentrifugation can be used to separate CNT from metallic impurities, and metallic impurity-CNT composites, by exploiting the differences in the density of CNTs and metallic nanoparticles. However, by using gradient centrifugation over a 2.5 hour period, Sun et al. [201] demonstrated that similar separation can be achieved by gradient centrifugation, with the higher density metallic particles and composites separated by controlled sedimentation. It is therefore envisioned that the metallic impurity content of the selected SWNT will be further reduced after centrifugation.

As mentioned previously, the quality of a pharmaceutical excipient lies partly in identifying the impurities present in the sample. To this end, qualitative electron dispersive x-ray spectroscopy (EDS/EDX) will be used to identify the metallic impurities in the six SWNT samples.

4.3   Qualitative EDX Analysis of SWNT Samples

4.3.1   Results and Discussion –SWNT Quality by EDX

Backscattering electron images confirm the non-homogenous nature of all SWT samples analyzed. The backscattering electron images of the EDS analyses show the presence of impurities as sharp bright spots, contrasted from the carbon mass (containing CNTs and graphitic impurities), allowing for detecting subtle variations in the chemical composition of the material

(material with heavier elements appear brighter). Table 4.3 contains a summary of the reported metallic impurities, and metallic impurities identified in our analysis. EDS backscattering images and plots can be found in Appendix A.

AP-SWNT samples are shown to contain Ni and Y as particles (0.5-1 μm). The accompanying elemental analysis from the supplier indicates the sample contains 40-60 % SWNT and 30 % residual catalyst of Ni/Y catalyst.

Table 4.3   EDS backscattering analysis of SWNT

SWNT	Reported Impurities	Impurities by EDX
AP-SWNT	Ni/Y	Ni/Y
NA-SWNT	Al, Cl, Co and S.	Si, Cr-Fe-Co Fe-Cr-Mo.
		Trace amounts of Al, Cl, Co, S and Fe,
HMS-SWNT	None	Fe, Co, S and Si
CT-SWNT	Al, Cl, Co and S	Fe, Cr, S, Si, Al, Ca, Ti, Cl,
P2-SWNT	Ni, Cl, S, Si, Y	Ni, Cl, S, Si, Y

CT1*- SWNT sample purchased from CheapTubes in 2005, whiles CT2* were purchased (also from CheapTubes) in 2007.

For N&A-SWNT sample, a piece of Si as individual shard is visible (see accompanying SEM spectra), while other particles were identified to contain Al-Si (<1 μm), Cr-Fe-Co (100-500 nm) and Fe-Cr-Mo (100-200 nm). The carbon mass has trace amounts of Co, Fe, Cl, S, Al. The accompanying elemental analysis (in certificate of analysis) indicates the sample consists of 96.30 % C, 0.08 % Al, 0.41 % Cl, 2.91 % Co and 0.29 % S. For the purity of SWNT samples, a quote of the carbon content is of little significance; this includes all other allotropes of carbon. The results do show the presence of all the listed elements, and additionally, Fe and Si were

found in the sample as well. The presence of Si in the sample is thought to originate from the packaging (glass vial) of the material, or the substrate upon which the SWNT were synthesized.

HMS-SWNT samples contained significantly large particles of Co (10 μm) and minor amounts of Fe. The rest of the carbon mass has trace amounts of Fe, S, and Si. The presence of this large micron sized Co may be traced to remnants of metallic catalysts used in the synthetic process.

In the material analysis data sheet accompanying the SWNT, the purity has been quoted as >90 %, with < 5% amorphous carbon, and < 2 % ash. There is no information as to the possible existence of metallic impurities in the sample, contrary to our finding. The presence of metallic impurities can be accounted for in the reported chemical vapour deposition (CVD) synthetic method used to produce these CNTs.

CT-SWNT backscattering images indicated the presence of Fe with minor Cr as particle (< 1 μm), as well as Fe-Cr with minor particles of Ca, S, Ti as particle (<1 μm) and particles of Si (1-2 μm). The carbon mass contains trace amounts of Fe, Cr, Ca, Cl, S, Si. The accompanying elemental analysis (in certificate of analysis) indicates the sample consists of 96.32 % C, 0.08 % Al, 0.40 % Cl, 2.90 % Co and 0.29 % S. For the purity of SWNT samples, a quote of the carbon content is of little significance; this includes all other allotropes of carbon. The results do show the presence of all the listed elements, and additionally, Fe and Si were found in the sample as well.

The EDX analysis of P2-SWNT showed the presence of Ni as particle (100-300 nm). Carbon mass contains minor Ni, Cl, S, Si, Y. These are reported by the manufacturers to contain 70-90 % SWNT and 7-10 % residual catalysts from Ni/Y. The results indicate the presence of

additional impurities; Cl, S and Si, which have been listed by the supplier as possible

contaminants.

4.3.2 Conclusions from SWNT Purity analysis

The analyzed samples appear to contain mainly carbonaceous mass, as non-reflective

background, compared to the reflective metallic particles. However, there are particulates of

metal catalysts residues in each of the analyzed samples, often containing additional impurities

not stated in the material analysis data sheet. This could arise from contamination, or the use of a

less sensitive analytical technique to identify the impurities.

The results show that the qualitative impurity identity of the CNT materials is often

understated. Of the six samples analyzed, only two (AP-SWNT and P2-SWNT) have listed all

the impurities confirmed by our independent analysis. Interestingly, for HMS-SWNT, no

mention was made of either the starting metallic catalysts, or the possible impurities. NA-SWNT

and CT-SWNT and have been demonstrated to contain impurities that were not listed.

4.4 Dispersion of SWNT in selected pharmaceutical solvents

From pharmaceutical view point, it is essential that solubility be obtained prior to the use

of CNT in therapeutic formulations. Despite the abundance of literature regarding CNT

dispersion, there are no agreed methods of evaluating a dispersion [202].

Ultraviolet spectroscopy has been used to evaluate the dispersion efficiency of CNTs and

the colloidal stability of the resultant dispersion. It has been used to monitor the exfoliation of

both SWNTs [109, 130, 203-205] and MWNTs [109, 206-208] in surfactant solutions. Jiang *et

al.* [209] and Marsh *et al.*[207] independently evaluated the colloidal stability of CNT

dispersions by monitoring the sedimentation of dispersed CNT over time by the UV absorbance

of the supernatant. Yu *et al*. [206] monitored the exfoliation of bundles MWNTs in SDS solution in a time-dependent study. It was suggested that bundled MWNTs are minimally active in the UV region, due to tunnel coupling between metallic and semiconductive SWNTs, allowing for the concentration of exfoliated CNTs in solution could be determined. For a given MWNT:surfactant ratio, the maximum exfoliation achievable was reported when the UV absorbance was a maximum [205].

However, even though UV spectroscopy has been used to comparatively evaluate the efficiency of exfoliation in individual/smaller bundles of CNTs no publications indicate the use of this technique in determining the absolute concentration of individually exfoliated CNTs in solution. This is mainly because of the UV activity of smaller sized bundles. For our purpose therefore, UV spectroscopy will be used to monitor the exfoliation efficiency. This has been used to monitor the extent of exfoliation of SWNT in gemini surfactant (12-3-12) and SDS.

Microscopy techniques such as TEM, SEM and AFM are suited for CNT size and purity analysis. However, as these techniques typically measure samples in a dry state, they do not adequately represent the suspension state of CNT. The simplest qualitative estimation of CNT dispersion is by visual estimation. Several methods have been reported to quantitatively estimate dispersion in solution. The most common approaches are UV-Vis absorbance [114, 130, 164, 210-214], resonant Raman scattering [109, 211, 212, 214-218], small angle scattering [116, 211, 219-222]. These techniques are best used in combination to confirm dispersion [162].

The concentration estimates of dispersed CNT have been obtained by UV absorbance measurements. However, our preliminary investigation indicates that these estimates could be misleading, if the amount of non-dispersed material (CNT, carbonaceous impurities, and catalyst residue) is not accounted for.

4.4.1 Preliminary classification of dispersions based on morphology of dispersions

The single most significant contributor to the dispersion efficiency of CNT lies in the choice of an appropriate dispersing agent. Besides the dispersing agent, dispersions are often accomplished by sonication, and centrifugation to obtain a nano-dispersion (dispersion into individual nanotubes or nanosized bundles). These nano-dispersions tend to yield stable dispersions, with no visible aggregation over several months.
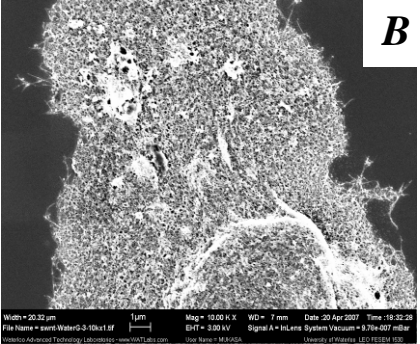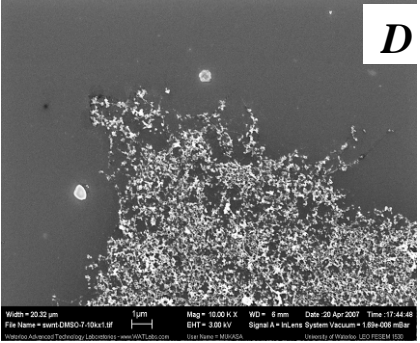
To characterize SWNT dispersions in the selected surfactants, pharmaceutical solvents, and biocompatible solvents, the morphology of the resultant dispersions were investigated by visual observation, light microscopy, and SEM imaging. It was observed that all nanotube dispersions appear homogeneous immediately following sonication. However, a time study of the dispersion stability was the criteria used to evaluate the dispersants suitability for nanosized CNT dispersions.

We have investigated the dispersibility of CNTs in a series of pharmaceutical solvents [130], and present visible, microscopic, and SEM images of CNTs in three representative solvents using a three-category assessment of dispersibility - aggregated/insoluble, swollen, and dispersed based on visual observation. CNTs show no signs of aggregation and phase separation resulting in a stable and uniform suspension indicated by a uniform light black/brown colour. The dispersed SWNTs show no visible signs of aggregation and phase separation several months after sonication. There are currently few techniques that can be used to assess the extent of CNT dispersion. A measure of the stability of the dispersion (i.e. formation of visible precipitates over time) is typically a good indicator of the dispersion efficiency, however, this approach is incapable of distinguishing individual from bundle suspensions of CNT [223].

Within an hour of sonication, non-dispersed SWNT aggregate and sediment to the bottom of vial, while the swollen and nano-dispersed dispersions have a similar visual appearance within 24 hours. The nano-dispersed samples are expected to contain both mixture of individual SWNT, and small sized bundles as centrifugation at 10,000 g is not expected to completely remove smaller sized bundles.

Table 4.4 is a collation of the descriptive information of the three categories of dispersion, with optical images showing aggregated, swollen and stable dispersions, with their corresponding light, and SEM micrographs. Table 4.4 A depicts the aggregation of AP-SWNT in deionized water (representative of aggregated/precipitated state). The SWNT are observed to aggregate and sediment to the bottom of the vial in less than 2 hours after sonication. In a light microscope, these precipitates are clearly discernible as clusters, under an optical microscope (40X) as shown (Table 4.4 A). The corresponding SEM images of these aggregated clusters confirm the presence of SWNT, and bundled morphology of the SWNT (Table 4.4 B). Similar aggregated samples as in Table 4.4 A and B, were obtained for dispersion in benzalkonium chloride, poloxamers 338, 407, and 188, Tween 60 and 20 and Span 40. Dispersion of SWNT in 100 % DMSO, propylene glycol and glycerol gave a non-uniform quiescent dispersion of the carbonaceous materials (Table 4.4 C and D), which do not aggregate into larger clusters, but persists as suspension for several weeks and are described as swollen. Images of a swollen dispersion in Table 4.4 C and D were taken of SWNT dispersion in DMSO. Light micrographs of the dispersed samples depict the efficient dispersion of carbonaceous material. These dispersions are characterized by a uniform distribution of small particles in the light microscope (Table 4.4, insert E).

Table 4.4 Morphology of CNT dispersion

Type of Dispersion	Optical Micrographs	SEM
Aggregated- Optical microscopy and SEM images of SWNT dispersed in deionized water. Aggregation and sedimentation sets-in soon after sonication, falling out of solution and settling at the bottom of the vial		
Swollen - dispersion of SWNT in DMSO. Optical micrograph (9 months after sonication) shows both aggregates in suspension and at the bottom of the vial. SEM images reveal smaller aggregates/bundles of CNT.		

Dispersed - Optical micrographs of 0.1 %($^w/_v$) 12-3-12 gemini surfactant show no aggregates, while SEM micrographs show exfoliated CNT, resulting in individual/nanosized bundles
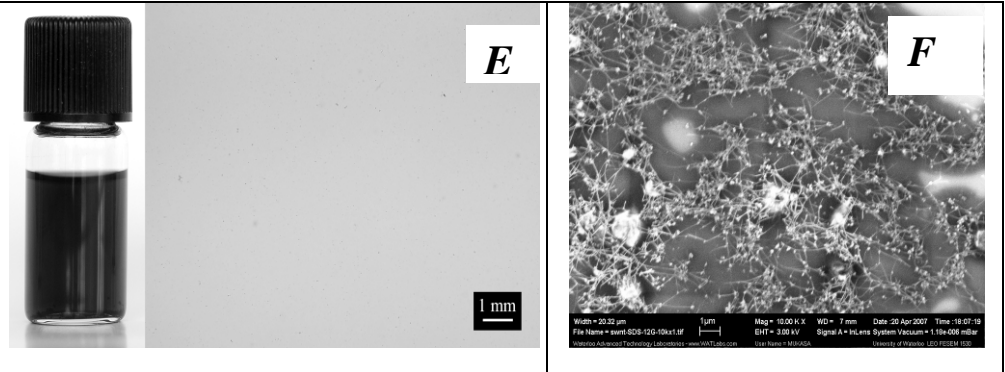
However, due to the presence of other non-CNT carbonaceous impurities in the sample, coupled with the limitation of the bath sonication process, some amount of sediment is observed, albeit much smaller than the aggregates in non-dispersed micrographs (Table 4.4 inserts A and C). The SEM micrographs of the dispersions give more detail as the aggregation states of the dispersions are visible. SEM images of non-dispersed SWNT (Table 4.4, insert B) show them as a thick and dense aggregate. The presence of SWNT is only discernible at the edges of the images as needle-like spikes. For the intermediate dispersion (swollen), SWNTs clusters appear to be smaller and more loosely aggregated [224] (Table 4.4, insert D), while for dispersed samples, shows a relatively less bundled smaller sized aggregates of SWNT. The SEM image of CNTs in SDS and 12-3-12 show de-bundled CNTs and very small SWNT bundles [130].

Table 4.5 summarizes the various dispersion states, the chemical structure, mean dispersion particle size represented by the hydrodynamic diameter (D_H), and the zeta (ζ) potential obtained for the selected dispersion agents. The dispersion agents have also been categorized into the surfactant types (cationic, anionic and non-ionic). Under this category, non-surfactant based dispersions are designated as not applicable (N/A). Dispersions prepared using non-surfactant based dispersing agents such as solvents; deionized water (DDH$_2$O), dimethylsulfoxide (DMSO), ethanol, propylene glycol, and glycerol, were prepared at 0.1 mg/ml P2-SWNT in 100 % of the dispersing agent, whiles all surfactant based dispersions were in 0.1 % ($^w/_v$) of surfactant in deionized water.
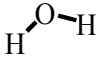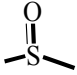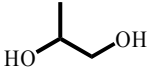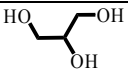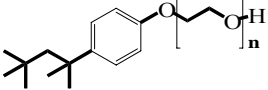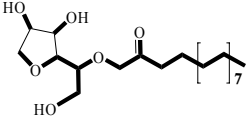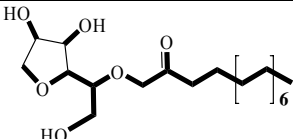
The reported particle size and zeta potential measurements were taken 24 hours after sonication (dispersions in DDH$_2$O and ethanol were taken immediately after sonication and again after 24 hours).
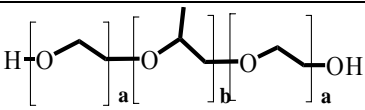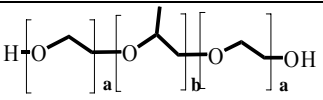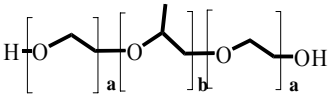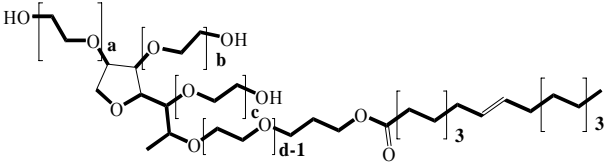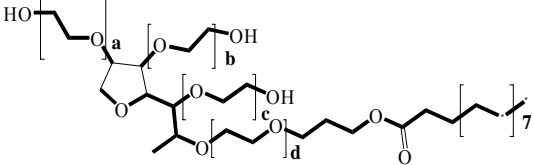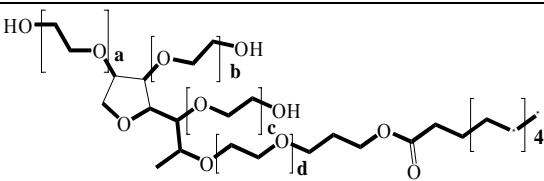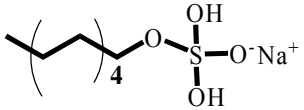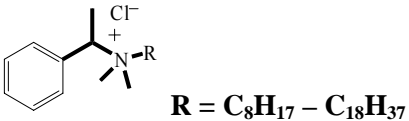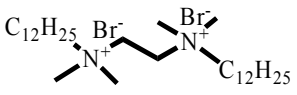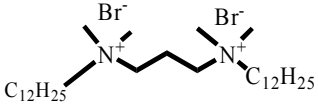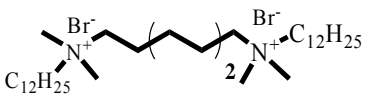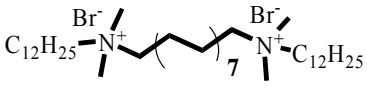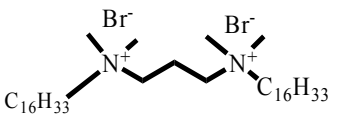
In ionic surfactant dispersion, colloidal stabilization is explained by the Derjaguin–Landau–Verwey–Overbeek (DLVO) theory. The ζ-potential of the dispersions is based on the Smoluchowski equation (as an approximation to the anisotropic rather than spherical morphology of the SWNT). Zeta (ζ) potential measurements of the dispersed SWNT show typically have values of magnitude > ±25 mV, while non-dispersed samples have a magnitude less than +20 mV. The stability of these colloidal dispersions could be attributed to two factors. Models have been proposed [116, 124, 166, 225, 226] for the orientation of the surfactant molecules on SWNT. In case of Gemini surfactants, their hydrophobic alkyl groups provide the binding with the hydrophobic surface of SWNTs, while the positive charges of gemini head groups provide compatibility with the polar solvent aqueous media, thereby preventing aggregation due to electrostatic repulsion.

Unlike ionic dispersions where the colloidal dispersion is a function of the magnitude of the electrostatic repulsion between like charged particles, the major driving force for non-ionic stabilized colloidal dispersions is a function of steric stabilization [227]. The three tri-block copolymers (Pol. 188, 407 and 338) were chosen with varying molecular weight. Stabilization via polymer block copolymers relies on the dual interaction of one block with the solvent while the other block interacts with the surface of the particles. However, no difference in dispersing capability was observed for the triblock copolymers used in this study.

Table 4.5 **Structure, classification of excipients and dispersion states**

Name	Surfactant Type	Average D_H (nm) [#]	ζ-potential (mV)	Chemical Structure of surfactant/excipient	Dispersion State
DDH$_2$O	N/A	> 6000	- 14.64 ± 5.69		Aggregated
DMSO	N/A	*DNSA	*DNSA		Swollen
Isopropyl Alcohol	N/A	-	-10.6 ± 12.3		Aggregated
Propylene Glycol	N/A	*DNSA	*DNSA		Swollen
Glycerol	N/A	700	*DNSA		Swollen
TX100	Non-ionic	294	- 9.65 ± 8.25		Aggregated
Span 60	Non-ionic	94.6	- 18.6 ± 10.52		Dispersed
Span 40	Non-ionic	331	- 27.6 ± 9.69		Aggregated

Pol. 338/ Pluronic F108	Non-ionic	206	-21.0 ± 6.34	where a = 141, b = 44	Dispersed
Pol. 407/ Pluronic F127	Non-ionic	141	-12.9 ± 5.85	where a = 101, b = 56	Dispersed
Pol. 188/ Pluronic F68	Non-ionic	196	-15.0 ± 4.98	where a = 80, b = 27	Dispersed
Tween 80	Non-ionic	164	- 7.39 ± 6.52	where a+b+c+d = 20	Dispersed
Tween 60	Non-ionic	234	-11.25 ± 12.36	where a+b+c+d = n	Aggregated
Tween 20	Non-ionic	332	-3.54 ± 4.68	where a+b+c+d = n	Aggregated

		264			
SDS	Anionic	81.4 *	-60.54	$\text{H}_3\text{C}(\text{CH}_2)_4\text{O}-\overset{\overset{\text{OH}}{\|}}{\underset{\underset{\text{OH}}{\|}}{\text{S}}}-\text{O}^-\text{Na}^+$	Dispersed
BAC	Cationic	268	+28.5 ± 9.36	Ph–CH(CH$_3$)–N$^+$(CH$_3$)$_2$–R Cl$^-$ **R = C$_8$H$_{17}$ – C$_{18}$H$_{37}$**	Aggregated
12-2-12	Cationic	227	+39.7±15.1	C$_{12}$H$_{25}$–N$^+$(CH$_3$)$_2$–CH$_2$CH$_2$–N$^+$(CH$_3$)$_2$–C$_{12}$H$_{25}$ 2 Br$^-$	Dispersed
12-3-12	Cationic	308	+66.0 ± 18.5	C$_{12}$H$_{25}$–N$^+$–(CH$_2$)$_3$–N$^+$–C$_{12}$H$_{25}$ 2 Br$^-$	Dispersed
12-7-12	Cationic	232	+62.0±15.3	C$_{12}$H$_{25}$–N$^+$–(CH$_2$)$_2$–N$^+$–C$_{12}$H$_{25}$ 2 Br$^-$	Dispersed
12-16-12	Cationic	205 +64.9 ±29.5			C$_{12}$H$_{25}$–N$^+$–(CH$_2$)$_7$–N$^+$–C$_{12}$H$_{25}$ 2 Br$^-$	Dispersed
16-3-16	Cationic	357	+48.3.0 ± 15.8	C$_{16}$H$_{33}$–N$^+$–(CH$_2$)$_3$–N$^+$–C$_{16}$H$_{33}$ 2 Br$^-$	Dispersed

[#] Reported values are the average hydrodynamic diameter of aggregates

| a | * DNSA- Data not suitable for nalysis.

The higher molecular weight surfactants and polymers increased the dispersion of CNT, due to steric stabilization by adsorbed surfactant/polymer onto the walls of the CNT, impeding CNT aggregation. This may explain the dispersion trend within the Tween (20, 60 and 80) non-ionic surfactants with molecular weights (MW) of 1227.54, 1283.65 and 1309.68 g respectively. Considering these have the same hydrophilic head-group, the difference in dispersion can also be explained by the degree of hydrophobicity of the alkyl tail.

Having established the general dispersibility of CNT in selected pharmaceutical dispersing agents, the focus of the dispersion was further narrowed down to dispersion in gemini surfactants, specifically, the 12-3-12 gemini surfactant. At a surfactant concentration of 0.1 % w/v, SWNT was dispersed in all the gemini surfactants investigated. It is suggested that the stabilization of SWNT in dispersion results from a perpendicular orientation of surfactant molecules to the CNT axis, resulting in a monolayer coating. The hydrophobic tail of the surfactants are adsorbed onto the graphitic CNT wall via van der Waals interactions, while the hydrophilic head-group of the surfactants are oriented away from the CNT wall, and towards the aqueous phase. A dispersion of this monolayer of cylindrical surfactant (ionic) coating on the CNT surface will be stabilized by electrostatic repulsion induced by the net charges on the surfactant coated CNTs [226, 228, 229].

The dispersion of CNTs in pharmaceutical solvents and surfactants is due to the adsorption of these dispersion agents onto the surface of the CNTs. For ionic surfactants, the stability of the dispersion results from the creation of a distribution of charges (either negative or positive), on the surface of the CNTs, preventing the aggregation of the dispersed tubes by coulombic repulsion. However, the mechanism of the adsorption onto the surface of CNTs, and

the orientation of the adsorbed molecules is not obvious. Several postulates have been put

forward to explain the binding mechanism, and the structure of the resultant CNT-moiety.

There has been suggestions however, that a more energetically stable surfactant coating, rather

than the formation of the cylindrical micelles is possible [228]. In a parallel conformation (i.e. to

the tube axis), hydrophobic tails can interact with the CNT sidewalls by van der Waal's forces;

the magnitude of which will depend on the hydrophobicity of that moiety.

Using this model of increased stability via van der Waals interactions, coupled with the

electrostatic repulsion, dispersion stability will be dependent on the magnitude of the

hydrophobic surfactant tail-CNT van der Waal's interaction and the charge and size of the

hydrophilic head-group of the surfactant [124].Islam et al. [124] speculated that surfactant

dispersed SWNT stabilization is dependent on the interaction between molecules oriented

parallel to the tube axis and the hydrophobic CNT surface. The dispersions are improved if the

hydrophobic chains are aligned parallel to the tube axis, rather than perpendicular.

By this mechanism, hemimicelle formation results from micelle collapse near the CNT

surface, resulting in increased absorption near the *CMC* of the surfactant [230]. However,

considering the structural stability of hemimicelles, these are stable upon a flat surface [230,

231], rather than on high curvature structures such as CNTs [226], thus suggesting that the

formation of hemimicelles is an unlikely mechanism for stabilizing dispersions.

It has been suggested that the absence of any structural information from small-angle

neutron scattering experiments for the dispersion of SWNT using 0.1-1 mg/mL of SDS for a

final SWNT concentration of 7-12 mg/mL of SWNT [116], suggests the absence of the models

proposed. Baskaran et al. [232] suggest a random model, where interactions between the

surfactant and CNT is of random fashion, with no consistent orientation of either the

hydrophobic moieties or the polar head-groups. Due to the extensive π-network due to the aromatic rings, CNTs are an electron rich moiety, capable of acting as electron donors in donor-acceptor complexes. Secondly, due to the extensive aromatic network, they are also capable non-covalent π-π interactions with electron rich moieties.

These proposed mechanisms for the dispersions are based on the model that CNTs do not have structural imperfections. However, the presence of structural defects makes such predictions even more complicated. It is known that the CNTs are electron-rich molecules and any electron-deficient molecules can interact with them and form donor-acceptor complexes, much the same way as the electron-rich molecules form π-π complexes. The π-π interactions of CNTs with electron-rich molecules have been used for noncovalent functionalization.

The polysorbate series of excipients (Tween 20, 60, and 80) were selected due to their use as emulsifiers and stabilizers for emulsions and suspensions, while the pluronic (Poloxamer 118, Poloxamer 338, and Poloxamer 407) surfactants are routinely used in pharmaceutical formulations. Both of these classes of compounds are reported to have a relatively low toxicity, and nonirritating properties.

From the chemical structure of Pluronics, it is postulated that the interaction between the hydrophobic polyoxypropylene block to the CNT surface on one hand, and that between the hydrophilic polyoxyethylene chain interacts with the aqueous phase, resulting in steric stabilization [133]. However, at the concentration of 0.1 % Pluronics, there was no observable dispersion of the AP-SWNTs whereas visible dispersion was observed for P2-SWNT. Moore et al. [118] reported the dispersion of SWNTs in Pluronics with mass percentage conversions up to 9.4 %.

4.4.2 Method development-SWNT in gemini surfactants

It is essential that SWNT dispersions be well characterized and preparations reproducible. This is necessary considering the disparity reported for the maximum dispersion of SWNTs; as much as two orders of magnitude [124, 131, 229]. These inconsistencies can be traced to one or more of several factors. The methods are developed in different laboratories using different processing conditions and different SWNT samples (from different sources). In our method development, we will investigate the effect of SWNT source (from five commercial sources) and purity on the dispersion efficiency (UV absorbance), optimize the sonication time required by monitoring the UV absorbance of the dispersion with time, establish an optimized centrifugation speed that will yield CNT dispersions with hydrodynamic diameters (size) <100 nm using the selected gemini surfactant (12-3-12).

4.4.2.1   Sonication and evaluation of SWNT Samples

Sonication in itself enhances the micro-scale dispersion of nanotubes within the dispersing medium [233]. However, the conditions used by various researchers vary considerably [117, 132, 234]. Sonication of CNT dispersions is the source of mechanical energy required to exfoliate the bundles of CNT into individual robes and smaller sized bundles. The simultaneous addition of stabilizers such as surfactants, retains the exfoliated CNTs in a dispersed state for periods of time [124, 130, 132, 203]. The mechanical energy from sonication is required to overcome the van der Waals interactions in the CNT bundles, resulting in tube exfoliation. The efficient dispersion of CNTs depends on an optimized sonication procedure, an optimized dispersant concentration and CNT concentration.

Initial reports suggested that exfoliation and dispersion efficiency was a function of sonication power [203]. However, even with sonication, optimized power is required, beyond

which the exfoliation process becomes dynamic; the rate of re-aggregation of the individual

CNTs, equals the rate of exfoliation [215]. Figure 4.3 shows the exfoliation profile of SWNTs

from five different commercial sources, monitored by UV spectroscopy. The degree of

exfoliation was monitored by UV spectroscopy appears to plateau after 10 hours of sonication.

Even though the exfoliation process might not be complete, the attainment of a plateau after ~10

hours suggests the exfoliation process attains a dynamic equilibrium.

In all five SWNT samples evaluated, a common feature was the attainment of a threshold

maximum (i.e. UV absorbance plateaus with sonication) [132]. As indicated, the optimized

exfoliation condition is dependent on both the dispersant and SWNT concentrations and the

strength of the inter-tube attractive van der Waal's forces in a given sample. The initial

evaluation of surfactant to SWNT starting weight ratio of 0.1 mg/mL of SWNT dispersed in 0.1

% w/v of surfactant was selected on the basis of the reported surfactant aided SWNT dispersion

ratios published in the literature [124, 132, 217, 235]. However, it is well established that the

maximum dispersion of CNT varies with dispersion agent. Hence all SWNT samples were

evaluated using the same dispersion agent/medium (0.1% ($^w/_v$) 12-3-12).

To optimize the length of sonication required to obtain the maximum exfoliation, the UV

absorbance of all SWNT dispersed in the same solvent was monitored over a 24 hr period

(Figure 4.3).
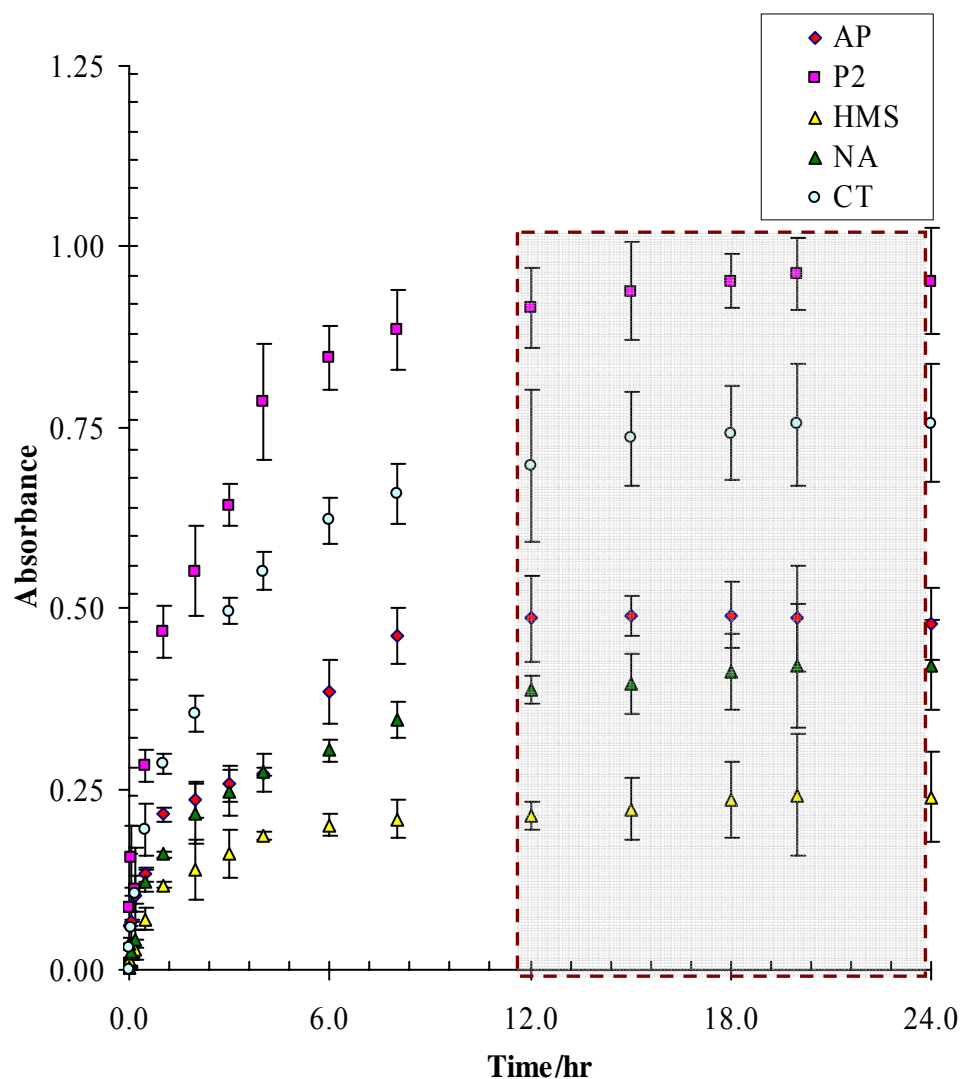
Figure 4.3   UV spectroscopy (λ =500 nm) monitoring of the exfoliation profile of 0.1mg/mL sonication aided dispersion of SWNTs from four commercial source (SWNT-AP2 Batch # 155 and P2-SWNT (70-90 % purity) from Carbon Solutions Inc, HMS from Helix Materials (90 % SWNT purity), and NA from Nanostructured and Amorphous Materials Inc (C1284YJ 7440-44-0, 95 % CNT, 90 % SWNT) in 0.1 % w/v of an aqueous solution of 12-3-12 gemini surfactant) with sonication of 50/60 kHz over a 24 hr period. The UV absorbance of the dispersion increases from 0-12 hrs, stabilizing thereafter (grey area) for all five SWNT sample (n=4)

Sonication is used as a source of the mechanical energy, to overcome the strong inter-tube attractive van der Waals forces inherent in the bundled/aggregated SWNTs, leading to the disentanglement and dispersion of exfoliated SWNTs. The shapes of the dispersion patterns are the same for all the SWNT samples investigated (i.e. UV absorbance increases for the first 12 hrs, and plateauing thereafter). However, P2-SWNT and AP-SWNT have a higher absorbance value at the maximum exfoliation. These differences can be attributed to two possible routes; the weaker intertube van der Waal's forces in EAD synthesized SWNT (AP-SWNT and P2-SWNT), compared to the CVD synthesized SWNTs (CT-SWNT, NA-SWNT and HMS-SWNT), or the lower SWNT content of the CVD synthesized SWNTs. In the former, higher energy input will be required to disrupt the intertube forces to obtain comparable (to AP- and P2-SWNT) exfoliation, and hence UV absorbance. The latter presupposes that a higher SWNT content of the EAD synthesized SWNTs, will yield a higher population of exfoliated SWNTs, resulting in their observed higher UV absorbance values.

The choice of UV spectroscopy as a quantitative measure of SWNT exfoliation is justified by the fact that only exfoliated CNTs are UV active in the wavelength region between 200 and 1200 nm, whereas the bundled and aggregated CNTs are not active due to tunnel coupling between metallic and semiconducting SWNTs [132]. However, since the non-UV active bundles/aggregates, significantly contribute to scattering the lower UV region, hence 500 nm was chosen to monitor the UV absorbance. Similarly, UV measurements were taken without centrifugation.

Continuous exfoliation from bundled SWNT aggregates, into individual SWNTs is observed by a corresponding increase in UV absorbance. It also implies that at the point of maximum UV absorbance (i.e. where the UV absorbance plateaus after 12 hours), a dynamic

equilibrium of exfoliation and re-aggregation of previously exfoliated SWNTs, is attained. The continuous increase in absorbance from 0-12 hr of sonication indicates an increase in exfoliation, attaining equilibrium as evidenced at the highest absorbance value, corresponding to the maximum exfoliation for each SWNT sample.

However, exfoliation does not mean the existence of SWNT as individual entities in dispersion. This is because, exfoliated SWNTs could still be very loosely entangled aggregates in solution, considering the rather high aspect ratios of these materials. By extrapolation, UV method has also been used as an indicator of the measure of colloidal stability of SWNT dispersions, by monitoring the UV absorbance over time. Under the experimental conditions, we conclude that to obtain the maximum exfoliation, the dispersion should be sonicated for a minimum of 12 hours.

4.4.2.2 *Centrifugation of SWNT dispersion*

Ultracentrifugation is the most common approach used to remove non-soluble carbonaceous impurities, remnant metallic particles, and bundles of CNT above a predefined size cut-off [103, 115, 125, 131, 204, 225, 236-240]. The defined size cut-off point is usually set at the size of the individual tube diameter [103]. However, this is often achieved with a loss of a significant amount of CNTs [103].

Rather than using the approach of ultracentrifugation to obtain isolated CNTs/small sized bundles, Bergin et al. [104, 106] found that a systematic dilution of sonicated CNTs in an appropriate solvent/dispersion medium is a superior technique to obtaining individual/small sized bundles of CNT dispersions. A concentration-dependent CNT bundle diameter distribution was obtained for CNT concentrations less than 0.05 mg/mL, with a size saturation of 2 nm. These

findings suggest that the extreme conditions of ultracentrifugation are not necessarily required to obtain exfoliated CNTs.

Using this approach of dilution instead of ultracentrifugation, Cathcart et al. [103] postulated that the increased proportion of individual CNTs via dilution results from the lowered probability of single CNTs re-aggregating due to the increased intertube separation upon dilution.

Centrifugation has been used in the separation of individually exfoliated SWNTs from bundled/aggregated SWNTs, carbonaceous impurities, and residual metallic particles. This has been achieved by exploiting the differences in the rate of centrifugal sedimentation of these components [241]. Also, considering that only exfoliated SWNTs are UV active, a continuous monitoring of the absorbance, with a corresponding increase in centrifugal force, will ascertain the optimum force required to separate the aggregated/bundled SWNTs, and the residual catalytic materials, from the exfoliated SWNTs. Since the UV absorbance of CNTs is proportional to the amount in suspension, monitoring the absorbance with varying centrifugation is used to quantitatively establish, the speed at which UV responsive dispersed CNTs begin to be removed from solution. To optimize the centrifugation speed (removing non-dispersed component), UV absorbance was used to monitor this process as for 0.1 mg/mL P2-SWNT in 0.1 % [12-3-12] (diluted in 1:20 for UV reading), centrifuged at varying speed/force (g).

Figure 4.4 shows the variation of UV absorbance ($\lambda = 500$ nm) with varying centrifugal force for a dispersion 0.1 mg/mL AP-SWNT in 0.1 % w/v 12-3-12. The UV absorbance of the dispersion appears to remain stable at 2.3 from 0-10,000 g. However, there is a continuous sedimentation of black precipitates as the centrifugal force increased from 0 to 10,000 g, without a change in UV absorbance. It is suspected that these dark precipitates consist of the non-UV active aggregated/bundled SWNTs, and remnants of the catalytic starting material.

However, beyond 10,000 g, the UV absorbance value begins to decrease consistently from a value of 2.3 at 10,000 g, to 1.6 at 24,000 g. Going by the premise that only exfoliated SWNTs, are UV active, we conclude that 10,000 g, is the optimum force of centrifugation, beyond which exfoliated SWNTs are additionally removed from the dispersion. Hence, the optimized centrifugation speed was therefore established to be 10,000 g.
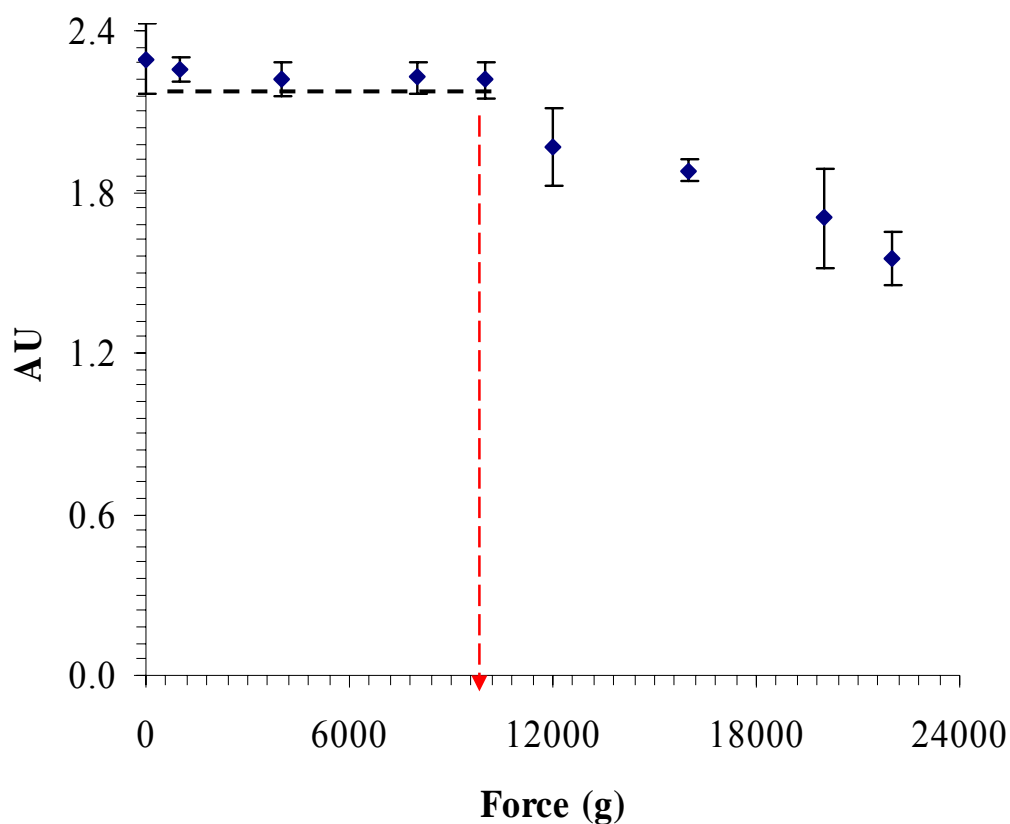
Figure 4.4   The effect of centrifugation on the UV absorbance of the 0.1 mg/mL AP-SWNT dispersed in 0.1 % w/v [12-3-12] aqueous gemini solution. The UV active dispersants remain in the dispersion until the threshold value of 10,000 g (arrow). Beyond 10,000 g, the heavier aggregates begin to sediment resulting in a lower UV absorbance.

To establish the presence of nano-sized dispersion (<100 nm) in solution, we monitored the particle size distribution (hydrodynamic diameter, D_H), of the dispersions above by dynamic light scattering. Even though SWNT are rod-like in nature, the Stokes-Einstein relationship approximation can be used for size analysis. However, since the polydispersity index (pdi) value for these dispersions is over the critical value of 0.2, the particle size distribution will be considered as polydispersed. This is understandable considering that there is a wide variation in AP-SWNT lengths from 1-5 μm (Table 4.1), and an expected variation in tube diameter. The polydispersity is therefore expected to arise from the varying sizes of SWNTs-surfactant conjugates.

Table 4.6   **Particle size distribution of AP-SWNT in 0.1 % (w/v) 12-3-12 gemini surfactant after centrifugation**

Centrifugal Forge (g)	D_H Peak Peak 1	Peak 2	Intensity Intensity 1	Intensity 2
24000	91	615.1	12.9	0.4
20000	91	615.8	11.5	0.3
16000	91	1990	11.3	0.1
12000	91	712.4	13.6	0.3
10000	91	458.7	13.5	0.6
8000	91	5560	12.2	0.2
5000	122.4	5560	12.2	0.2
2000	141.8	5560	11.6	0.2
1000	190.1	1106	13.3	0.4
0	295.3	5560	8.2	0.7

The dispersions obtained at all centrifugation speeds yielded a mixture of nano-sized particles (<100 nm) and macro-dispersions (from metallic and carbonaceous impurities and non-exfoliated bundles) resulting in the poly-dispersed sizes shown in Fig. 4.5 (0 centrifugation). The size of the particles in the CNT dispersions are difficult to interpret due to the polydispersity

imposed by the varying sizes of individual bundles, and aggregates of non-dispersed carbonaceous impurities.

Hence, an interpretation of the size distribution will focus on minimum D_H at the defined centrifugal force, and the corresponding intensity at the defined hydrodynamic diameter (Figure 4.5). Figure 4.5 A shows a plot of the particle size distribution for each sample, while figure 4.5 B shows in detail, the shift towards smaller diameter (particle size), as the centrifugal force is increased.

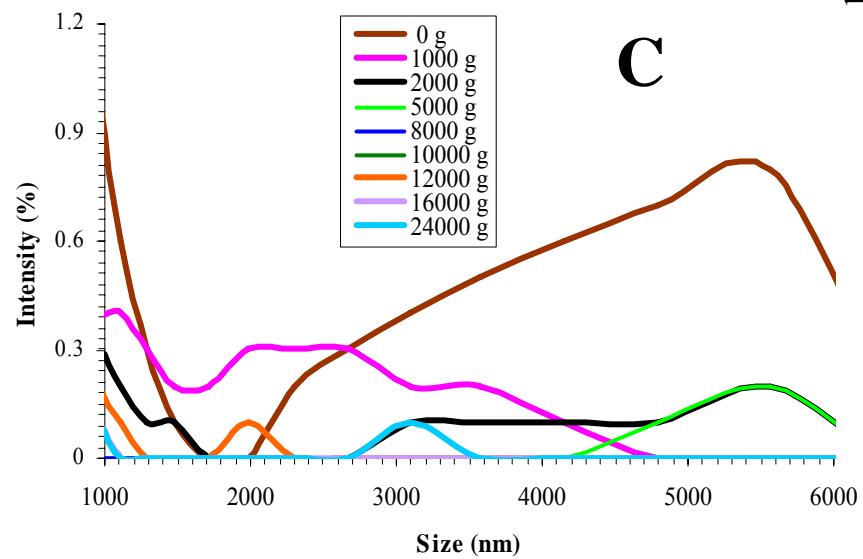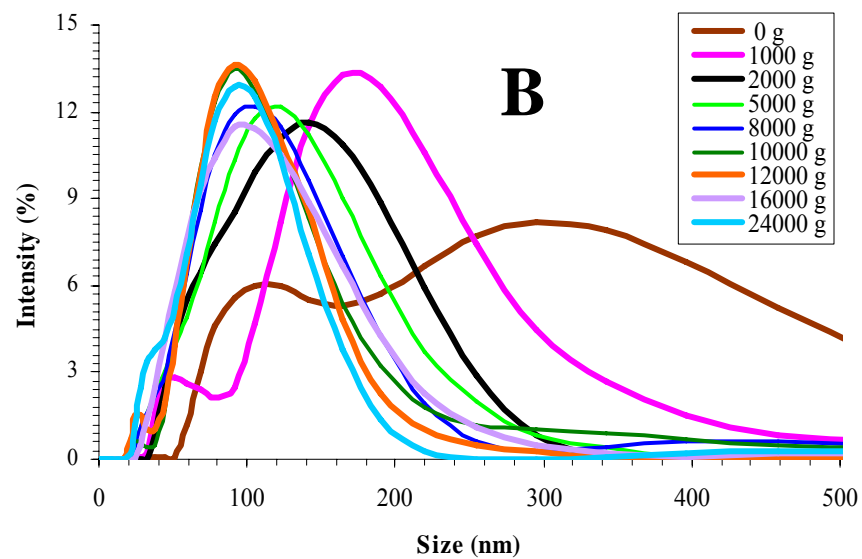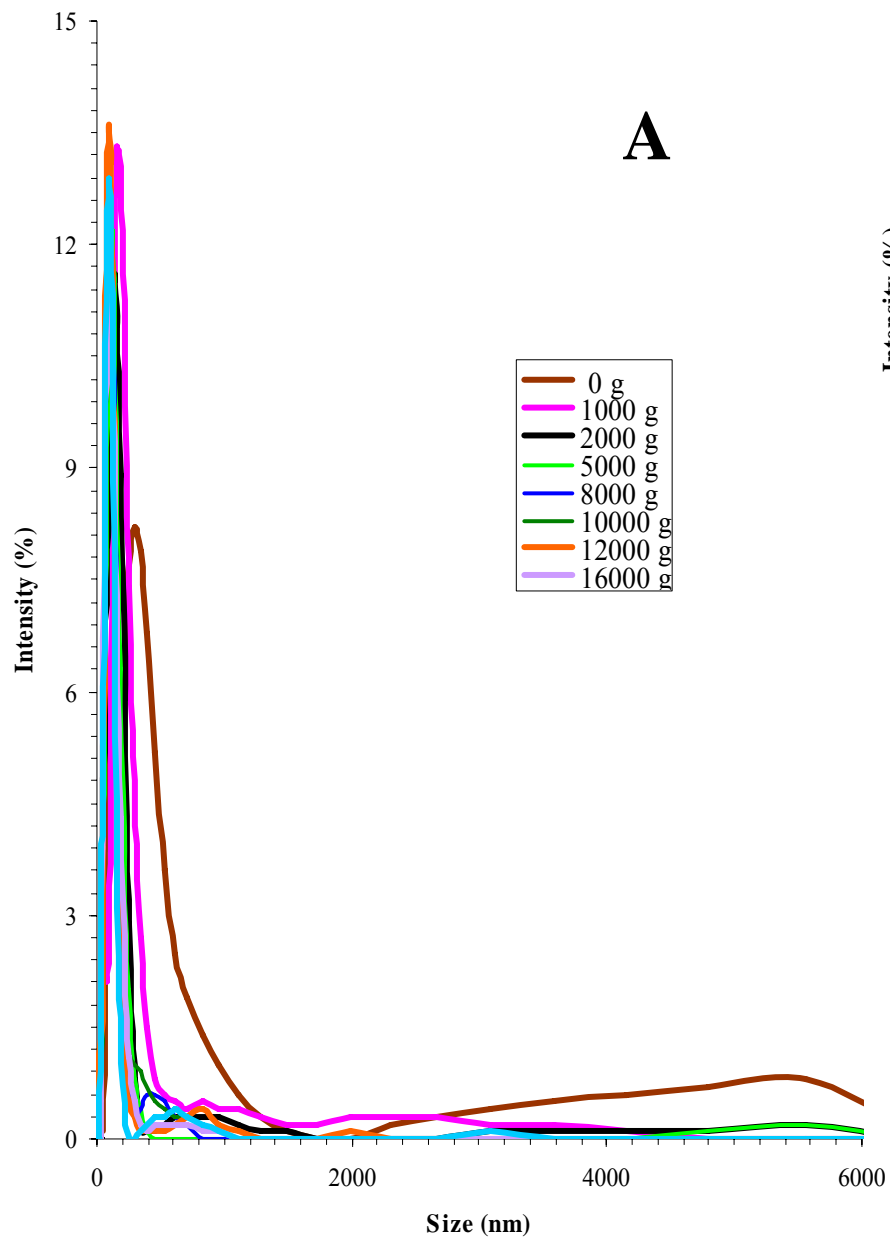Figure 4.5   The hydrodynamic size (diameter) distribution of 0.1 mg/mL AP-SWNT (dispersed in 0.1 w/v 12-3-12 gemini surfactant) with varying centrifugal speed. (A) General distribution shows a size distribution spanning from 100 nm to macro sized particles of size > 6000 (B) Increasing the centrifugation from 0-10000 g results in a reduced minimum size value <100 nm, and (C) a corresponding absence larger aggregates > 100 nm

A look at the plots for the size distribution using this approach shows the removal of larger sized particles (>1 μm). A reduction in the particle size distribution of AP-SWNT is observed as the centrifugal force is increased from 0 to 8,000 g. An increase in the centrifugal force beyond 8,000 g, does not result in a further reduction D_H of 91 nm (See Table 4.4), with a relatively stable peak intensity of 11.3 -13.5 %. Similarly, all samples centrifuged at > 8000 g (except for 16,000 g) have only one other significant peak (i.e. with intensity > 0.1 %) after peak 1, has a size less than 500 nm (0.5 μm). However, for centrifugation below 8000 g, peak 1 appears to decrease as the centrifugal force is increased from 0 g (i.e 295.3 nm) through 5000 g (122.4), with a significant particle population of peak 2 at 5560 nm (except for 1000 g).

Based on the size distribution of AP-SWNT and the corresponding UV absorbance results, we conclude that the optimized centrifugal force of 10,000 g, removes most of the aggregated SWNT bundles/impurities, while yielding an increase in population of exfoliated SWNT in 0.1 w/v % 12-3-12.

4.4.2.3 *Optimizing dispersant concentration for maximum exfoliation*

For dispersion of SWNTs, it is necessary to identify the minimum amount of surfactant that produces a stable dispersion for obvious reasons. To this end, zeta potential of the as prepared dispersions, are used as a measure of stability for the dispersion. Hence, a consistently increasing zeta potential is an indication of binding of surfactant molecules onto the SWNT surface, while a saturation of absorbed surfactant molecules onto the SWNT surface is reflected by a stable zeta potential value. Figure 4.6 shows a zeta titration of 0.1 mg/mL AP-SWNT with 0.1 % w/v 12-3-12 gemini surfactant. Similar results have been obtained for P2-SWNT.
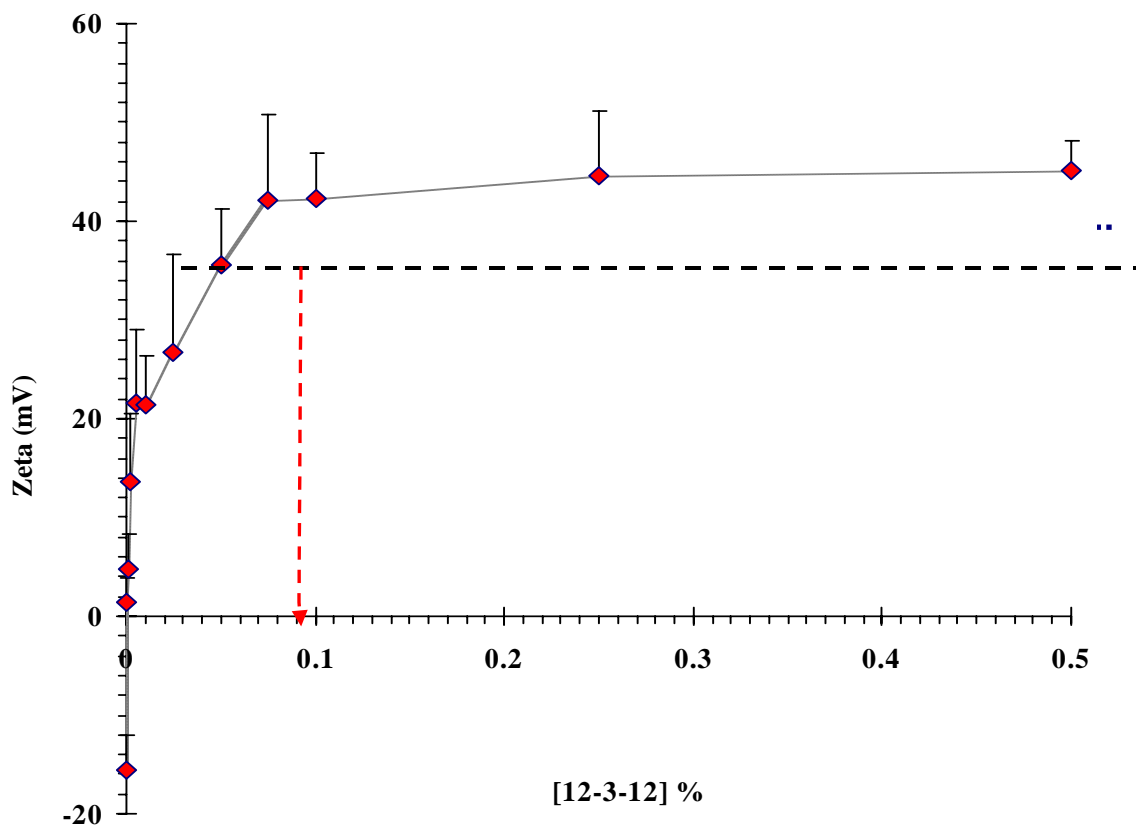
Figure 4.6   Concentration dependence of the ζ-potential (Zeta) distribution of 12-3-12 in 0.1mg/mL AP-SWNT. The zeta potential increases from -15 to 40 mV with a corresponding increase from 0 to~0.075 mg/mL of gemini surfactant. Above a concentration of 0.075 mg/mL, there is little change in the zeta potential, suggesting a saturation of binding to SWNT surface.

Dispersion of SWNT by ionic surfactants results from the interactions of the hydrophobic tail of the surfactant and the hydrophobic walls of the SWNT on one hand, and the polar head group with the polar solvent. By the Derjaguin, Landau, Verwey and Overbeek (DLVO) theory, a stable dispersion is expected for ionic dispersions with a -35 mV>ζ>35 mV. Figure 4.6 shows the ζ-potential titration of 12-3-12 in 0.10 mg/mL SWNT to determine the minimum amount of surfactant to produce high enough ζ-potential for a stable dispersion. For the 12-3-12 gemini surfactant, the minimum concentration required for dispersion is 0.05 % (dotted red line). The ζ-potential increased with increasing concentration over the range of 0 - 0.75 % ($^w/_v$), suggesting the continuous absorption of the 12-3-12 onto the SWNT. Beyond this range, the ζ-potential remains relatively constant indicating a saturation of the amount of gemini adsorbed onto the surface. It is observed that below the critical micelle concentration (*cmc*) of the 12-3-12 (0.89 mmol L^{-1} $\equiv$ 0.056 % ($^w/_v$)), the ζ-potential is not sufficient to retain SWNT in dispersion. Hence for the dispersion by subsequent gemini surfactants, the surfactant concentrations were chosen to be above their relative *cmc* values.

The hydrophobic alkyl tails of gemini surfactant provides the binding with the hydrophobic surface of SWNTs, while the positive charges of gemini head groups provide compatibility with the polar solvent aqueous media, thereby preventing aggregation due to electrostatic repulsion.

4.4.2.4   *Raman Spectroscopy*

The effectiveness of SWNT dispersion can be monitored by the increase in peak intensity of peaks in the RBM mode, and/or a shift in peak in the G-band [215, 242]. The interaction between nanotubes and dispersing agent is reflected by a peak shift or a peak

width change. The presence of binding to the exterior SWNT walls results in a shift in the vibration frequencies of both radial and tangential movement of the carbon atoms, which is generally indicative of strong attractive forces between a moiety and the CNT [109, 243]. Figures 4.7 and 4.8 show the Raman spectra of aqueous dispersions of SWNT in gemini surfactants and anionic and non-ionic surfactants respectively.

Dispersion of SWNT is accompanied by an observable shift in peak is observed in the G-band of the Raman spectrum for the gemini dispersion of SWNT (Figure 4.7). For all the gemini surfactants investigated, the G-band of the dispersion showed an upward peak shift from 1574.5 cm^{-1} (using SWNT dispersed in DDH_2O as reference-arrowed peak) to 1573.2 cm^{-1}. Generally, a shift in peak is indicative of an interactive force between the dispersing agent, and the SWNT.
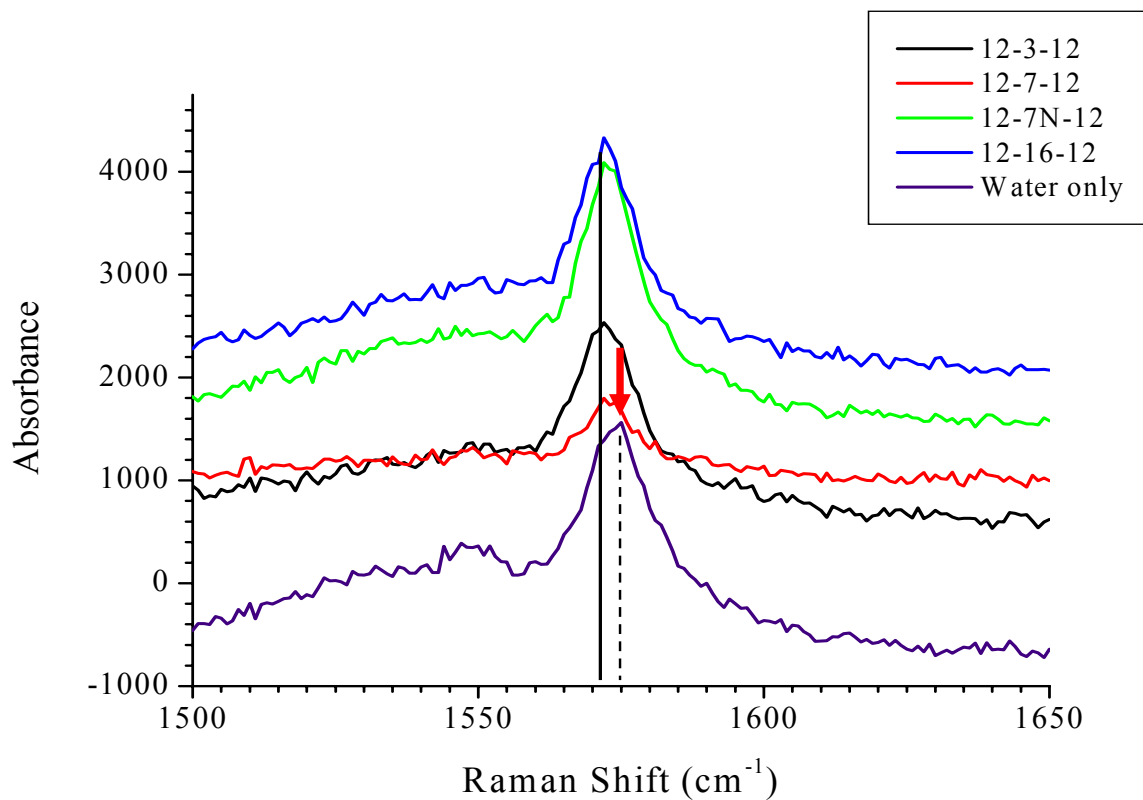
Figure 4.7   Raman spectra of aqueous dispersions of SWNT in 0.1 % w/v gemini
surfactant solutions, showing the G-band peak shift from 1574.5 cm^{-1} (for
the reference aggregated/precipitated dispersion in water) to ~1573.2 cm^{-1}
for the resulting stable dispersions SWNT in water.

Sinani et al. [109] explained the shift in peak as a consequence of the wrapping of the surfactant/polymer around the exfoliated SWNT. For the gemini surfactants, we postulate that an energetically favorable interaction will consist of a hydrophobic interaction between the alkyl tails of the surfactants and graphene walls of the SWNTs on one hand, and the interaction of the polar quaternary amine head-group of the gemini's with the solvent. This favourable interaction increases the effective diameter of the SWNT, and hence the energy required for vibrations to occur. This is reflected in the shift to higher frequency of Raman peaks [109].

The initial peak position is assumed to be that obtained for the non-dispersed SWNT in DDH_2O at 1574.5 cm^{-1} (Figure 4.8), while the dispersions have a consistent downshifted value of 1573.5 cm^{-1}. Irrespective of the mode of interaction, a positive interaction will invariably lead to an increase in the harmonic oscillator, and hence a shift.

Comparing the collated spectra, it is observed that, on successful dispersion of SWNTs in surfactants via sonication followed by centrifugation, individual exfoliation of SWNTs is achieved. This is revealed by the peak position of the G band peak.
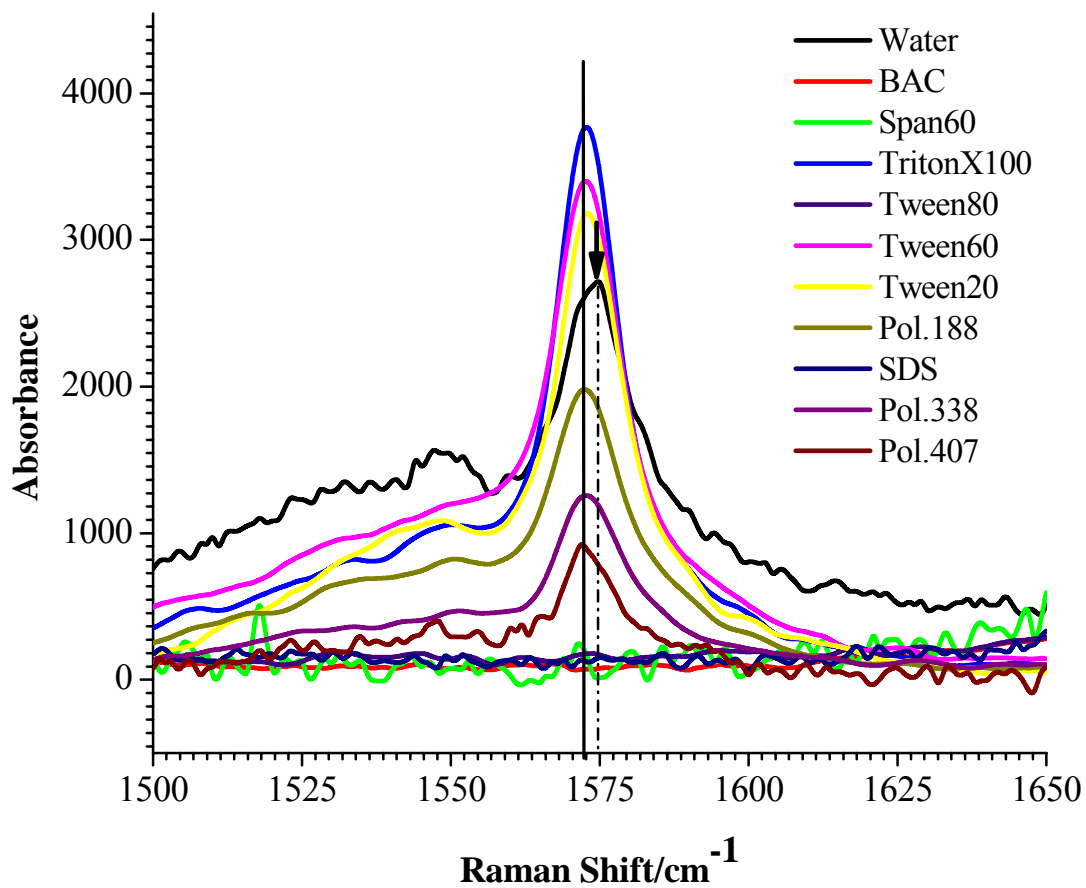
Figure 4.8   Raman spectra of the shift in G-band peak for SWNT dispersed in selected pharmaceutical excipients, relative to the non-dispersed (Water). The peak shift for nanodispersions is indicated by a peak shift, relative to the reference dispersion in water 1574.5 cm^{-1}(dotted line).

5.0 CONCLUSION AND FUTURE WORK

The findings of this research work shows that the long term goal of nanofluidic delivery of pharmaceutical agents using SWNTs can be explored after the two major issues of purity. The application of SWNTs in biological systems depends on their compatibility with hydrophilic environments; therefore, the solubilization of SWNTs in pharmaceutical solvents is essential. The dispersion of SWNTs depends on the purity and method of dispersion, and the characterization of the dispersion states of SWNTs (i.e. ascertaining that exfoliated SWNTs are present), can be achieved via sonication, followed by centrifugation.

5.1 Purity of SWNTs as potential pharmaceutical excipients
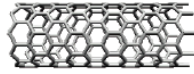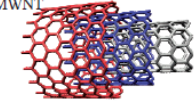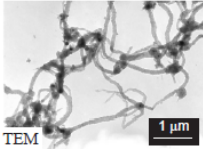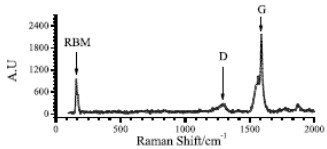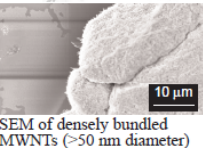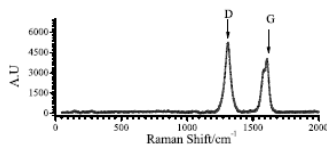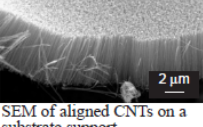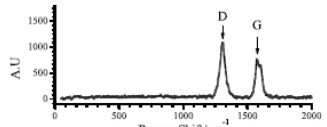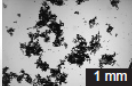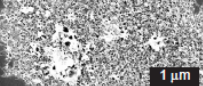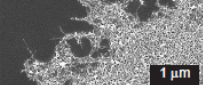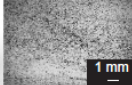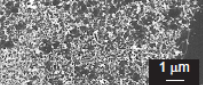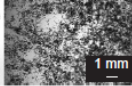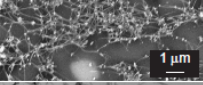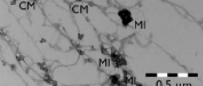
For purposes of pharmaceutical and biomedical uses, it is apparent that the quality of SWNTs could obviate research findings, mainly due to presence of unlisted impurities. This concern has led to formation of a working group by the International Organization for Standardization (ISO- TC229/WG2), mandated to establish and recommend protocols and standards for the measurement of CNT purity [244]. The work reported in this thesis, of inconsistent terminology used in describing the purity of SWNTs by various SWNT commercial sources, and the methods used to establish purity, buttress the need for these protocols and standards.

Additional to establishing the purity (amount of SWNT by weight), there is a need to identify the various impurities/residual catalytic materials present in each batch of material. It is therefore necessary that a paradigm of quality control and standards be established for these materials.

To this end, a mini-monograph is compiled (Figure 5.1), and serves as a starting reference, upon which a more complete monograph on the subject of CNTs as pharmaceutical materials can be developed. Issues of SWNT purity have been raised, and comparative evaluation methods such as EDX and Raman spectroscopy suggested. However, to make these methods stand alone, it is absolutely necessary to have an industry standard (reference material). As potential pharmaceutical excipients SWNTs are regarded as inert/nonactive components of dosage forms, but they are essential and necessary components of pharmaceutical preparations. Below is a summary of a collection of data to initiate the description of CNTs in general as pharmaceutical excipients (Figure 5.1).

A second stage of this discussion will involve the establishment of limits for the impurities inherent in the SWNTs (metallic and carbonaceous). However, these values can only be set after the toxicity of the impurities have been established and quantitative methods establishing the concentration of such impurities in a given sample.

Pharmaceutically relevant properties of carbon nanotubes

	Description	Specific data		
Chemical name (synonyms)	Carbon fullerene (carbon nanotubes, CNTs)			
Chemical family	Synthetic graphite	CAS number 7782-42-5 (graphite)		
Structural formula	Carbon (C)	Molecular weight 840 to >10 million	Purity > 95% desired	Melting point > 1000°C Specific gravity > 1
Types	SWNT	Diameter Outer: 1.0–3.0 nm Inner: 0.6–2.4 nm	Length Short: 0.5–2 µm Standard: 0.5–100 µm Specific surface area (typical) 300–600 m²/g	Electronic properties Metallic (armchair; 10,10) Semi-conducting (zig-zag; 10,0)
	MWNT	Diameter Outer: 2.5–100 nm Inner: 1.5–15 nm Interlayer separation 0.3–0.4 nm	Length Short: 0.5–2 µm Standard: 0.5–200 µm Specific surface area (typical) 40–300 m²/g	Electronic properties Mixture of conducting and semiconducting tubes

Physical and chemical properties

		Visible	EM	Raman spectra
Organoleptic properties	SWNT Granular or fluffy black power		TEM	
	MWNT Granular or fluffy black power		SEM of densely bundled MWNTs (>50 nm diameter)	
	Aligned CNTs Black fluffy velvet-like sheet of aligned CNTs*		SEM of aligned CNTs on a substrate support	

	Solution medium	Visible	EM	Description of visible and EM images
Solubility properties of pristine SWNTs†	Water: insoluble			Visible: Light micrograph of SWNTs falling out of water. Insert shows SWNTs fall out of water soon after sonication. SEM: Loosely packed arrangement of SWNTs dispersed in water.
	Ethanol: insoluble			Visible: Light micrograph of SWNTs falling out of ethanol. Insert shows SWNTs fall out of ethanol soon after sonication. SEM: SWNT dispersed in ethanol, showing network of SWNT bundles.
	Propylene glycol: swollen			Visible: Light micrograph of swollen dispersion of SWNTs in propylene glycol. SEM: Dispersion shows less aggregation of SWNTs in propylene glycol.
	DMSO: swollen			Visible: Light micrograph of swollen dispersion of SWNTs in DMSO. SEM: Dispersion shows less aggregation of SWNTs in DMSO.
	SDS: soluble			Visible: Light micrograph of well-dispersed SWNTs in SDS, showing few aggregates. SEM: Dispersion shows smaller bundles of SWNTs.
Impurities	Metal oxides: in SWNT <5% Carbonaceous material: 0.1-90% w/w			TEM image of SWNTs. Impurities appear as dark blotches, labeled metallic impurities (MI) and carbonaceous material (CM), on the SWNT bundle.

* Visible and SEM images of CNTs courtesy of Dr, Jun Chen, Intelligent Polymer Research Institute, Univ. of Wollongong, Australia

Figure 5.1   A collation of the physical properties of CNTs, organoleptic properties, and dispersion states in representative pharmaceutical solvents [59, 64].

5.2   Dispersion of SWNT

The dispersion of SWNT in pharmaceutical excipients is the first step towards their incorporation towards their incorporation in drug delivery. Even though SWNT dispersion has been achieved with a variety of pharmaceutical solvents, the dispersion technique, facilitate reproducible and quantifiable dispersions. Evaluation of SWNT dispersions using the methods of microscopy, Raman spectroscopy to ascertain exfoliation of bundles, colloidal dispersion stability (ζ-potential) of the exfoliated bundles and a time dependent stability study of SWNT dispersions using pharmaceutical excipients established that dispersion in ionic surfactants, such as the dicationic gemini surfactant 12-3-12, depends largely on ζ-potential. SWNT dispersion should have a uniform dark brown/black coloration, with no visible particulates when examined under a light microscope.

5.3   Future Work

5.3.1   Magnetism

To effectively deliver therapeutic molecules across *stratum corneum* membrane as envisaged in our initial model, three main issues will have to be investigated; the source of magnetism observed for aggregated SWNTs, and the optimized magnetic field strength required to effectively penetrating the intact membrane.

5.3.2 Purity of SWNT

Haven qualitatively established the presence of metallic impurities in SWNT samples, it is essential that the quantitative amounts of these impurities be established to enable the establishment of limits for quantified impurities within a sample. To this end, the following can be investigated;

i.   The quantitative determination of the carbonaceous impurities by TGA

ii. The quantitative evaluation of metallic impurity concentration in SWNT samples

5.3.3 Dispersion and Characterization

The dispersion results presented in this thesis clearly the efficient dispersion of SWNTs in selected pharmaceutical solvents/surfactants.

Considering the promise of gemini surfactants, the relation between surfactant concentration, and the dispersion efficiency is not clear. Further information, possibly leading to a better understanding of the factors controlling dispersion can be achieved by;

i.   Establishing the minimum concentration of gemini surfactants investigated required to produce a stable dispersion, for all gemini surfactants investigated, and

ii.   Establish if the minimum amount of gemini surfactant required for dispersion is a factor of SWNT purity

For the non-ionic surfactants, it is essential to investigate the relation between the HLB values, and the respective molecular weights of the surfactants. This will also include a

i.   Comparison of the dispersion efficiency of at least six surfactants within the same family of surfactants with different MW and HLB values (pluronics and poloxamers), and

ii.   Investigate the effect HLB values for mixed dispersing solvents on dispersion efficiency (HLB values from 4-20).

REFERENCES

1.   A. Bianco, K. Kostarelos, C.D. Partidos, and M. Prato, Biomedical applications of functionalised carbon nanotubes, Chem Commun (Camb). (2005) 571-577.

2.   K. Heilmann, Innovations in drug delivery systems, Curr Med Res Opin. 8 Suppl 2 (1983) 3-9.

3.   N. Venkatesan, J. Yoshimitsu, Y. Ito, N. Shibata, and K. Takada, Liquid filled nanoparticles as a drug delivery tool for protein therapeutics, Biomaterials. 26 (2005) 7154-7163.

4.   W. Wu, S. Wieckowski, G. Pastorin, M. Benincasa, C. Klumpp, J.P. Briand, R. Gennaro, M. Prato, and A. Bianco, Targeted delivery of amphotericin B to cells by using functionalized carbon nanotubes, Angew Chem Int Ed Engl. 44 (2005) 6358-6362.

5.   J. Chen, M.A. Hamon, H. Hu, Y. Chen, A.M. Rao, P.C. Eklund, and R.C. Haddon, Solution properties of single-walled carbon nanotubes, Science. 282 (1998) 95-98.

6.   Z. Yinghuai, A.T. Peng, K. Carpenter, J.A. Maguire, N.S. Hosmane, and M. Takagaki, Substituted carborane-appended water-soluble single-wall carbon nanotubes: new approach to boron neutron capture therapy drug delivery, J Am Chem Soc. 127 (2005) 9875-9880.

7.   J. Chattopadhyay, F. Cortez, S. Chakraborty, N. Slater, and W. Billups, Synthesis of water soluble PEGylated single-walled carbon nanotubes, Chem. Mater. 18 (2006) 6864-5868.

8.   H. Liu, W. Cai, L. He, N. Nakayama, K. Chen, X. Sun, X. Chen, and H. Dai, *In vivo* biodistribution and highly efficient tumor targeting of carbon nanotubes in mice, Nature Nanotech. 2 (2007) 47-52.

9.   N.W. Kam, Z. Liu, and H. Dai, Functionalization of carbon nanotubes via cleavable disulfide bonds for efficient intracellular delivery of siRNA and potent gene silencing, J Am Chem Soc. 127 (2005) 12492-12493.

10.   Z. Liu, S.M. Tabakman, Z. Chen, and H. Dai, Preparation of carbon nanotube bioconjugates for biomedical applications, Nat. Protoc. 4 (2009) 1372-1382.

11.   D. Pantarotto, J.P. Briand, M. Prato, and A. Bianco, Translocation of bioactive peptides across cell membranes by carbon nanotubes, Chem Commun (Camb). (2004) 16-17.

12.   N.W. Kam, Z. Liu, and H. Dai, Carbon nanotubes as intracellular transporters for proteins and DNA: An investigation of the uptake mechanism and pathway, Angew Chem Int Ed Engl. 45 (2006) 577-581.

13. C. Salvador-Morales, E. Flahaut, E. Sim, J. Sloan, M.L. Green, and R.B. Sim, *Complement activation and protein adsorption by carbon nanotubes*, Mol Immunol. 43 (2006) 193-201.

14. D. Pantarotto, C.D. Partidos, J. Hoebeke, F. Brown, E. Kramer, J.P. Briand, S. Muller, M. Prato, and A. Bianco, *Immunization with peptide-functionalized carbon nanotubes enhances virus-specific neutralizing antibody responses*, Chem Biol. 10 (2003) 961-966.

15. D. Pantarotto, C.D. Partidos, R. Graff, J. Hoebeke, J.P. Briand, M. Prato, and A. Bianco, *Synthesis, structural characterization, and immunological properties of carbon nanotubes functionalized with peptides*, J Am Chem Soc. 125 (2003) 6160-6164.

16. N.W. KamH. Dai, *Carbon nanotubes as intracellular protein transporters: generality and biological functionality*, J Am Chem Soc. 127 (2005) 6021-6026.

17. N.W. Kam, T.C. Jessop, P.A. Wender, and H. Dai, *Nanotube molecular transporters: internalization of carbon nanotube-protein conjugates into Mammalian cells*, J Am Chem Soc. 126 (2004) 6850-6851.

18. A. Bianco, J. Hoebeke, S. Godefroy, O. Chaloin, D. Pantarotto, J.P. Briand, S. Muller, M. Prato, and C.D. Partidos, *Cationic carbon nanotubes bind to CpG oligodeoxynucleotides and enhance their immunostimulatory properties*, J Am Chem Soc. 127 (2005) 58-59.

19. Z. Zhang, X. Yang, Y. Zhang, B. Zeng, S. Wang, T. Zhu, R.B. Roden, Y. Chen, and R. Yang, *Delivery of telomerase reverse transcriptase small interfering RNA in complex with positively charged single-walled carbon nanotubes suppresses tumor growth*, Clin Cancer Res. 12 (2006) 4933-4939.

20. A. Bianco, *Carbon nanotubes for the delivery of therapeutic molecules*, Expert Opin Drug Deliv. 1 (2004) 57-65.

21. D. Pantarotto, R. Singh, D. McCarthy, M. Erhardt, J.P. Briand, M. Prato, K. Kostarelos, and A. Bianco, *Functionalized carbon nanotubes for plasmid DNA gene delivery*, Angew Chem Int Ed Engl. 43 (2004) 5242-5246.

22. R. Singh, D. Pantarotto, D. McCarthy, O. Chaloin, J. Hoebeke, C.D. Partidos, J.P. Briand, M. Prato, A. Bianco, and K. Kostarelos, *Binding and condensation of plasmid DNA onto functionalized carbon nanotubes: toward the construction of nanotube-based gene delivery vectors*, J Am Chem Soc. 127 (2005) 4388-4396.

23. D. Cai, J.M. Mataraza, Z.H. Qin, Z. Huang, J. Huang, T.C. Chiles, D. Carnahan, K. Kempa, and Z. Ren, *Highly efficient molecular delivery into mammalian cells using carbon nanotube spearing*, Nat Methods. 2 (2005) 449-454.

24. N.W. Kam, M. O'Connell, J.A. Wisdom, and H. Dai, Carbon nanotubes as multifunctional biological transporters and near-infrared agents for selective cancer cell destruction, Proc Natl Acad Sci U S A. 102 (2005) 11600-11605.

25. F. Barthel, J.S. Remy, J.P. Loeffler, and J.P. Behr, Gene transfer optimization with lipospermine-coated DNA, DNA Cell Biol. 12 (1993) 553-560.

26. A.J. Lin, N.L. Slack, A. Ahmad, I. Koltover, C.X. George, C.E. Samuel, and C.R. Safinya, Structure and structure-function studies of lipid/plasmid DNA complexes, J Drug Target. 8 (2000) 13-27.

27. M. Nahar, T. Dutta, S. Murugesan, A. Asthana, D. Mishra, V. Rajkumar, M. Tare, S. Saraf, and N.K. Jain, Functional polymeric nanoparticles: an efficient and promising tool for active delivery of bioactives, Crit Rev Ther Drug Carrier Syst. 23 (2006) 259-318.

28. M.R. McDevitt, D. Chattopadhyay, B.J. Kappel, J.S. Jaggi, S.R. Schiffman, C. Antczak, J.T. Njardarson, R. Brentjens, and D.A. Scheinberg, Tumor targeting with antibody-functionalized, radiolabeled carbon nanotubes, J Nucl Med. 48 (2007) 1180-1189.

29. X. Zhang, L. Meng, Q. Lu, Z. Fei, and P.J. Dyson, Targeted delivery and controlled release of doxorubicin to cancer cells using modified single wall carbon nanotubes, Biomaterials. 30 (2009) 6041-6047.

30. R. Yang, X. Yang, Z. Zhang, Y. Zhang, S. Wang, Z. Cai, Y. Jia, Y. Ma, C. Zheng, Y. Lu, R. Roden, and Y. Chen, Single-walled carbon nanotubes-mediated in vivo and in vitro delivery of siRNA into antigen-presenting cells, Gene Ther. 13 (2006) 1714-1723.

31. V. Lovat, D. Pantarotto, L. Lagostena, B. Cacciari, M. Grandolfo, M. Righi, G. Spalluto, M. Prato, and L. Ballerini, Carbon nanotube substrates boost neuronal electrical signaling, Nano Lett. 5 (2005) 1107-1110.

32. M.P. Mattson, R.C. Haddon, and A.M. Rao, Molecular functionalization of carbon nanotubes and use as substrates for neuronal growth, J Mol Neurosci. 14 (2000) 175-182.

33. H. Hu, Y. Ni, V. Montana, R.C. Haddon, and V. Parpura, Chemically functionalized carbon nanotubes as substrates for neuronal growth, Nano Lett. 4 (2004) 507-511.

34. H. Hu, Y. Ni, S.K. Mandal, V. Montana, B. Zhao, R.C. Haddon, and V. Parpura, Polyethyleneimine functionalized single-walled carbon nanotubes as a substrate for neuronal growth, J Phys Chem B Condens Matter Mater Surf Interfaces Biophys. 109 (2005) 4285-4289.

35.   X. Zhang, S. Prasad, S. Niyogi, A. Morgan, M. Ozkan, and C. Ozkan, Guided neurite growth on patterned carbon nanotubes, Sensors and Actuators B. 106 (2005) 843–850.

36.   K. Matsumoto, C. Sato, Y. Naka, A. Kitazawa, R.L. Whitby, and N. Shimizu, Neurite outgrowths of neurons with neurotrophin-coated carbon nanotubes, J Biosci Bioeng. 103 (2007) 216-220.

37.   E. JanN.A. Kotov, Successful differentiation of mouse neural stem cells on layer-by-layer assembled single-walled carbon nanotube composite, Nano Lett. 7 (2007) 1123-1128.

38.   A.V. Liopo, M.P. Stewart, J. Hudson, J.M. Tour, and T.C. Pappas, Biocompatibility of native and functionalized single-walled carbon nanotubes for neuronal interface, J Nanosci Nanotechnol. 6 (2006) 1365-1374.

39.   K. Wang, H.A. Fishman, H. Dai, and J.S. Harris, Neural stimulation with a carbon nanotube microelectrode array, Nano Lett. 6 (2006) 2043-2048.

40.   T. Gabay, E. Jakobs, E. Ben-Jacob, and Y. Hanein, Engineered self-organization of neural networks using carbon nanotube clusters, Physica A. 350 (2005) 611-621.

41.   R. Sorkin, T. Gabay, P. Blinder, D. Baranes, E. Ben-Jacob, and Y. Hanein, Compact self-wiring in cultured neural networks, J Neural Eng. 3 (2006) 95-101.

42.   Y. Ni, H. Hu, E.B. Malarkey, B. Zhao, V. Montana, R.C. Haddon, and V. Parpura, Chemically functionalized water soluble single-walled carbon nanotubes modulate neurite outgrowth, J Nanosci Nanotechnol. 5 (2005) 1707-1712.

43.   J.L. McKenzie, M.C. Waid, R. Shi, and T.J. Webster, Decreased functions of astrocytes on carbon nanofiber materials, Biomaterials. 25 (2004) 1309-1317.

44.   K. Shaitan, Y. Tourleigh, D. Golik, and M. Kirpichnikov, Computer-aided molecular design of nanocontainers for inclusion and targeted delivery of bioactive compounds, J Drug Del Sci Tech. 16 (2006) 253-258.

45.   A. Leonhardt, I. Monch, A. Meye, S. Hampel, and B. Buchner, Synthesis of ferromagnetic filled carbon nanotubes and their biomedical application, Advances in Science and Tech. 49 (2006) 74-78.

46.   B.M. Kim, S. Qian, and H.H. Bau, Filling carbon nanotubes with particles, Nano Lett. 5 (2005) 873-878.

47.   E. Dujardin, T.W. Ebbesen, H. Hiura, and K. Tanigaki, Capillary wetting of carbon nanotubes, Science. 265 (1994) 1850-1852.

48. D. Ugarte, A. Chatelain, and W. de Heer, Nanocapillarity and chemistry in carbon nanotubes, Science. 274 (1996) 1897-1899.

49. G. Korneva, H. Ye, Y. Gogotsi, D. Halverson, G. Friedman, J.C. Bradley, and K.G. Kornev, Carbon nanotubes loaded with magnetic particles, Nano Lett. 5 (2005) 879-884.

50. M. Majumder, N. Chopra, R. Andrews, and B.J. Hinds, Nanoscale hydrodynamics: enhanced flow in carbon nanotubes, Nature. 438 (2005) 44.

51. D. Cui, C. Ozkan, Y. Kong, and H. Gao, Encapsulation of Pt-labeled DNA inside carbon nanotubes, MCB. 1 (2004) 113-121.

52. T. Kaneko, T. Okada, and R. Hatakeyama, DNA encapsulation inside carbon nanotubes using micro electrolyte plasmas, Contrib. Plasma Phys. 47 (2007) 57-63.

53. I.C. YehG. Hummer, Nucleic acid transport through carbon nanotube membranes, Proc Natl Acad Sci U S A. 101 (2004) 12177-12182.

54. A.H. Barber, S.R. Cohen, and H.D. Wagner, Static and dynamic wetting measurements of single carbon nanotubes, Phys Rev Lett. 92 (2004) 186103.

55. S. Nadarajan, P. Katsikis, and E. Papazoglou, Loading carbon nanotubs with viscous fluids and nanoparticles-a simpler approach, Appl. Phys. A. 89 (2007) 437-442.

56. L. Huang, S.P. Lau, H.Y. Yang, E.S. Leong, S.F. Yu, and S. Prawer, Stable superhydrophobic surface via carbon nanotubes coated with a ZnO thin film, J Phys Chem B Condens Matter Mater Surf Interfaces Biophys. 109 (2005) 7746-7748.

57. L. Zhu, J. Xu, Y. Xiu, Y. Sun, D.W. Hess, and C.P. Wong, Electrowetting of aligned carbon nanotube films, J Phys Chem B Condens Matter Mater Surf Interfaces Biophys. 110 (2006) 15945-15950.

58. A.D. Maynard, P.A. Baron, M. Foley, A.A. Shvedova, E.R. Kisin, and V. Castranova, Exposure to carbon nanotube material: aerosol release during the handling of unrefined single-walled carbon nanotube material, J Toxicol Environ Health A. 67 (2004) 87-107.

59. M. FoldvariM. Bagonluri, Carbon nanotubes as functional excipients for nanomedicines: II. Drug delivery and biocompatibility issues, Nanomedicine. 4 (2008) 183-200.

60. A. Bianco, J. Hoebeke, K. Kostarelos, M. Prato, and C.D. Partidos, Carbon nanotubes: on the road to deliver, Curr Drug Deliv. 2 (2005) 253-259.

61.   A. Bianco, K. Kostarelos, and M. Prato, Applications of carbon nanotubes in drug delivery, Curr Opin Chem Biol. 9 (2005) 674-679.

62.   V. Georgakilas, K. Kordatos, M. Prato, D.M. Guldi, M. Holzinger, and A. Hirsch, Organic functionalization of carbon nanotubes, J Am Chem Soc. 124 (2002) 760-761.

63.   R. Krajcik, A. Jung, A. Hirsch, W. Neuhuber, and O. Zolk, Functionalization of carbon nanotubes enables non-covalent binding and intracellular delivery of small interfering RNA for efficient knock-down of genes, Biochem Biophys Res Commun. 369 (2008) 595-602.

64.   M. FoldvariM. Bagonluri, Carbon nanotubes as functional excipients for nanomedicines: I. Pharmaceutical properties, Nanomedicine. 4 (2008) 173-182.

65.   C. Klumpp, K. Kostarelos, M. Prato, and A. Bianco, Functionalized carbon nanotubes as emerging nanovectors for the delivery of therapeutics, Biochim Biophys Acta. 1758 (2006) 404-412.

66.   S. Dhar, Z. Liu, J. Thomale, H. Dai, and S.J. Lippard, Targeted single-wall carbon nanotube-mediated Pt(IV) prodrug delivery using folate as a homing device, J Am Chem Soc. 130 (2008) 11467-11476.

67.   W.Z. Yuan, J.Z. Sun, Y. Dong, M. Ha?ussier, F. Yang, H.P. Xu, A. Qin, J.W.Y. Lam, Q. Zheng, and B.Z. Tang, Wrapping carbon nanotubes in pyrene-containing poly(phenylacetylene) chains: Solubility, stability, light emission, and surface photovoltaic properties, Macromolecules. 39 (2006) 8011-8020.

68.   Z. Liu, K. Chen, C. Davis, S. Sherlock, Q. Cao, X. Chen, and H. Dai, Drug delivery with carbon nanotubes for in vivo cancer treatment, Cancer Res. 68 (2008) 6652-6660.

69.   M.E. Itkis, D.E. Perea, R. Jung, S. Niyogi, and R.C. Haddon, Comparison of analytical techniques for purity evaluation of single-walled carbon nanotubes, J Am Chem Soc. 127 (2005) 3439-3448.

70.   J. Giles, Growing nanotech trade hit by questions over quality, Nature. 432 (2004) 791.

71.   R.G. Manning, S. Lane, S. Dressman, W.W. Hauck, R.L. Williams, P.J. Palermo, M.W. Borer, D. Fay, A.R. Gomas, S. Jin, J. Lee, and M.I. Santoro, The application of uncertainty to USP's compendial reference standards program: Certified reference materials, Pharmacopeial Forum. 33 (2007) 1300-1305.

72.   R.L. Williams, Official USP Reference Standards: metrology concepts, overview, and scientific issues and opportunities, J Pharm Biomed Anal. 40 (2006) 3-15.

73. C.W. Lam, J.T. James, R. McCluskey, S. Arepalli, and R.L. Hunter, A review of carbon nanotube toxicity and assessment of potential occupational and environmental health risks, Crit Rev Toxicol. 36 (2006) 189-217.

74. C.W. Lam, J.T. James, R. McCluskey, and R.L. Hunter, Pulmonary toxicity of single-wall carbon nanotubes in mice 7 and 90 days after intratracheal instillation, Toxicol Sci. 77 (2004) 126-134.

75. A.A. Shvedova, V. Castranova, E.R. Kisin, D. Schwegler-Berry, A.R. Murray, V.Z. Gandelsman, A. Maynard, and P. Baron, Exposure to carbon nanotube material: assessment of nanotube cytotoxicity using human keratinocyte cells, J Toxicol Environ Health A. 66 (2003) 1909-1926.

76. D.B. Warheit, B.R. Laurence, K.L. Reed, D.H. Roach, G.A. Reynolds, and T.R. Webb, Comparative pulmonary toxicity assessment of single-wall carbon nanotubes in rats, Toxicol Sci. 77 (2004) 117-125.

77. J. Muller, F. Huaux, N. Moreau, P. Misson, J.F. Heilier, M. Delos, M. Arras, A. Fonseca, J.B. Nagy, and D. Lison, Respiratory toxicity of multi-wall carbon nanotubes, Toxicol Appl Pharmacol. 207 (2005) 221-231.

78. A.A. Shvedova, E.R. Kisin, R. Mercer, A.R. Murray, V.J. Johnson, A.I. Potapovich, Y.Y. Tyurina, O. Gorelik, S. Arepalli, D. Schwegler-Berry, A.F. Hubbs, J. Antonini, D.E. Evans, B.K. Ku, D. Ramsey, A. Maynard, V.E. Kagan, V. Castranova, and P. Baron, Unusual inflammatory and fibrogenic pulmonary responses to single-walled carbon nanotubes in mice, Am J Physiol Lung Cell Mol Physiol. 289 (2005) L698-708.

79. K. Pulskamp, S. Diabate, and H.F. Krug, Carbon nanotubes show no sign of acute toxicity but induce intracellular reactive oxygen species in dependence on contaminants, Toxicol Lett. 168 (2007) 58-74.

80. C. Gao, W. Li, H. Morimoto, Y. Nagaoka, and T. Maekawa, Magnetic carbon nanotubes: synthesis by electrostatic self-assembly approach and application in biomanipulations, J Phys Chem B Condens Matter Mater Surf Interfaces Biophys. 110 (2006) 7213-7220.

81. C.M. Sayes, F. Liang, J.L. Hudson, J. Mendez, W. Guo, J.M. Beach, V.C. Moore, C.D. Doyle, J.L. West, W.E. Billups, K.D. Ausman, and V.L. Colvin, Functionalization density dependence of single-walled carbon nanotubes cytotoxicity in vitro, Toxicol Lett. 161 (2006) 135-142.

82. M.S. Dresselhaus, G. Dresselhaus, J.C. Charlier, and E. Hernandez, Electronic, thermal and mechanical properties of carbon nanotubes, Philos Transact A Math Phys Eng Sci. 362 (2004) 2065-2098.

83. E. Joselevich, Electronic structure and chemical reactivity of carbon nanotubes: a chemist's view, Chemphyschem. 5 (2004) 619-624.

84. D. Danailov, P. Keblinski, S. Nayak, and P.M. Ajayan, Bending properties of carbon nanotubes encapsulating solid nanowires, J Nanosci Nanotechnol. 2 (2002) 503-507.

85. H. Trotter, R. Phillips, B. Ni, Y. Hu, S.B. Sinnott, P.T. Mikulski, and J.A. Harrison, Effect of filling on the compressibility of carbon nanotubes: predictions from molecular dynamics simulations, J Nanosci Nanotechnol. 5 (2005) 536-541.

86. S. Iijima, Helical microtubules of graphitic carbon, Nature. 354 (1991) 56-58.

87. K. Awasthi, A. Srivastava, and O.N. Srivastava, Synthesis of carbon nanotubes, J Nanosci Nanotechnol. 5 (2005) 1616-1636.

88. Y. Wang, Z. Zhang, H. Liu, X. Xu, G. Pan, Z. Guo, Y. Liu, X. Han, and G. Lan, The effect of catalyst concentration on the synthesis of single-wall carbon nanotubes, Spectrochim Acta A Mol Biomol Spectrosc. 58 (2002) 2089-2095.

89. J.B. Nagy, G. Bister, A. Fonseca, D. Mehn, Z. Konya, I. Kiricsi, Z.E. Horvath, and L.P. Biro, On the growth mechanism of single-walled carbon nanotubes by catalytic carbon vapor deposition on supported metal catalysts, J Nanosci Nanotechnol. 4 (2004) 326-345.

90. A. Thess, R. Lee, P. Nikolaev, H. Dai, P. Petit, J. Robert, C. Xu, Y.H. Lee, S.G. Kim, A.G. Rinzler, D.T. Colbert, G.E. Scuseria, D. Tomanek, J.E. Fischer, and R.E. Smalley, Crystalline ropes of metallic carbon nanotubes, Science. 273 (1996) 483-487.

91. M. Jose-Yacaman, Catalytic growth of carbon microtubules with fullerene structure, Appl Phys Letts. 62 (1993) 657-659.

92. M.S. Dresselhaus, G. Dresselhaus, A. Jorio, A.G. Souza Filho, M.A. Pimenta, and R. Saito, Single nanotube Raman spectroscopy, Acc Chem Res. 35 (2002) 1070-1078.

93. R. Vajtai, B.Q. Wei, and P.M. Ajayan, Controlled growth of carbon nanotubes, Philos Transact A Math Phys Eng Sci. 362 (2004) 2143-2160.

94. B.O. Boskovic, V. Stolojan, R.U. Khan, S. Haq, and S.R. Silva, Large-area synthesis of carbon nanofibres at room temperature, Nat Mater. 1 (2002) 165-168.

95. C. BaddourC. Briens, Carbon nanotube synthesis: A review, Int J Chem Reactor Eng. 3 (2005) R3-R9.

96. B. Kleinsorge, V.B. Golovko, S. Hofmann, J. Geng, D. Jefferson, J. Robertson, and B.F. Johnson, Growth of aligned carbon nanofibres over large areas using colloidal catalysts at low temperatures, Chem Commun (Camb). (2004) 1416-1417.

97.   E. Joselevich, H. Dai, J. Liu, K. Hata, and A.H. Windle, *Carbon Nanotube Synthesis and Organization*, in *Carbon Nanotubes, Topics Appl. Physics*, A. Jorio, et al., Editors. 2008, Springer-Verlag Berlin Heidelberg: Berlin.

98.   A. Jorio, R. Saito, J.H. Hafner, C.M. Lieber, M. Hunter, T. McClure, G. Dresselhaus, and M.S. Dresselhaus, Structural (n, m) determination of isolated single-wall carbon nanotubes by resonant Raman scattering, Phys Rev Lett. 86 (2001) 1118-1121.

99.   P.M. Raja, J. Connolley, G.P. Ganesan, L. Ci, P.M. Ajayan, O. Nalamasu, and D.M. Thompson, Impact of carbon nanotube exposure, dosage and aggregation on smooth muscle cells, Toxicol Lett. 169 (2007) 51-63.

100.   K. Soto, K.M. Garza, and L.E. Murr, Cytotoxic effects of aggregated nanomaterials, Acta Biomater. 3 (2007) 351-358.

101.   P. Wick, P. Manser, L.K. Limbach, U. Dettlaff-Weglikowska, F. Krumeich, S. Roth, W.J. Stark, and A. Bruinink, The degree and kind of agglomeration affect carbon nanotube cytotoxicity, Toxicol Lett. 168 (2007) 121-131.

102.   K.K. Kim, S.-M. Yoon, J.-Y. Choi, J. Lee, B.-K. Kim, J.M. Kim, J.-H. Lee, U. Paik, M.H. Park, C.W. Yang, K.H. An, Y. Chung, and Y.H. Lee, Design of dispersants for the dispersion of carbon nanotubes in an organic solvent, Advanced Functional Materials. 17 (2007) 1775-1783.

103.   H. Cathcart, S. Quinn, V. Nicolosi, J.M. Kelly, W.J. Blau, and J.N. Coleman, Spontaneous debundling of single-walled carbon nanotubes in DNA-based dispersions, Journal of Physical Chemistry C. 111 (2007) 66-74.

104.   S. Giordani, S.D. Bergin, V. Nicolosi, S. Lebedkin, M.M. Kappes, W.J. Blau, and J.N. Coleman, Debundling of single-walled nanotubes by dilution: Observation of large populations of individual nanotubes in amide solvent dispersions, Journal of Physical Chemistry B. 110 (2006) 15708-15718.

105.   S. Giordani, S. Bergin, V. Nicolosi, S. Lebedkin, W.J. Blau, and J.N. Coleman, Fabrication of stable dispersions containing up to 70% individual carbon nanotubes in a common organic solvent, Physica Status Solidi (B) Basic Research. 243 (2006) 3058-3062.

106.   S.D. Bergin, V. Nicolosi, H. Cathcart, M. Lotya, D. Rickard, Z. Sun, W.J. Blau, and J.N. Coleman, Large populations of individual nanotubes in surfactant-based dispersions without the need for ultracentrifugation, Journal of Physical Chemistry C. 112 (2008) 972-977.

107.   U.J. Kim, C.A. Furtado, X. Liu, G. Chen, and P.C. Eklund, Raman and IR spectroscopy of chemically processed single-walled carbon nanotubes, J Am Chem Soc. 127 (2005) 15437-15445.

108. V.N. Khabashesku, W.E. Billups, and J.L. Margrave, Fluorination of single-wall carbon nanotubes and subsequent derivatization reactions, Acc Chem Res. 35 (2002) 1087-1095.

109. V.A. Sinani, M.K. Gheith, A.A. Yaroslavov, A.A. Rakhnyanskaya, K. Sun, A.A. Mamedov, J.P. Wicksted, and N.A. Kotov, Aqueous dispersions of single-wall and multiwall carbon nanotubes with designed amphiphilic polycations, J Am Chem Soc. 127 (2005) 3463-3472.

110. S.D. Bergin, V. Nicolosi, S. Giordani, A.D. Gromard, L. Carpenter, W.J. Blau, and J.N. Coleman, Exfoliation in ecstasy: Liquid crystal formation and concentration- dependent debundling observed for single-wall nanotubes dispersed in the liquid drug *y*-butyrolactone, Nanotechnology. 18 (2007).

111. S.D. Bergin, V. Nicolosi, P.V. Streich, S. Giordani, Z. Sun, A.H. Windle, P. Ryan, N.P.P. Niraj, Z.-T.T. Wang, L. Carpenter, W.J. Blau, J.J. Boland, J.P. Hamilton, and J.N. Coleman, Towards solutions of single-walled carbon nanotubes in common solvents, Advanced Materials. 20 (2008) 1876-1881.

112. J.Y. Shin, T. Premkumar, and K.E. Geckeler, Dispersion of single-walled carbon nanotubes by using surfactants: are the type and concentration important?, Chemistry. 14 (2008) 6044-6048.

113. Z. Sun, V. Nicolosi, D. Rickard, S.D. Bergin, D. Aherne, and J.N. Coleman, Quantitative evaluation of surfactant-stabilized single-walled carbon nanotubes: Dispersion quality and its correlation with zeta potential, Journal of Physical Chemistry C. 112 (2008) 10692-10699.

114. Y. TanD. Resasco, Dispersion of single-walled carbon nanotubes of narrow diameter distribution, J Phys Chem B. 109 (2005) 14454-14460.

115. D. Yoon, J.-B. Choi, C.-S. Han, Y.-J. Kim, and S. Baik, The quantitative characterization of the dispersion state of single-walled carbon nanotubes using Raman spectroscopy and atomic force microscopy, Carbon. 46 (2008) 1530-1534.

116. K. Yurekli, C.A. Mitchell, and R. Krishnamoorti, Small-angle neutron scattering from surfactant-assisted aqueous dispersions of carbon nanotubes, J Am Chem Soc. 126 (2004) 9902-9903.

117. S. Attal, R. Thiruvengadathan, and O. Regev, Determination of the concentration of single-walled carbon nanotubes in aqueous dispersions using UV-visible absorption spectroscopy, Anal Chem. 78 (2006) 8098-8104.

118. V.C. Moore, M.S. Strano, E.H. Haroz, R.H. Hauge, R.E. Smalley, J. Schmidt, and Y. Talmon, Individually Suspended Single-Walled Carbon Nanotubes in Various Surfactants, Nano Letters. 3 (2003) 1379-1382.

119. H. Wang, W. Zhou, D.L. Ho, K.I. Winey, J.E. Fischer, C.J. Glinka, and E.K. Hobbie, Dispersing single-walled carbon nanotubes with surfactants: A small angle neutron scattering study, Nano Letters. 4 (2004) 1789-1793.

120. Q. Wang, Y. Han, Y. Wang, Y. Qin, and Z.X. Guo, Effect of surfactant structure on the stability of carbon nanotubes in aqueous solution, J Phys Chem B. 112 (2008) 7227-7233.

121. G. Ciofani, V. Raffa, V. Pensabene, A. Menciassi, and P. Dario, Dispersion of multi-walled carbon nanotubes in aqueous pluronic F127 solutions for biological applications, Fullerenes Nanotubes and Carbon Nanostructures. 17 (2009) 11-25.

122. A. Di Crescenzo, D. Demurtas, A. Renzetti, G. Siani, P. De Maria, M. Meneghetti, M. Prato, and A. Fontana, Disaggregation of single-walled carbon nanotubes (SWNTs) promoted by the ionic liquid-based surfactant 1-hexadecyl-3-vinyl-imidazolium bromide in aqueous solution, Soft Matter. 5 (2009) 62-66.

123. Y. KangT.A. Taton, Micelle-encapsulated carbon nanotubes: a route to nanotube composites, J Am Chem Soc. 125 (2003) 5650-5651.

124. M. Islam, R. Rojas, D. Bergey, A. Johnson, and A. Yodh, High Weight Fraction Surfactant Solubilization of Single-Wall Carbon Nanotubes in Water, Nano Lett. 3 (2003) 269-273.

125. M.J. O'Connell, S.M. Bachilo, C.B. Huffman, V.C. Moore, M.S. Strano, E.H. Haroz, K.L. Rialon, P.J. Boul, W.H. Noon, C. Kittrell, J. Ma, R.H. Hauge, R.B. Weisman, and R.E. Smalley, Band gap fluorescence from individual single-walled carbon nanotubes, Science. 297 (2002) 593-596.

126. Q. Wang, Y. Han, Y. Wang, Y. Qin, and Z.-X. Guo, Effect of surfactant structure on the stability of carbon nanotubes in aqueous solution, Journal of Physical Chemistry B. 112 (2008) 7227-7233.

127. K. Ausman, R. Piner, O. Lourie, and R. Ruoff, Organic solvent dispersion of single-walled carbon nanotubes: Towards solutions of pristine nanotubes, J. Phys. Chem. B. 104 (2000) 8911-8915.

128. J. Bahr, E. Mickelson, M. Bronikowski, R. Smalley, and J. Tour, Dissolution of small diameter single-wall carbon nanotubes in organic solvents?, Chem. Comm. (2001) 193-194.

129. B.J. Landi, H.J. Ruf, J.J. Worman, and R.P. Raffaelle, Effects of alkyl amide solvents on the dispersion of single-wall carbon nanotubes, Journal of Physical Chemistry B. 108 (2004) 17089-17095.

130. H.T. Ham, Y.S. Choi, and I.J. Chung, An explanation of dispersion states of single-walled carbon nanotubes in solvents and aqueous surfactant solutions using solubility parameters, J Colloid Interface Sci. 286 (2005) 216-223.

131. V. Moore, M. Strano, E. Haroz, R. Hauge, and R. Smalley, Individually suspended single-walled carbon nanotubes in various surfactants, Nano Lett. 3 (2003) 1379-1382.

132. N. Grossiord, O. Regev, J. Loos, J. Meuldijk, and C.E. Koning, Time-dependent study of the exfoliation process of carbon nanotubes in aqueous dispersions by using UV-visible spectroscopy, Anal Chem. 77 (2005) 5135-5139.

133. L. Vaisman, H.D. Wagner, and G. Marom, The role of surfactants in dispersion of carbon nanotubes, Adv Colloid Interface Sci. 128-130 (2006) 37-46.

134. G.S. McKeeK.S. Vecchio, Thermogravimetric analysis of synthesis variation effects on CVD generated multiwalled carbon nanotubes, J Phys Chem B Condens Matter Mater Surf Interfaces Biophys. 110 (2006) 1179-1186.

135. P.H. Li, Y.L. Qu, X.J. Xu, Y.W. Zhu, T. Yu, K.C. Chin, J. Mi, X.Y. Gao, C.T. Lim, Z.X. Shen, A.T. Wee, W. Ji, and C.H. Sow, Synthesis of "cactus" top-decorated aligned carbon nanotubes and their third-order nonlinear optical properties, J Nanosci Nanotechnol. 6 (2006) 990-995.

136. V. Georgakilas, D. Voulgaris, E. Vazquez, M. Prato, D.M. Guldi, A. Kukovecz, and H. Kuzmany, Purification of HiPCO carbon nanotubes via organic functionalization, J Am Chem Soc. 124 (2002) 14318-14319.

137. P. Eklund, J. Holden, and R. Jishi, Vibrational modes of carbon nanotubes; Spectroscopy and theory, Carbon. 33 (1995) 959-972.

138. A.M. Rao, E. Richter, S. Bandow, B. Chase, P.C. Eklund, K.A. Williams, S. Fang, K.R. Subbaswamy, M. Menon, A. Thess, R.E. Smalley, G. Dresselhaus, and M.S. Dresselhaus, Diameter-selective Raman scattering from vibrational modes in carbon nanotubes, Science. 275 (1997) 187-191.

139. A.C. Dillon, M. Yudasaka, and M.S. Dresselhaus, Employing Raman spectroscopy to qualitatively evaluate the purity of carbon single-wall nanotube materials, J Nanosci Nanotechnol. 4 (2004) 691-703.

140. U.J. Kim, X.M. Liu, C.A. Furtado, G. Chen, R. Saito, J. Jiang, M.S. Dresselhaus, and P.C. Eklund, Infrared-active vibrational modes of single-walled carbon nanotubes, Phys Rev Lett. 95 (2005) 157402.

141. K. Fu, W. Huang, Y. Lin, D. Zhang, T.W. Hanks, A.M. Rao, and Y.P. Sun, Functionalization of carbon nanotubes with bovine serum albumin in homogeneous aqueous solution, J Nanosci Nanotechnol. 2 (2002) 457-461.

142. G. Pastorin, W. Wu, S. Wieckowski, J.P. Briand, K. Kostarelos, M. Prato, and A. Bianco, Double functionalization of carbon nanotubes for multimodal drug delivery, Chem Commun (Camb). (2006) 1182-1184.

143.   H. Peng, L.B. Alemany, J.L. Margrave, and V.N. Khabashesku, Sidewall carboxylic acid functionalization of single-walled carbon nanotubes, J Am Chem Soc. 125 (2003) 15174-15182.

144.   C.E. Banks, A. Crossley, C. Salter, S.J. Wilkins, and R.G. Compton, Carbon nanotubes contain metal impurities which are responsible for the "electrocatalysis" seen at some nanotube-modified electrodes, Angewandte Chemie - International Edition. 45 (2006) 2533-2537.

145.   S. Costa, E. Borowiak-Palen, A. Bachmatiuk, M.H. Ru?mmeli, T. Gemming, and R.J. Kalen?czuk, Filling of carbon nanotubes for bio-applications, Physica Status Solidi (B) Basic Research. 244 (2007) 4315-4318.

146.   S. Khan, Z.H. Khan, K.N. Tripathi, and M. Husain, Synthesis of carbon nanotubes using Ni95Ti5 nanocrystalline film as a catalyst., Journal of nanoscience and nanotechnology. 7 (2007) 1855-1859.

147.   S.L. Zhang, K.H. Tam, A.B. Djurisic, and Y.F. Hsu, The influence of source material composition on morphology and optical properties of ZnO nanostructures, J Nanosci Nanotechnol. 8 (2008) 1295-1300.

148.   J.P. Trigueiro, G.G. Silva, R.L. Lavall, C.A. Furtado, S. Oliveira, A.S. Ferlauto, R.G. Lacerda, L.O. Ladeira, J.W. Liu, R.L. Frost, and G.A. George, Purity evaluation of carbon nanotube materials by thermogravimetric, TEM, and SEM methods, J Nanosci Nanotechnol. 7 (2007) 3477-3486.

149.   G.G. Bortoleto, S.S.d.O. Borges, and M.I.M.S. Bueno, X-ray scattering and multivariate analysis for classification of organic samples: A comparative study using Rh tube and synchrotron radiation, Analytica Chimica Acta. 595 (2007) 38-42.

150.   M. Pumera, Carbon nanotubes contain residual metal catalyst nanoparticles even after washing with nitric acid at elevated temperature because these metal nanoparticles are sheathed by several graphene sheets, Langmuir. 23 (2007) 6453-6458.

151.   Y. Hayashi, T. Fujita, T. Tokunaga, K. Kaneko, T. Butler, N. Rupesinghe, J.D. Carey, S.R.P. Silva, and G.A.J. Amaratunga, Encapsluation of Co and Pd multi-metal nanowires inside multiwalled carbon nanotubes by microwave plasma chemical vapor deposition, Diamond and Related Materials. 16 (2007) 1200-1203.

152.   X. He, F. Wu, and M. Zheng, The synthesis of carbon nanoballs and its electrochemical performance, Diamond and Related Materials. 16 (2007) 311-315.

153.   H.-Q. Wu, P.-S. Yuan, H.-Y. Xu, D.-M. Xu, B.-Y. Geng, and X.-W. Wei, Controllable synthesis and magnetic properties of Fe-Co alloy nanoparticles

attached on carbon nanotubes, Journal of Materials Science. 41 (2006) 6889-6894.

154. D. Chattapadhyay, I. Galeska, and F. Papadimitrakopoulos, Complete elimination of metal catalysts from single wall carbon nanotubes, Carbon. 40 (2002) 985*988.

155. C. DykeJ. Tour, Overcoming the insolubility of carbon nanotubes through high degrees of sidewall functionalization, Chemistry. 10 (2004) 812-817.

156. C. DykeJ. Tour, Solvent-free functionalization of carbon nanotubes, J Am Chem Soc. 125 (2003) 1156-1157.

157. L. ZhaoL. Gao, Stability of multi-walled carbon nanotubes dispersion with copolymer in ethanol, Colloids and Surfaces A. 224 (2003) 127-134.

158. M. Sano, A. Kamino, J. Okamura, and S. Shinkai, Self-organization of *PEO*-graft-single-walled carbon nanotubes in solutions and Langmuir-Blodgett films, Langmuir. 17 (2001) 5125-5128.

159. J.Y. Lee, J.S. Kim, K.H. An, K. Lee, D.Y. Kim, D.J. Bae, and Y.H. Lee, Electrophoretic and dynamic light scattering in evaluating dispersion and size distribution of single-walled carbon nanotubes, J Nanosci Nanotechnol. 5 (2005) 1045-1049.

160. X. Gao, T. Hu, L. Liu, and Z. Guo, Self-assembly of modified carbon nanotubes in toluene, Chem. Phys. Lett. 370 (2003) 661-664.

161. L. Vaisman, G. Marom, and H. Wagner, Dispersion of surface-modified carbon nanotubes in water-soluble and water-insoluble polymers, Adv. Funct. Mater. 16 (2006) 357-363.

162. Z. Li, G. Luo, W. Zhuo, F. Wei, R. Xiang, and Y. Liu, The quantitative characterization of the concentration and dispersion of multi-walled carbon nanotubes in suspension by spectrophotometry, Nanotechnology. 17 (2006) 3692-3698.

163. J. Riggs, D. Walker, D. Carroll, and Y. Sun, Optical limiting properties of suspended and solubilized carbon nanotubes, J Phys Chem B. 104 (2000) 7071-7076.

164. K. Kelley, P.E. Pehrsson, L.M. Ericson, and W. Zhao, Optical pH response of DNA wrapped HiPco carbon nanotubes, J Nanosci Nanotechnol. 5 (2005) 1041-1044.

165. A. Ryabenko, T. Dorofeeva, and G. Zvereva, UV–VIS–NIR spectroscopy study of sensitivity of single-wall carbon nanotubes to chemical processing and Van-der-Waals SWNT/SWNT interaction. Verification of the SWNT content measurements by absorption spectroscopy, Carbon. 42 (2004) 1523-1535.

166.   M. O'Connell, S. Bachilo, C. Huffman, V. Moore, M. Strano, E. Haroz, K. Railon, P. Boul, W. Noon, C. Kittrell, J. Ma, R. Hauge, R. Weisman, and R. Smalley, Band gap fluorescence from individual single-walled carbon nanotubes, Science. 297 (2002) 593-596.

167.   A. Nish, J.-Y. Hwang, J. Doig, and R.J. Nicholas, Highly selective dispersion of single-walled carbon nanotubes using aromatic polymers, Nature Nanotechnology. 2 (2007) 640-646.

168.   S.M. Bachilo, M.S. Strano, C. Kittrell, R.H. Hauge, R.E. Smalley, and R.B. Weisman, Structure-assigned optical spectra of single-walled carbon nanotubes, Science. 298 (2002) 2361-2366.

169.   J. Lefebvre, D.G. Austing, J. Bond, and P. Finnie, Photoluminescence imaging of suspended single-walled carbon nanotubes, Nano Lett. 6 (2006) 1603-1608.

170.   J.S. Lauret, C. Voisin, G. Cassabois, C. Delalande, P. Roussignol, O. Jost, and L. Capes, Ultrafast carrier dynamics in single-wall carbon nanotubes, Phys Rev Lett. 90 (2003) 057404.

171.   J.-S. Lauret, C. Voisin, G. Cassabois, P. Roussignol, C. Delalande, A. Filoramo, L. Capes, E. Valentin, and O. Jost, Bandgap photoluminescence of semiconducting single-wall carbon nanotubes, Physica E: Low-Dimensional Systems and Nanostructures. 21 (2004) 1057-1060.

172.   S.D. WettigR.E. Verrall, Thermodynamic Studies of Aqueous m-s-m Gemini Surfactant Systems, J Colloid Interface Sci. 235 (2001) 310-316.

173.   M. Donkuru, *Non-viral gene delivery with pH-sensitive gemini nanoparticles : synthesis of gemini surfactant building blocks, characterization and in vitro screening of transfection efficiency and toxicity*, in *College of Pharmacy and Nutrition*. 2008, University of Saskatchewan: Saskatoon.

174.   K.M. Jenkins, *Thermodynamic studies of bis(quanternary ammonium) and (N-alkyl-) ionic surfactants*, in *Department of Chemsitry*. 2000, University of Saskatchewan: Saskatoon.

175.   J.E. Thompson, A Practical Guide to Comtemporary Pharmacy Practice. Third ed, Philadelphia: LWW.

176.   O.-K. Kim, J. Je, J.W. Baldwin, S. Kooi, P.E. Pehrsson, and L.J. Buckley, Solubilization of single-wall carbon nanotubes by supramolecular encapsulation of helical amylose, Journal of the American Chemical Society. 125 (2003) 4426-4427.

177.   A. Ikeda, T. Hamano, K. Hayashi, and J. Kikuchi, Water-solubilization of nucleotides-coated single-walled carbon nanotubes using a high-speed vibration milling technique, Org Lett. 8 (2006) 1153-1156.

178. R. Rastogi, R. Kaushal, S.K. Tripathi, A.L. Sharma, I. Kaur, and L.M. Bharadwaj, *Comparative study of carbon nanotube dispersion using surfactants,* Journal of Colloid and Interface Science. (2008).

179. W. Zhou, S. Lv, and W. Shi, *Preparation of micelle-encapsulated single-wall and multi-wall carbon nanotubes with amphiphilic hyperbranched polymer,* European Polymer Journal. 44 (2008) 587-601.

180. F. Chen, Y. Xue, V.G. Hadjiev, C.W. Chu, P. Nikolaev, and S. Arepalli, *Fast characterization of magnetic impurities in single-walled carbon nanotubes,* Applied Physics Letters. 83 (2003) 4601-4603.

181. Y.V. ShtogunL.M. Woods, *Electronic and magnetic properties of deformed and defective single wall carbon nanotubes,* Carbon. 47 (2009) 3252-3262.

182. S. Kyatskaya, J.R.G. MascarÃ³s, L. Bogani, F. Hennrich, M. Kappes, W. Wernsdorfer, and M. Ruben, *Anchoring of rare-earth-based single-molecule magnets on single-walled carbon nanotubes,* Journal of the American Chemical Society. 131 (2009) 15143-15151.

183. T. KolodiazhnyiM. Pumera, *Towards an ultrasensitive method for the determination of metal impurities in carbon nanotubes,* Small. 4 (2008) 1476-1484.

184. E.-S.M. DuraiaK.A. Abdullin, *Ferromagnetic resonance of cobalt nanoparticles used as a catalyst for the carbon nanotubes synthesis,* Journal of Magnetism and Magnetic Materials. 321 (2009).

185. C. He, N. Zhao, C. Shi, J. Li, and H. Li, *Magnetic properties and transmission electron microscopy studies of Ni nanoparticles encapsulated in carbon nanocages and carbon nanotubes,* Materials Research Bulletin. 43 (2008) 2260-2265.

186. T. Makarova, *Unconventional magnetism in carbon based materials*, in *Frontiers in magnetic materials*, A. Narlikar, Editor. 2005, Springer: Berlin Heidelberg. p. 209-246.

187. Y. Fujiwara, H. Takegawa, H. Sato, K. Maeda, Y. Saito, T. Kobayashi, and S. Shiomi, *Magnetic properties of carbon nanotubes grown on Fe catalyst layer by microwave plasma enhanced chemical vapor deposition,* Journal of Applied Physics. 95 (2004) 7118-7120.

188. P. StamenovJ. Coey, *Magnetic susceptibility of carbon - experiment and theory,* Journal of Magnetism and Magnetic Materials. 290-291 (2005) 279-285.

189. X. Zhang, G. Wen, S. Huang, L. Dai, R. Gao, and Z. Wang, *Magnetic properties of Fe nanoparticles trapped at the tips of the aligned carbon nanotubes,* Journal of Magnetism and Magnetic Materials. 231 (2001) L9–L12.

190. P. Lehtinen, A. Krasheninnikov, A. Foster, and R. Nieminen, *The magnetic nature of intrinsic and irradiation-induced defects in carbon systems*, in *Carbon-based magnetism. An overview of the magnetism of metal free carbon-based compounds and materials*, T. Makarova and F. Palacio, Editors. 2006, Elsevier: Amsterdam. p. 371-396.

191. K.-P. Dinse, J. van Tol, A. Ozarowski, and B. Corzilius, Multi-frequency EPR and DC conductivity of itinerant spins in single-wall carbon nanotubes, Applied Magnetic Resonance. 37 (2009) 595-603.

192. J.R. Alvarez Collado, Calculation of the paramagnetism of large carbon nanotubes, using a parameter-independent molecular orbital model, International Journal of Quantum Chemistry. 108 (2008) 257-264.

193. L.E. HelsethT. Skodvin, Optical monitoring of low-field magnetophoretic separation of particles, Measurement Science and Technology. 20 (2009).

194. R. Afshar, Y. Moser, T. Lehnert, and M.A.M. Gijs, Magnetic particle dosing and size separation in a microfluidic channel, Sensors and Actuators, B: Chemical.

195. P. Eklund, J. Holden, and R. Jishi, Vibrational modes of carbon nanotubes;Spectroscopy and theory, Carbon. 33 (1995) 959-972.

196. U. Venkateswaran, A.M. Rao, E. Richter, M. Menon, A. Rinzler, R. Smalley, and P. Eklund, Probing the single-wall carbon nanotube bundle: Raman scattering under high pressure, Phys. Rev. B. 59 (1999) 10928-10934.

197. A. FerrariJ. Robertson, Resonant Raman spectroscopy of disordered, amorphous, and diamondlike carbon, Phys. Rev. B. 64 (2001) 075414-075414(-075413).

198. A. FerrariJ. Robertson, Interpretation of Raman spectra of disordered and amorphous carbon, Phys. Rev. B. 61 (2000) 14095-14107.

199. A.C. FerrariJ. Robertson, Raman spectroscopy of amorphous, nanostructured, diamond-like carbon, and nanodiamond, Philos Transact A Math Phys Eng Sci. 362 (2004) 2477-2512.

200. R.A. DiLeo, B.J. Landi, and R.P. Raffaelle, Purity assessment of multiwalled carbon nanotubes by Raman spectroscopy, Journal of Applied Physics. 101 (2007).

201. X. Sun, S.M. Tabakman, W.S. Seo, L. Zhang, G. Zhang, S. Sherlock, L. Bai, and H. Dai, Separation of nanoparticles in a density gradient: FeCo@C and gold nanocrystals, Angew Chem Int Ed Engl. 48 (2009) 939-942.

202. J.A. Fagan, B.J. Landi, I. Mandelbaum, J.R. Simpson, V. Bajpai, B.J. Bauer, K. Migler, A.R. Walker, R. Raffaelle, and E.K. Hobbie, Comparative measures of

single-wall carbon nanotube dispersion, *J Phys Chem B Condens Matter Mater Surf Interfaces Biophys.* 110 (2006) 23801-23805.

203.   N. Grossiord, O. Regev, J. Loos, J. Meuldijk, and C.E. Koning, Time-dependent study of the exfoliation process of carbon nanotubes in aqueous dispersions by using UV-visible spectroscopy, *Analytical Chemistry.* 77 (2005) 5135-5139.

204.   Y. TanD.E. Resasco, Dispersion of single-walled carbon nanotubes of narrow diameter distribution, *J Phys Chem B.* 109 (2005) 14454-14460.

205.   N. Grossiord, P. Schoot, J. Meuldijk, and C.E. Koning, Determination of the surface coverage of exfoliated carbon nanotubes by surfactant molecules in aqueous solution, *Langmuir.* 23 (2007) 3646-3653.

206.   J. Yu, N. Grossiord, C.E. Koning, and J. Loos, Controlling the dispersion of multi-wall carbon nanotubes in aqueous surfactant solution, *Carbon.* 45 (2007) 618-623.

207.   D.H. Marsh, G.A. Rance, M.H. Zaka, R.J. Whitby, and A.N. Khlobystov, Comparison of the stability of multiwalled carbon nanotube dispersions in water, *Physical Chemistry Chemical Physics.* 9 (2007) 5490-5496.

208.   Z.F. Li, G.H. Luo, W.P. Zhou, F. Wei, R. Xiang, and Y.P. Liu, The quantitative characterization of the concentration and dispersion of multi-walled carbon nanotubes in suspension by spectrophotometry, *Nanotechnology.* 17 (2006) 3692-3698.

209.   L. Jiang, L. Gao, and J. Sun, Production of aqueous colloidal dispersions of carbon nanotubes, *J Colloid Interface Sci.* 260 (2003) 89-94.

210.   M.S. Arnold, M.O. Guler, M.C. Hersam, and S.I. Stupp, Encapsulation of carbon nanotubes by self-assembling peptide amphiphiles, *Langmuir.* 21 (2005) 4705-4709.

211.   J.A. Fagan, B.J. Landi, I. Mandelbaum, J.R. Simpson, V. Bajpai, B.J. Bauer, K. Migler, A.R. Walker, R. Raffaelle, and E.K. Hobbie, Comparative measures of single-wall carbon nanotube dispersion, *J Phys Chem B Condens Matter Mater Surf Interfaces Biophys.* 110 (2006) 23801-23805.

212.   S.S. Karajanagi, H. Yang, P. Asuri, E. Sellitto, J.S. Dordick, and R.S. Kane, Protein-assisted solubilization of single-walled carbon nanotubes, *Langmuir.* 22 (2006) 1392-1395.

213.   B. Gigliotti, B. Sakizzie, D.S. Bethune, R.M. Shelby, and J.N. Cha, Sequence-independent helical wrapping of single-walled carbon nanotubes by long genomic DNA, *Nano Lett.* 6 (2006) 159-164.

214.   R.J. ChenY. Zhang, Controlled precipitation of solubilized carbon nanotubes by delamination of DNA, J Phys Chem B Condens Matter Mater Surf Interfaces Biophys. 110 (2006) 54-57.

215.   M.S. Strano, V.C. Moore, M.K. Miller, M.J. Allen, E.H. Haroz, C. Kittrell, R.H. Hauge, and R.E. Smalley, The role of surfactant adsorption during ultrasonication in the dispersion of single-walled carbon nanotubes, J Nanosci Nanotechnol. 3 (2003) 81-86.

216.   J. Foster, S. Singamaneni, R. Kattumenu, and V. Bliznyuk, Dispersion and phase separation of carbon nanotubes in ultrathin polymer films, J Colloid Interface Sci. 287 (2005) 167-172.

217.   Y. TanD.E. Resasco, Dispersion of single-walled carbon nanotubes of narrow diameter distribution, J Phys Chem B Condens Matter Mater Surf Interfaces Biophys. 109 (2005) 14454-14460.

218.   K. Shen, S. Curran, H. Xu, S. Rogelj, Y. Jiang, J. Dewald, and T. Pietrass, Single-walled carbon nanotube purification, pelletization, and surfactant-assisted dispersion: a combined TEM and resonant micro-raman spectroscopy study, J Phys Chem B Condens Matter Mater Surf Interfaces Biophys. 109 (2005) 4455-4463.

219.   V. Weiss, R. Thiruvengadathan, and O. Regev, Preparation and characterization of a carbon nanotube-lyotropic liquid crystal composite, Langmuir. 22 (2006) 854-856.

220.   E.K. Hobbie, B.J. Bauer, J. Stephens, M.L. Becker, P. McGuiggan, S.D. Hudson, and H. Wang, Colloidal particles coated and stabilized by DNA-wrapped carbon nanotubes, Langmuir. 21 (2005) 10284-10287.

221.   J. Zhao, D.W. Schaefer, D. Shi, J. Lian, J. Brown, G. Beaucage, L. Wang, and R.C. Ewing, How does surface modification aid in the dispersion of carbon nanofibers?, J Phys Chem B Condens Matter Mater Surf Interfaces Biophys. 109 (2005) 23351-23357.

222.   B. Bauer, E. Bobbie, and M. Mecker, Small-angle neutron scattering from labeled single-wall carbon nanotubes, Macromolecules. 39 (2006) 2637-2642.

223.   S. Arepalli, P. Nikolaev, O. Gorelik, V. Hadjiev, W. Holmes, B. Files, and L. Yowell, Protocol for the characterization of single-wall carbon nanotube material quality, Carbon. 42 (2004) 1783-1791.

224.   M. BagonluriM. Foldvari. *Dispersion and debundling of carbon nanotubes (CNTs) using pharmaceutical excipients*. in *AAPS Annual Meeting and Exposition*. 2007.

225. R. Haggenmueller, S.S. Rahatekar, J.A. Fagan, J. Chun, M.L. Becker, R.R. Naik, T. Krauss, L. Carlson, J.F. Kadla, P.C. Trulove, D.F. Fox, H.C. Delong, Z. Fang, S.O. Kelley, and J.W. Gilman, Comparison of the quality of aqueous dispersions of single wall carbon nanotubes using surfactants and biomolecules, Langmuir. 24 (2008) 5070-5078.

226. O. Matarredona, H. Rhoads, Z. Li, J.H. Harwell, L. Balzano, and D.E. Resasco, Dispersion of single-walled carbon nanotubes in aqueous solutions of the anionic surfactant NaDDBS, Journal of Physical Chemistry B. 107 (2003) 13357-13367.

227. B. White, S. Banerjee, S. O'Brien, N. Turro, and I. Herman, Zeta-potential measurements of surfactant-wrapped individual single-walled carbon nanotubes, J. Phys. Chem. C. 111 (2007) 13684-13690.

228. C. Richard, F. Balavoine, P. Schultz, T.W. Ebbesen, and C. Mioskowski, Supramolecular self-assembly of lipid derivatives on carbon nanotubes, Science. 300 (2003) 775-778.

229. R. Haggenmueller, S.S. Rahatekar, J.A. Fagan, J. Chun, M.L. Becker, R.R. Naik, T. Krauss, L. Carlson, J.F. Kadla, P.C. Trulove, D.F. Fox, H.C. DeLong, Z. Fang, S.O. Kelley, and J.W. Gilrnan, Comparison of the quality of aqueous dispersions of single wall carbon nanotubes using surfactants and biomolecules, Langmuir. 24 (2008) 5070-5078.

230. S. Manne, J. Cleveland, H. Gaub, G. Stucky, and P. Hansma, Direct visualization of surfactant hemimicelles by force microscopyof the electrical double layer, Langmuir. 10 (1994) 4409-4413.

231. J.-F. LiuW.A. Ducker, Self-assembled supramolecular structures of charged polymers at the graphite/liquid interface, Langmuir. 16 (2000) 3467-3473.

232. D. Baskaran, J.W. Mays, and M.S. Bratcher, Noncovalent and nonspecific molecular interactions of polymers with multiwalled carbon nanotubes, Chemistry of Materials. 17 (2005) 3389-3397.

233. E. Rodriguez, Investigation and development of a continuous nanotube suspension fabrication process, in Engineering - Industrial Engineering. 2006, Florida State University.

234. Purity and Dispersion Measurement Issues Workshop on Single Wall Carbon Nanotubes (SWCNTs). 2003, NIST: Gaithersburg, Maryland,.

235. S. Attal, R. Thiruvengadathan, and O. Regev, Determination of the Concentration of Single-Walled Carbon Nanotubes in Aqueous Dispersions Using UV-Visible Absorption Spectroscopy, Anal Chem. 78 (2006) 8098-8104.

236. M. Zheng, A. Jagota, E.D. Semke, B.A. Diner, R.S. McLean, S.R. Lustig, R.E. Richardson, and N.G. Tassi, DNA-assisted dispersion and separation of carbon nanotubes, Nat Mater. 2 (2003) 338-342.

237. Y. Maeda, M. Kanda, M. Hashimoto, T. Hasegawa, S. Kimura, Y. Lian, T. Wakahara, T. Akasaka, S. Kazaoui, N. Minami, T. Okazaki, Y. Hayamizu, K. Hata, J. Lu, and S. Nagase, Dispersion and separation of small-diameter single-walled carbon nanotubes, J Am Chem Soc. 128 (2006) 12239-12242.

238. D. Yoon, S.J. Kang, J.B. Choi, Y.J. Kim, and S. Baik, The evaluation of individual dispersion of single-walled carbon nanotubes using absorption and fluorescence spectroscopic techniques, J Nanosci Nanotechnol. 7 (2007) 3727-3730.

239. D. Tasis, K. Papagelis, D. Douroumis, J.R. Smith, N. Bouropoulos, and D.G. Fatouros, Diameter-selective solubilization of carbon nanotubes by lipid micelles, J Nanosci Nanotechnol. 8 (2008) 420-423.

240. W.R. Small, C.D. Walton, J. Loos, and M. in het Panhuis, Carbon nanotube network formation from evaporating sessile drops, J Phys Chem B. 110 (2006) 13029-13036.

241. A. Yu, E. Bekyarova, M.E. Itkis, D. Fakhrutdinov, R. Webster, and R.C. Haddon, Application of centrifugation to the large-scale purification of electric arc-produced single-walled carbon nanotubes, J Am Chem Soc. 128 (2006) 9902-9908.

242. D. Heller, P. Barone, J. Swanson, R. Mayrhofer, and M. Strano, Using Raman spectroscopy to elucidate the aggregation state of single-walled carbon nanotubes, J Phys Chem B. 108 (2004) 6905-6909.

243. Q. ZhaoH.D. Wagner, Raman spectroscopy of carbon-nanotube-based composites, Philos Transact A Math Phys Eng Sci. 362 (2004) 2407-2424.

244. S. Ichimura, Current activities of ISO TC229/WG2 on purity evaluation and quality assurance standards for carbon nanotubes, Anal Bioanal Chem. 396 963-971.

APPENDICES

APPENDIX A -   COLLATED PROPERTIES OF CARBON NANOTUBES FROM SUPPLIERS

A1. NA-SWNT/N&A-SWNT - Single walled carbon nanotubes (described as 90 % regular SWNT, Stock#: 1284YJ) is the highest purity of the three non-functionalized SWNT samples from Nanostructured & Amorphous Materials, Inc.

Purchased: July 2007

Synthesis – Chemical Vapour Deposition

Parameter	Value	Method
Diameter (Outer)	1.1 nm	TEM
Length	5-30 μm	TEM
Purity*	90 % SWNT / 95 % MWNT	
Amorphous Carbon		
Metal Content (wt %)	3 % i.e. inferred from data	EDS
Ash		
Specific Surface Area	400 m^2/g	
Density at 20 ^{o}C	1.7 – 1.9 g/cm3	
Melting point/Melting range	3652-3697 ° C (subl/vac)	
Solubility	Insoluble in water	

Elemental Analysis by energy dispersive spectroscopy (EDS).

Components	Contents (%)
C	96.30
Al	0.08
Cl	0.41
Co	2.91
S	0.29

A2. **AP-SWNT** are single walled carbon nanotubes (described as 90 % regular SWNT, Batch#AP-155). The SWNT were synthesized by electric arc discharge, using Ni/Y catalysts. AP-SWNT is reported to be the highest purity as-produced SWNT (i.e. without further purification) using the electric arc method.

Purchased : May 2005

Synthesis – Electric arc discharge

Parameter	Value	Method
Diameter[#]	1.4 nm	▓
Length	0.5-3μm	▓
Purity*	40-60 %	Near Infrared (NIR)
Amorphous Carbon	▓	▓
Metal Content (wt %)	30 %	▓
Ash	▓	▓
Specific Surface Area	▓	▓
Density	1.2 to 1.5 g/cm^3	▓
Bundle Length	1-5μm	▓
Bundle Diameter	2-10nm	▓

[#] *Diameter does not specify whether internal or external diameter*

* Carbonaceous purity

Elemental Analysis

Stated that Ni/Y used as catalyst in synthesis.

A3. P2-SWNT - Single walled carbon nanotubes identified as P2-SWNT from Carbon Solutions Inc (P2-SWNT, Batch#02-254). These are described as purified (from AP-SWNT) SWNT by air oxidation, resulting in high purity SWNT, with reduced residual metal (catalyst) content. The purified material closely approximates the pristine state with low functionality and low chemical doping. Dispersibility is similar to that of the AP-SWNTs.

Purchased : July 2007

Synthesis – Electric arc discharge

Parameter	Value	Method
Diameter	1.4 nm	▓
Length	0.5-1.5 μm	▓
Purity*	70-90 %	Near Infrared (NIR)
Amorphous Carbon	N/A	▓
Metal Content (wt %)	7-10 %	TGA
Ash	▓	▓

Specific Surface Area		
Density	1.2 to 1.5 g/cm^3	
Bundle Length	500nm-1.5μm (~1.0μm)	
Bundle Diameter	4-5nm	

* Carbonaceous purity

Elemental Analysis

Stated that Ni/Y used as catalyst in synthesis

Samples are purified by air oxidation and subsequently treated to remove the catalyst. The purified material closely approximates the pristine state with low functionality.

A4. P3-SWNT are acid purified samples of AP-SWNT (Carbon Solutions Inc. Acid (nitric acid) purification results in a 3-6 % residual carboxylic acid groups on the tips and sidewalls, making the resultant P3-SWNT soluble in water.

Purchased : July 2005

Synthesis – Electric arc discharge

Parameter	Value	Method
External Diameter	1.4 nm	
Length	0.5-1.5 μm	
Purity*	80-90 %	Near Infrared (NIR)
Amorphous Carbon		
Metal Content (wt %)	5-10 %	TGA
Ash		
Specific Surface Area		
Density		
Bundle Length	500nm-1.5μm (~1.0μm)	
Bundle Diameter	4-5nm	

* Carbonaceous purity

Elemental Analysis

Stated that Ni/Y used as catalyst in synthesis

A5. HMS-SWNT are single walled carbon nanotubes described as high-purity single wall carbon nanotubes (Part No: SWNT-12900002-00, Lot No: BSCA 06310069) from Helix Material Solutions, Inc.

Purchased : July 2007

Synthesis – Chemical Vapour Deposition

Parameter	Value	Method
External Diameter	~ 1.3 nm	TEM, Raman
Length	0.5 ~ 40 μm	TEM, SEM
Purity	> 90%	TGA, SEM
Amorphous Carbon	< 5%	TGA
Ash	< 2 wt%	TGA
Specific Surface Area	300 – 600 m^2/g	BET

Samples were accompanied by an elemental analysis data sheet (described as spec sheet), listing the above methods used in determining the corresponding parameter. This also includes a Raman spectrum confirming the presence of the RBM, D and G-bands.

A6. CT-SWNT - Single walled carbon nanotubes described as high-purity (>90 %) single wall carbon nanotubes from Cheap Tubes Inc. These are now listed on the supplier's website as SWNT 90s (http://www.cheaptubesinc.com/SWNTs).

Purchased: June 2005

Synthesis – Chemical Vapour Deposition

Parameter	Value	Method
External Diameter	1-2 nm / 0.8-1.6nm	TEM, Raman
Length	5-30	SEM
Purity*	> 90 wt %	NA
Amorphous Carbon	NA	NA
Metal Content (wt %)	3 % (inferred from EDS analysis)	EDS
Ash	1.5 wt %	TEM

Specific Surface Area	407 m^2/g	TEM
Density at 20 ^{o}C	~ 2.1 g/cm³	TEM, Raman

* *Carbonaceous purity*

Reported elemental analysis by EDS

Components	Contents (%)
C	96.32
Al	0.08
Cl	0.40
Co	2.90
S	0.29

Samples were accompanied by an elemental analysis data sheet, TEM image, as well as a Raman spectrum to confirm the presence of the RBM, D and G-bands.

CNT Handling and Toxicity Information-Summary

The following information is extracted from the MSDS sheets for Nanostructured & Amorphous Materials Inc (N&A) and Cheap Tubes Inc, and Helix Materials Solutions Inc. These are generic for both SWNT and MWNT. As the toxicity of these materials has not been clearly identified, the exposure limits quoted by both N&A and CheapTubes are the values used for graphite exposure.

General protective and hygienic measures The usual precautionary measures for handling chemicals should be followed. Keep away from foodstuffs, beverages and feed. Remove all soiled and contaminated clothing immediately. Wash hands before breaks and at the end of work. Avoid contact with the eyes. Avoid contact with the eyes and skin.

Additional information about design of technical systems: Properly operating chemical fume hood designed for hazardous chemicals and having an average face velocity of at least 100 feet per minute.

Breathing equipment: Use suitable respirator when high concentrations are present.

• **Protection of hands:** Impervious gloves

• **Eye protection:** Safety glasses

Toxicity

- Acute toxicity

Note: The toxicity of CNTs are classified as acute as a precautionary measure as the toxicity is not fully known. There is as yet, no classification data on their carcinogenic properties available from the regulatory bodies such as EPA, IARC, NTP, OSHA or ACGIH.

Hazards identification

• **Hazard description:** Xi Irritant

• **Information pertaining to particular dangers for man and environment** R 36/37 Irritating to eyes and respiratory system.

Information for safe handling:

Keep container tightly sealed.

Store in cool, dry place in tightly closed containers.

Ensure good ventilation at the workplace.

Do not store together with strong oxidizing agents

Protection of hands: Impervious gloves

• **Eye protection:** Safety glasses

Appendix B – EDX Analysis of CNT samples

B1. EDS backscattering image of AP-SWNT: Ni and Y as particles (0.5 to 1 micrometer), carbon mass with Ni and Y. No distinguishable particles within mass. These are reported to contain 40-60 % SWNT and 30 % residual catalyst of Ni/Y catalyst.
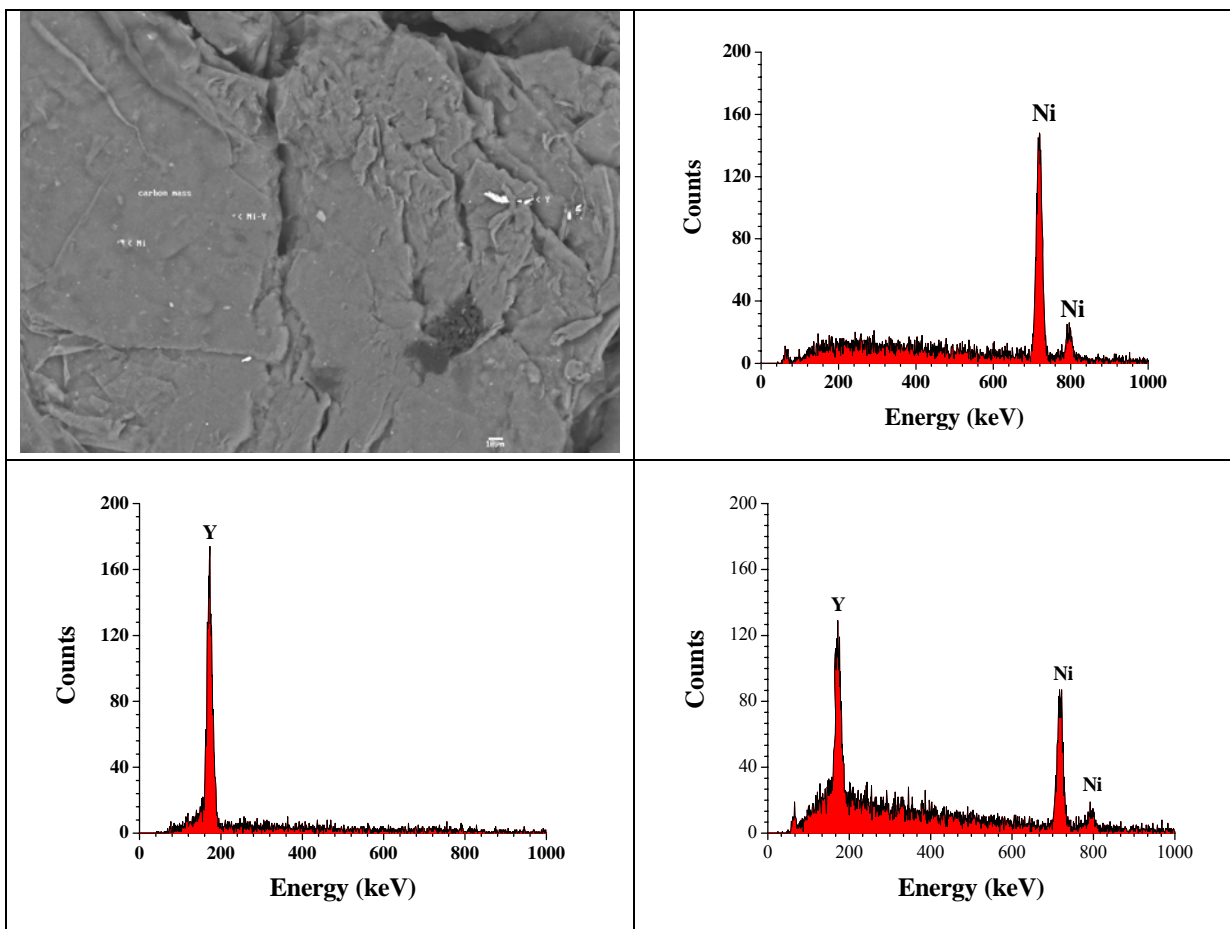

B2 EDS backscattering image of N&A-SWNT: A piece of Si as individual shard, Al-Si as particles (<1 μm), Cr-Fe-Co as particles (100-500 nanometers) and Fe-Cr-Mo (100-200 nanometers). Carbon mass has trace amounts of Co, Fe, Cl, S, Al.

The accompanying elemental analysis (in certificate of analysis) indicates the sample consists of 96.30 % C, 0.08 % Al, 0.41 % Cl, 2.91 % Co and 0.29 % S. The presence of Ni For the purity of SWNT samples, a quote of the carbon content is of little significance;

this includes all other allotropes of carbon. The results do show the presence of all the listed elements, and additionally, Fe and Si were found in the sample as well.
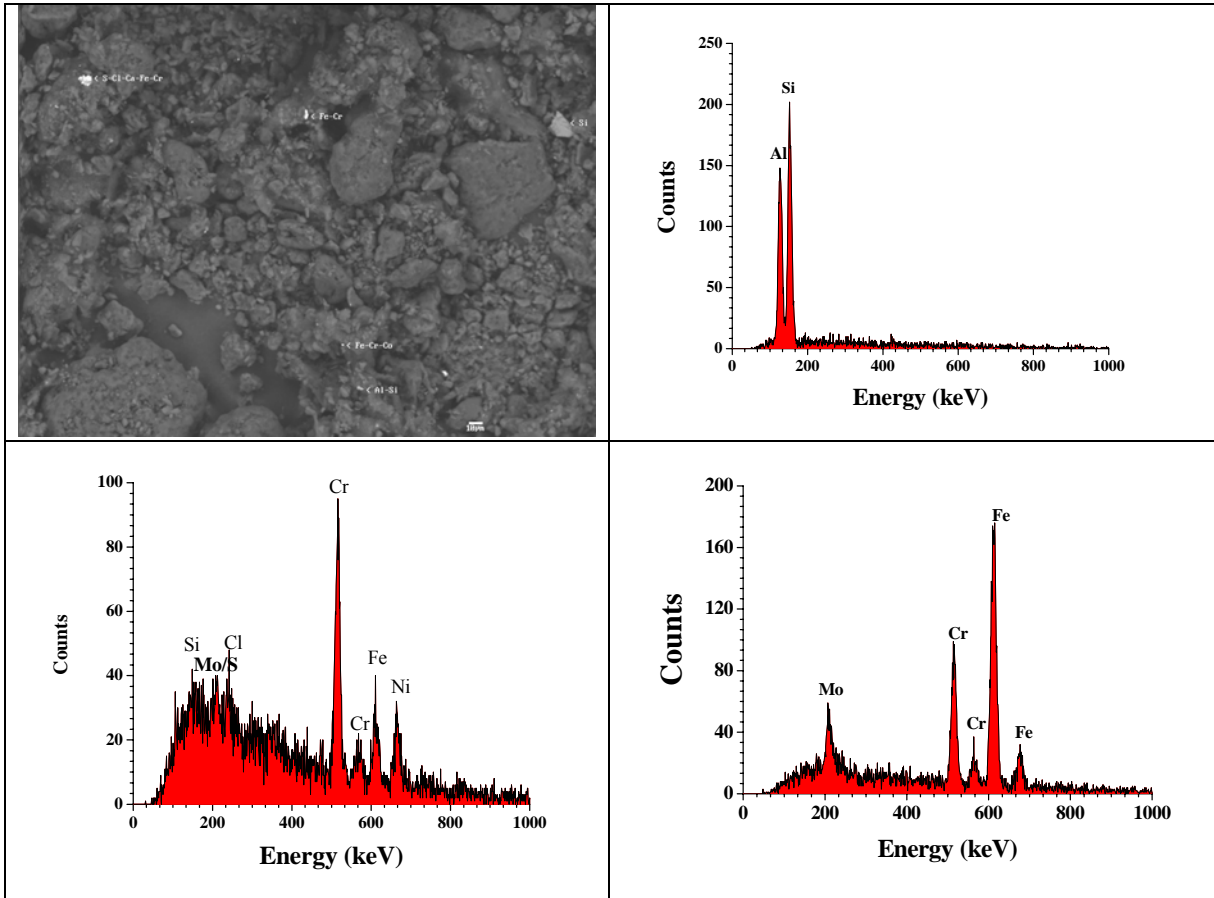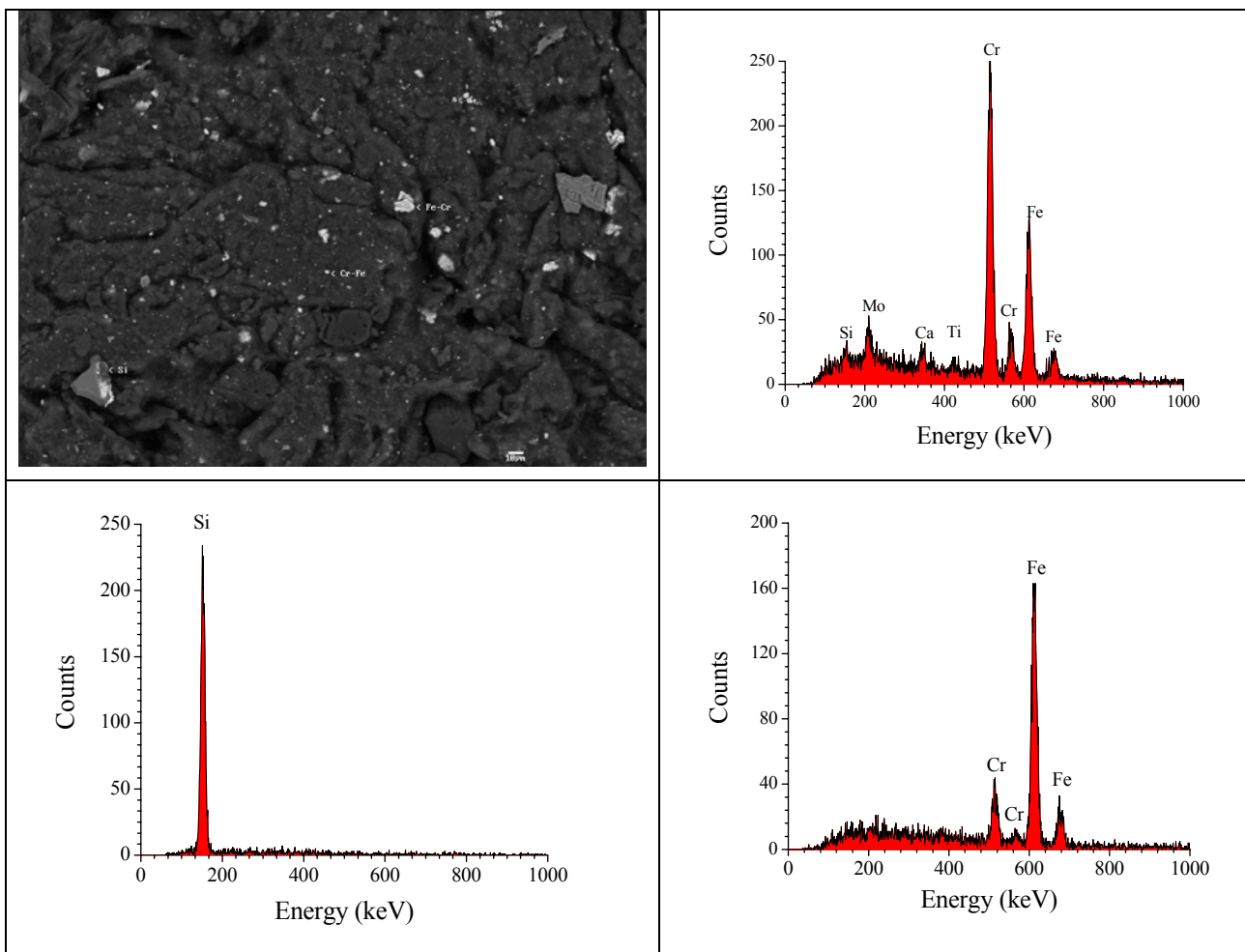

B3 EDS backscattering image of HMS-SWNT Fe-minor Co as particle (10 μm), Carbon mass has trace amounts of Fe, S, Si. In the material analysis data sheet accompanying the SWNT, the purity has been quoted as >90 %, with < 5% amorphous carbon, and < 2 % ash. There is no information as to the possible existence of metallic impurities in the sample, contrary to our finding. The presence of metallic impurities can be accounted for in the reported CVD synthetic method used to produce these CNTs.
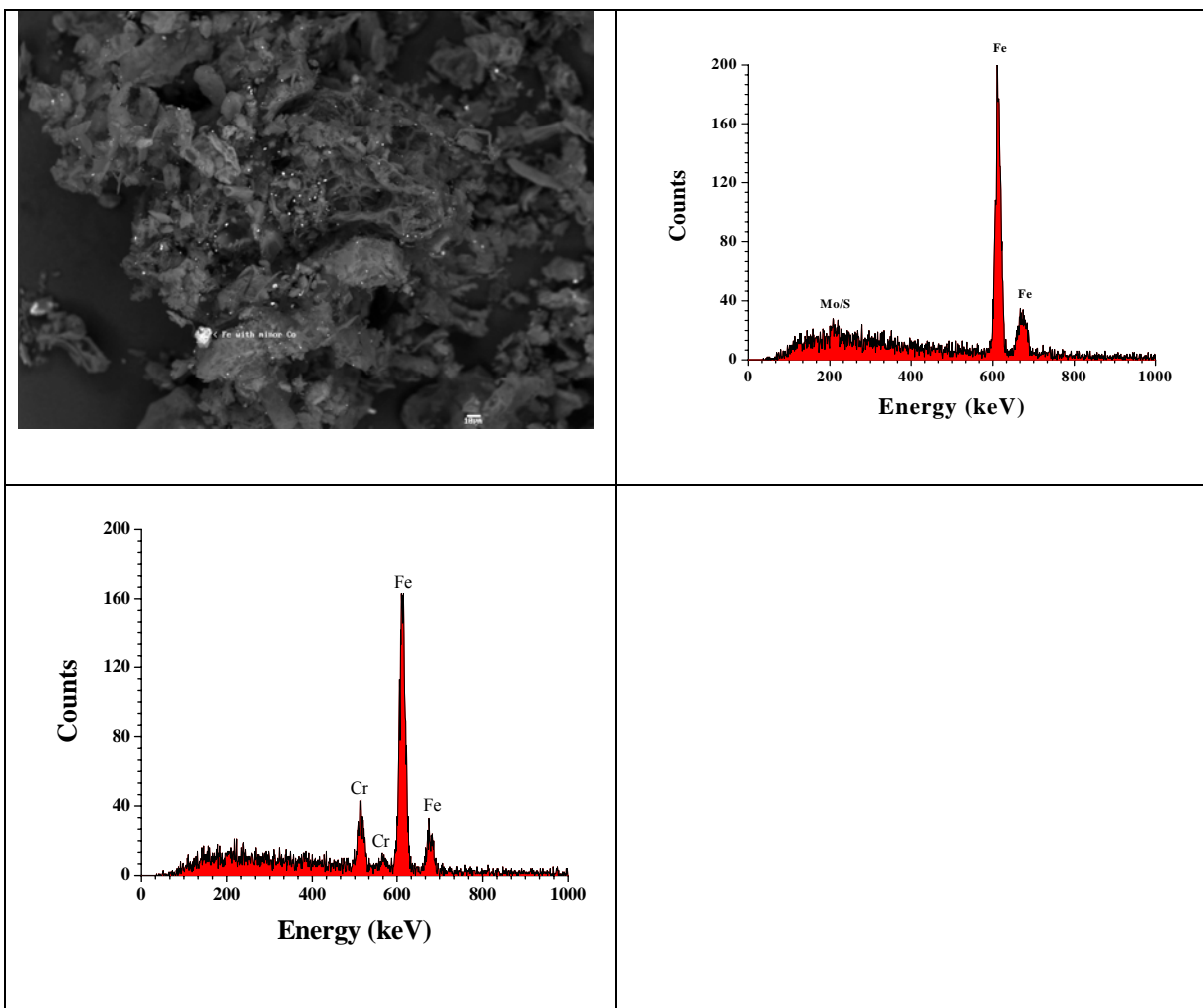
B4 EDS backscattering image of CT1-SWNT: Fe with minor Cr as particle (< 1 micrometer), Fe-Cr with minor Ca, S, Ti as particle (<1 micrometer), Si as particle (1-2 micrometers) Carbon mass contains trace amounts of Fe, Cr, Ca, Cl, S, Si.

The accompanying elemental analysis (in certificate of analysis) indicates the sample consists of 96.32 % C, 0.08 % Al, 0.40 % Cl, 2.90 % Co and 0.29 % S. For the purity of SWNT samples, a quote of the carbon content is of little significance; this includes all other allotropes of carbon.

The results do show the presence of all the listed elements, and additionally, Fe and Si were found in the sample as well.

B5   EDS backscattering image of CT2-SWNT: Si as particle (1-2 μm), Fe-Cr with minor S, Si, Al as particle (< 1 micrometer). The carbon mass contain trace amounts of Fe and S. This sample is similar to CT1-SWNT, except the two are from different batches.

The accompanying elemental analysis (in certificate of analysis) indicates the sample consists of 96.32 % C, 0.08 % Al, 0.40 % Cl, 2.90 % Co and 0.29 % S. For the purity of SWNT samples, a quote of the carbon content is of little significance; this includes all other allotropes of carbon.
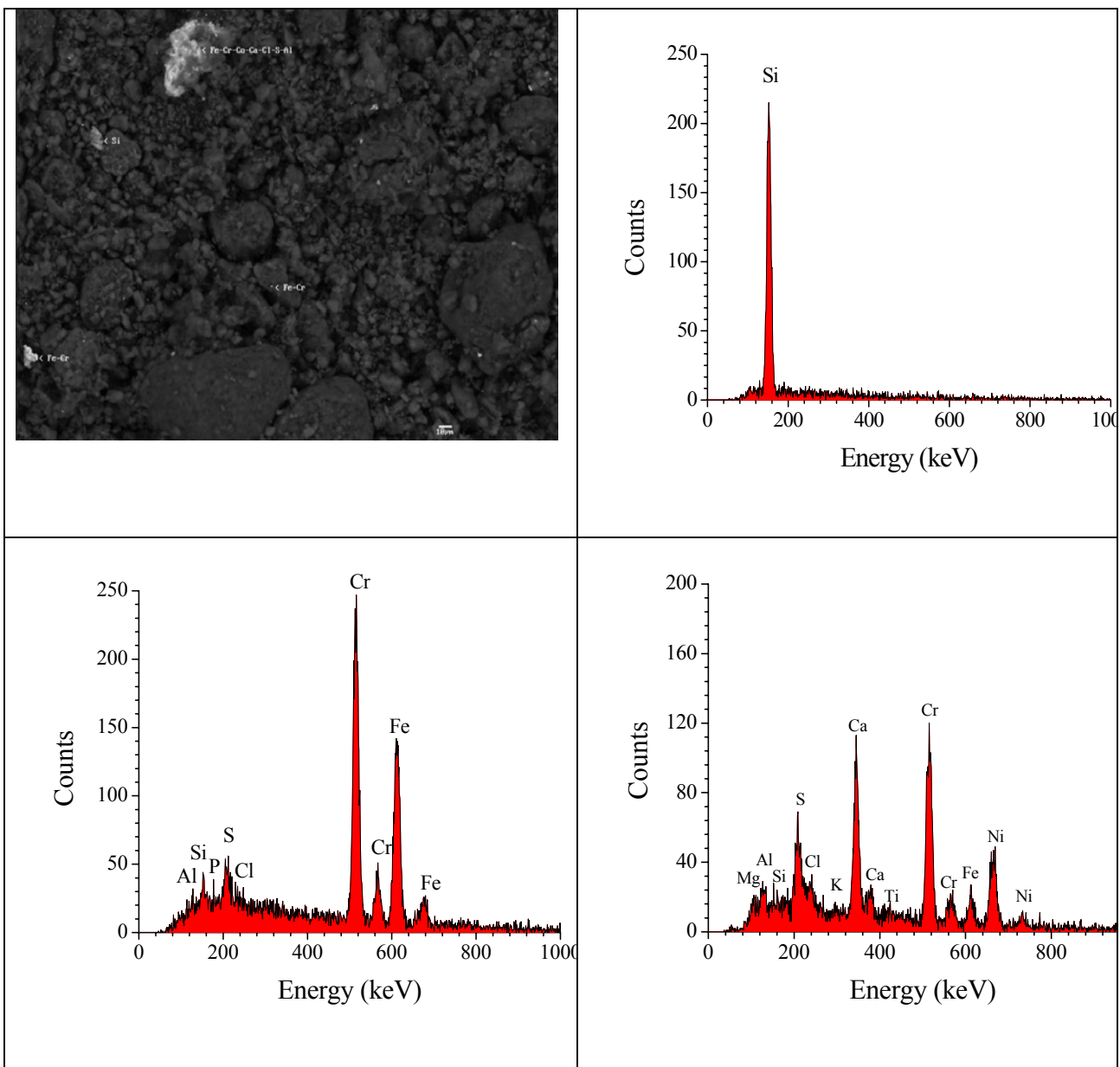
The spot appears to be heavily contaminated albeight in trace quantities (Mg, Si, P, Cr, Fe, Mg, Cr, Ti, K), together with Fe, Cr and Ni.

B6   **EDS backscattering image of P2-SWNT**: Ni as particle (100-300 nm). Carbon mass contains minor Ni, Cl, S, Si, Y. These are reported to contain 70-90 % SWNT and 7-10 % residual catalysts from Ni/Y, with low functionality.
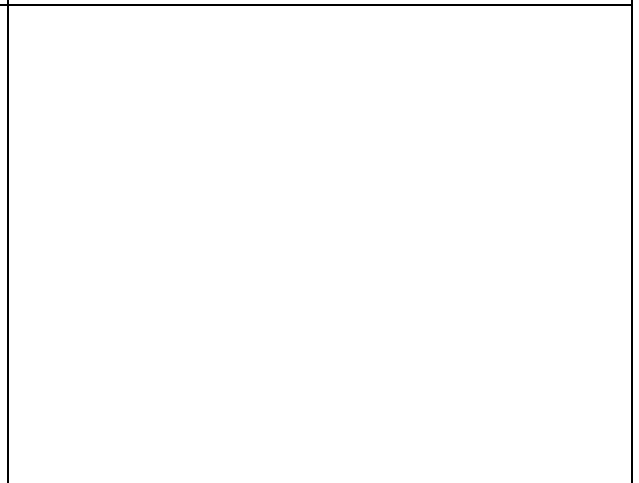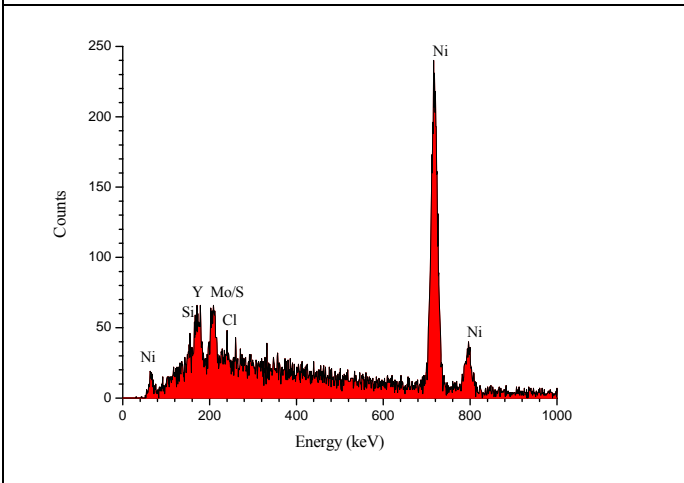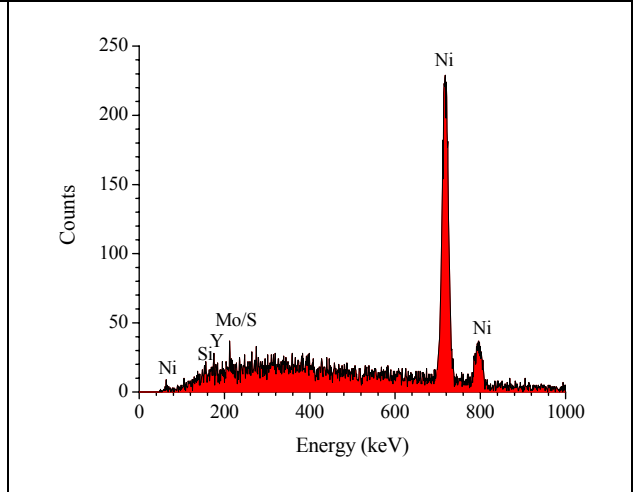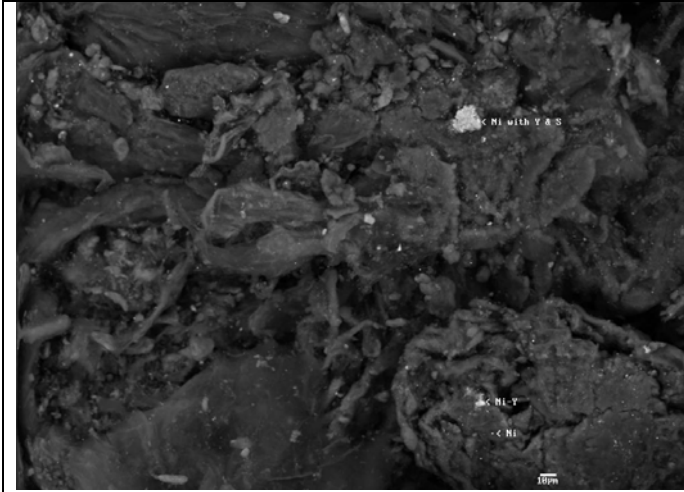
The results indicate the presence of additional impurities; Cl, S and Si.

APPENDIX C – HARVESTING HUMAN STRATUM CORNEUM

The *stratum corneum* was prepared from trimmed (removing the excess underlying subcutaneous tissue) excised human breast tissue by the trypsin technique. Pieces of the intact skin (with residual subcutaneous tissue removed) were cut into 4 x 4 cm^2, and placed in a tissue culture plate, with the stratum corneum facing upwards. Enough trypsin (1 % $^w/_v$ in water) solution was added to completely submerge the skin and incubated overnight at 37 ^{o}C. The detached *SC* with detached epidermal layer was placed on a flat surface, smoothed out, and the digested epidermis removed by gentle rubbing with moistened cotton tipped applicators. The now transparent *SC* sheets were rinsed with water.